UNIVERSITÀ DEGLI STUDI DI VERONA

Department of Biotechnology

Graduate school of Natural Sciences and Engineering

Doctoral Program in Biotechnology

XXXVII Cycle/2021-2024

A Metabolic Engineering Approach to Study the Biological Role of Tryptamine and Serotonin in the Model Species *Solanum lycopersicum*

S.S.D. BIO/01 – Botanica Generale

Coordinator: PROF.SSA FLAVIA GUZZO

Tutor: PROF.SSA FLAVIA GUZZO

Doctoral student: GIANLUCA GAMBACORTA

Table of contents

Summary

Tryptamine (TAM) and serotonin (SER) are tryptophan-derived compounds that belong to a widespread class of bioactive molecules known as indolamines or indole-alkaloids. In plants, TAM and SER are mainly known for being intermediates in the biosynthesis of melatonin, a well-studied molecule involved in important biological processes such as biotic and abiotic stress responses, ROS scavenging, embryo development, and plant morphogenesis. Although TAM and SER have been detected at very high concentrations (µg/g fw) in the edible fruits and seeds of numerous plant species, their biological functions in reproductive organs remain unclear, and their metabolic pathways still need to be fully elucidated. In plants, the biosynthesis of TAM and SER typically involves the consecutive decarboxylation and hydroxylation of tryptophan, catalyzed by tryptophan decarboxylase (TDC) and tryptamine 5-hydroxylase (T5H) enzymes, respectively. Our recent research has focused on the functional characterization of a three-member *TDC* gene family and a single *T5H* gene involved in TAM and SER biosynthesis in the model species *Solanum lycopersicum*. Our findings support a model wherein SlTDC1 promotes TAM accumulation in fruits, SlTDC2 mediates TAM production in aerial vegetative organs, SlTDC3 drives TAM synthesis in roots and seeds, and SlT5H is responsible for the conversion of TAM to SER in the entire plant. Following this model, we implemented a metabolic engineering strategy to modulate the levels of TAM and SER in different organs of the tomato plant to study their phenotypes. We chose to utilize two different genetic engineering techniques: one based on gene overexpression mediated by the strong constitutive 35S promoter from *Cauliflower mosaic virus* (CaMV), and the other based on CRISPR/Cas9-mediated gene knockout. Several engineered lines of Micro-Tom were produced, and some of these were characterized at the phenotypic and molecular levels. The results indicate a potential involvement of TAM and/or SER in the vegetative and reproductive development. In particular, the *SlTDC1*-overexpressing lines, characterized by elevated SER levels in the roots and mature leaves, exhibited a faster transition to the reproductive phase and an

earlier onset of anthesis compared to the *sltdc1* lines. In accordance with our model, the knockout of the *SlTDC1* gene resulted in the depletion of TAM and SER levels in both fruits and seeds. Interestingly, the seeds produced by the *sltdc1* lines exhibited dark pigmentation of the seed coat and a drastic reduction in germinability. Consistently, the knockout of the *SlT5H* gene resulted in a significant accumulation of TAM and complete depletion of SER. Only minimal levels of SER were detected in the leaves of *Slt5h* mutants, which may suggest the existence of an alternative pathway for SER production independent from the *SlT5H* gene. However, the *slt5h* lines displayed shortened stem compared to the control, suggesting a connection between this parameter and the altered levels of TAM and SER. In the *SlT5H*-overexpressing lines, no significant variations in TAM and SER levels were observed in the roots and leaves. Interestingly, in these genotypes the stem length is also negatively affected compared to the control, being it even shorter than that of *slt5h* lines. Moreover, a unique trait that was modulated by *SlT5H* overexpression was the emergence of floral buds, which was anticipated. In general, the interpretation of the observed phenotypes is hindered by several factors, including the overlap of roles attributed to SER and MEL, the existence of cross-talk between SER and MEL levels and other plant hormones such as auxin, cytokinins, ABA, and GA, and the structural similarity of indolamines to auxin, which may lead to interference in the signaling of this hormone. While the roles of TAM and SER in determining the observed phenotypes have not yet been clearly defined, the obtained results, together with the collection of engineered Micro-Tom genotypes generated in this project, represent an excellent starting point for deciphering the biological significance of plant TAM and SER in the model species *S. lycopersicum*.

Background and Aim of the Doctoral Project

This doctoral project is part of a research initiative started in 2018, which led to the identification of the genes involved in the biosynthesis of TAM and SER in the model species *S. lycopersicum* cv. Micro-Tom (Commisso et al., 2022). According to this model, the tomato genome includes three *TDC* genes and one *T5H* gene. The *TDC1* and *TDC2* genes exhibit tissue-specific activity and are responsible for converting tryptophan into TAM in fruits and seeds, and in aerial vegetative organs, respectively. The *TDC3* gene is characterized by a ubiquitous expression and works in synergy with the *SlT5H* gene to direct the production of SER throughout the plant, from roots to seeds.

The objective of this doctoral project is to study the biological roles of TAM and SER in *S. lycopersicum* cv. Micro-Tom. To achieve this goal, we decided to modulate the levels of TAM and SER in various plant organs by targeting the genes involved in their biosynthesis, using a metabolic engineering approach based on two distinct genetic engineering techniques: 35S-mediated gene overexpression, and the CRSIRP/Cas9-mediated gene knockout.

To analyze the effects of the depletion and/or accumulation of TAM and SER on the vegetative and reproductive development of Micro-Tom, the following genotypes were produced:

- *SlTDC1*-overxpresing lines to increase the production of TAM and SER in all plant organs;
- *SlTDC1*-knockout lines to induce the complete depletion of TAM and SER in fruits and seeds;
- *SlT5H*-overexpressing lines to induce the depletion of TAM in favor of increased SER production;
- *SlT5H1*-knockout to induce the accumulation of TAM and the complete depletion of SER;

- *SlTDC2*-knockout to induce the depletion of TAM and SER in aerial vegetative organs;
- Triple knockout lines (*SlTDC1/SlTDC2/SlTDC3*) to induce the complete depletion of TAM and SER in all plant organs and tissues.

Content and Structure of the Thesis:

This thesis is structured into the following seven chapters:

- **Chapter 1 –** Presents a general overview of the indolamines tryptamine (TAM) and serotonin (SER), focusing on the current state of knowledge regarding their biological functions and biosynthetic pathways in higher plants.

- **Chapter 2 –** Details all the materials and procedures used in the experiments.

- **Chapter 3 –** Presents the results obtained from the assembly of plant gene expression vectors and the stable genetic transformation of tomato plants mediated by *Agrobacterium tumefaciens*.

- **Chapter 4 –** Presents the results obtained from the phenotypic and molecular characterization of *SlTDC1*-overexpressing and *SlTDC1*-knockout lines.

- **Chapter 5 –** Presents the results obtained from the phenotypic and molecular characterization of *SlT5H*-overexpressing and *SlT5H*-knockout lines.

- **Chapter 6 –** Presents the results obtained from the preliminary implementation of a protocol for the exogenous administration of tryptamine (TAM) at the root level in wild-type Micro-Tom plants.

- **Chapter 7 –** Discusses the results obtained and outlines future perspectives related to this research project.

Chapter 1 – General Introduction

1.1 Plant metabolites: a complex network of primary and specialized functions

The metabolome encompasses the complete set of low molecular weight organic molecules (< 1500 Da) that can be found within a cell, tissue, organ, or organism at a given time (Wishart et al., 2007). The components of plant metabolome are conventionally categorized into primary metabolites (PMs), specialized secondary metabolites (PSMs), and plant hormones (Taiz et al., 2015). PMs, such as sugars, amino acids, nucleotides, and organic acids, are key players in central carbon metabolism and serve as the building blocks of all organic macromolecules (Wink, 2010). Consequently, PMs are highly conserved and are present in all living organisms, from prokaryotes to higher eukaryotes (Fernie and Pichersky, 2015). In contrast, PSMs are not directly involved in central metabolism and are often lineage-specific (Erb & Kliebenstein, 2020). These molecules enhance plant fitness by acting as primary defenses against herbivores and pathogens, modulating stress responses, and serving as signaling molecules in interspecific communication (Pang et al., 2021). Although a precise chemical distinction between PSMs and plant hormones cannot be made, the latter are defined as small organic molecules that regulate physiological processes at low concentrations (Davies, 2012), whereas PSMs are generally produced and accumulated in larger amounts. For decades, the functional classification of plant metabolites into PMs, PSMs, and plant hormones has provided a useful framework for research in plant biology. However, many PSMs not only mediate ecological interactions but also regulate plant growth and defense, blurring the traditional distinction between PMs and PSMs. (Erb & Kliebenstein, 2020). For instance, glucosinolates and their breakdown products are involved in the regulation of various physiological processes, such as callose deposition following bacterial infection, root growth, stomatal closure, and flowering time (Clay et al., n.d.; Kerwin et al., 2011; Khokon et al., 2011; Kliebenstein et al., 2001; Salehin et al.,

2019). Similarly, indolamines, such as melatonin (MEL), exhibit multifunctional roles, regulating both PSMs production and fundamental physiological processes. In plants, MEL can enhance photosynthetic efficiency by modulating stomatal conductance, and intercellular CO_2 levels (Arnao et al., 2022; Back, 2021). The multifunctionality of PSMs suggests that the traditional classification of plant metabolites may be overly simplistic. Rather than being viewed as secondary, PSMs should be considered integral components of dynamic metabolic networks shaped by environmental selection pressures. This new perspective can provide a deeper understanding of plant metabolism and plant-environment interactions. The biosynthesis of PSMs is tightly linked to primary metabolism, as it relies on key intermediates (i.e., amino acids, acetyl coenzyme A, shikimic acid, mevalonic acid and 1-deoxy-xylulose 5-phosphate) which are PMs or originate from central metabolic routes such as glycolysis, the Krebs cycle, and the shikimate pathway. These intermediates, are redirected into secondary metabolic pathways to form the backbone of almost all classes of PSMs, including terpenes, alkaloids, and phenolics (Böttger et al., 2018). To date, over 200,000 PSMs have been identified; however, it is estimated that their total number may exceed 500,000 (Wu & Baldwin, 2010; Yonekura-Sakakibara & Saito, 2009). Despite this huge structural diversity, the number of enzymes involved in the biosynthesis of PSMs does not reflect this abundance. This phenomenon can be partially explained by the fact that secondary metabolites are assembled from simpler precursors derived from primary metabolism, which can be combined in multiple ways. Moreover, the genes responsible for PSMs biosynthesis, such as terpene synthases, belong to large gene families that encode similar enzymes capable of producing different molecules from the same substrate. Even minor changes in an enzyme's active site can lead to the synthesis of distinct compounds from a single precursor (Köllner et al., 2004; Tholl et al., 2005). Modifying enzymes, such as carboxyl methyltransferases and acetyltransferases, exhibit low substrate specificity and can often utilize multiple substrates (Negre et al., 2003; Pichersky et al., 2006). In addition to enzymatic versatility, genetic mechanisms significantly contribute to

expanding the metabolic repertoire. Whole-genome and local gene duplication events are among the most important factors driving PSM diversity (Moore et al., 2014). Mutations in duplicated genes can lead to the loss of function, resulting in pseudogenes (Zhang, 2003), or neofunctionalization, where changes in substrate preferences or catalytic activities give rise to novel metabolites (Schwab, 2003). Additional genetic factors, such as promoter variations, single-nucleotide polymorphisms, and transposon-mediated insertions or deletions, might further enhance metabolic variability (Fernie & Tohge, 2025). The complex interplay between gene duplication, neo-functionalization, and enzymatic flexibility has enabled plants to develop, over the course of evolution, a vast biochemical arsenal known as the secondary or specialized metabolome. Considering recent discoveries highlighting the involvement of PSMs in various fundamental physiological processes, the term 'specialized metabolome' appears more appropriate, as it better reflects the heterogeneous distribution of PSMs and their essential biological role in ensuring the adaptability and survival of different plant species.

1.2 Indolamines: where, how, and why?

1.2.1 Occurrence of the indolamines tryptamine, serotonin in living organisms

Tryptamine (TAM) and serotonin (5-hydroxytryptamine, SER) are compounds derived from tryptophan, belonging to the class of indole alkaloids (Figure 1). More specifically, TAM and SER are indolamines, a group of secondary metabolites characterized by an indole backbone and an ethylamine side chain, both deriving from the amino acid tryptophan.

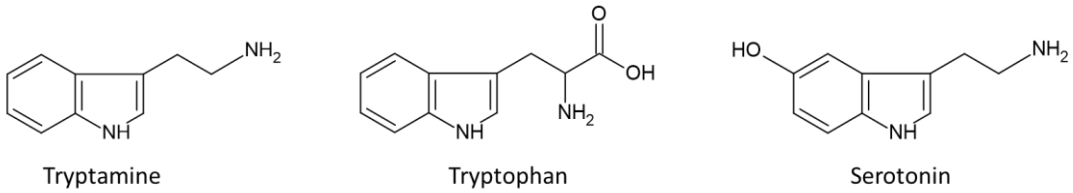

Figure 1. Molecular structure of tryptamine, tryptophan, and serotonin.

Although their distribution is heterogeneous, TAM and SER are widespread across all living kingdoms, where they fulfill diverse biological functions (Negri et al., 2021). In plants, TAM and SER are primarily recognized as intermediates in the biosynthesis of melatonin (N-acetyl-5-methoxytryptamine, MEL), a well-studied indolamine that plays important biological roles in both plants and humans (Arnao, Cano, and Hernández-Ruiz, 2022; Mannino et al., 2021). In higher plants, MEL biosynthesis starts with the conversion of L-tryptophan to TAM catalyzed by the enzyme tryptophan decarboxylase (TDC) (Mannino et al., 2021). Plant TDCs belong to a subgroup of aromatic acid decarboxylases (AACDs), a class of enzymes that operate at the interface between primary and secondary metabolism, producing biogenic amines that serve as precursors for a wide range of plant secondary metabolites (PSMs) (Facchini et al., 2000). Although TAM has been found in high concentrations in numerous edible plant species, its specific function remains unknown (Negri et al., 2021). In vertebrates, TAM does not serve as a serotonin precursor, but its trace presence in the human brain may suggest a functional role, possibly as a minor neuromodulator (Khan and Nawaz, 2016). While tryptamine is rarely found in prokaryotes, certain bacteria within the human gut microbiota, particularly *Ruminococcus gnavus* and *Clostridium sporogenes*, are

capable of producing tryptamine through the activity of TDC enzymes. Interestingly, TAM produced by these bacteria can accelerate the host's whole-gut transit by binding to specific receptors in the intestinal epithelium (Bhattarai et al., 2018; Williams et al., 2014). This ability to modulate intestinal transit in animal hosts suggests a role for tryptamine in interspecific communication. The hypothesis is further supported by findings showing that a mutant strain of the entomopathogenic fungus *Metarhizium acridum*, which accumulates elevated levels of TAM, exhibits increased virulence against various species of phytophagous insects, including *Locusta migratoria* (Tong et al., 2020). TAM has also been identified in certain basidiomycete fungi, such as *Psilocybe carpophores*, where it serves as a precursor in the biosynthesis of substituted tryptamines, including the psychedelic tryptamines psilocybin and psilocin (Araújo et al., 2015). The second step in the plant MEL biosynthetic pathway is the conversion of TAM into SER, catalyzed by the enzyme tryptamine 5-hydroxylase (T5H). In animals, SER biosynthesis follows a different pathway, where tryptophan is first hydroxylated by tryptophan hydroxylase (TPH) to form 5-hydroxytryptophan, which is subsequently decarboxylated by AADC to produce SER (Mannino et al., 2021). Despite these differences, both plant and animal kingdoms share the downstream enzymatic steps leading from SER to MEL. This evolutionary convergence highlights the biological significance of these versatile molecules. Given the strong antioxidant properties of both SER and MEL, some authors have hypothesized that early aerobic and photosynthetic organisms acquired the ability to produce these indolamines over 2.5–3.5 billion years ago as a means to cope with oxidative stress generated by their metabolism (Manchester et al., 2015; Turlejski, 1996). However, SER is rarely found in prokaryotic organisms, with only a few species of bacteria capable of producing this indolamine (Gonçalves et al., 2022; Muszyńska et al., 2011). Recently, some authors have reported the involvement of SER in various bacterial biological processes, such as stress response, biofilm formation, and quorum sensing (Gonçalves et al., 2022; Knecht et al., 2016). Interestingly, in *in-vitro* assays, SER has been shown to exert antifungal activities against certain

species of human pathogenic fungi belonging to the genera *Aspergillus* and *Candida* (Lass-Flörl et al., 2003; Perkhofer et al., 2007). In animals, SER primarily acts as a neurotransmitter, regulating mood, sleep, and appetite, but it is also involved in other processes such as platelet aggregation and intestinal peristalsis (Mohammad-Zadehet al., 2008; Oliver et al., 1998; Veenstra-Vanderweele et al., 2000). Unlike TAM, the role of SER in higher plants has been extensively studied in recent decades. As will be discussed later in this chapter, in plants, SER is involved in key physiological functions related to growth regulation and development, as well as responses to biotic and abiotic stress (Sun et al., 2021). Despite this, the mechanisms of action of SER remain ambiguous, and its role in plants is still unclear.

1.3 State of the art concerning the biological roles of tryptamine and serotonin in angiosperms

1.3.1 Biochemical fate and putative biological roles of plant tryptamine

In plants, TAM serves as a precursor for a wide array of bioactive molecules recognized for their important pharmacological properties, including the potent anti-cancer monoterpenoid indole alkaloids vincristine and vinblastine (Dewick, 2002). This unique characteristic of TAM has garnered considerable interest from researchers aiming to elucidate the downstream pathways associated with TAM to discover new compounds, while also leveraging the versatility of its molecular scaffold for developing semi-synthetic derivatives (Bradley et al., 2023; Sravanthi and Manju, 2016; Runguphan et al., 2009). As a result, many of the enzymes involved in the biosynthesis of plant indolamines and their derivatives have been identified and characterized (Mannino et al., 2021; Dewick, 2002). The enzyme TDC, along with its product TAM, represents a major entry point for carbon and nitrogen in the specialized metabolism of plants (Negri et al., 2021). TAM is synthesized in the cytosol, and once produced, it can undergo several fates:

i) being channeled into the indoleamine pathway (of which MEL is the final product).

ii) serving as a precursor for a wide range of specialized metabolites containing the indole moiety, such as monoterpenoid indole alkaloids, indole-alkylamines, and β-carbolines.

iii) being accumulated.

Moreover, the existence of an alternative pathway for auxin biosynthesis involving TAM has been proposed; however, the genes potentially involved have not yet been identified, and the hypothesis currently lacks confirmation (Bajguz and Piotrowska-Niczyporuk, 2023). Plant TAM is produced from tryptophan through the action of the enzyme TDC. First characterized in the species *Catharanthus roseus* (De Luca et al., 1988), several orthologs of the *TDC* gene have been identified in various angiosperm species. In some cases, such as in kiwi (*Actinidia*

deliciosa), the *TDC* gene is present in a single copy, while in others, small gene families consisting of two or three members are found (Li et al., 2016 a; Negri et al., 2021), as observed in *Aegilops variabilis,* rice (*Oryza sativa*), and tomato (*S. lycopersicum*). Interestingly, in the latter species, the three copies of the *TDC* gene have shown variable activity depending on the organ and developmental stage, suggesting specific functions for the products of the biosynthetic pathway, particularly TAM and SER, which often accumulate in high quantities (Commisso et al., 2022). To date, TAM has been detected in various edible plant species, such as tomato, kiwi, apple, rice, etc., where it primarily accumulates in reproductive organs such as fruits and seeds, but is also present in aerial vegetative organs, like leaves and in underground organs, such as roots, rhizomes, and tubers, in quantities ranging from a few nanograms to tens of micrograms of fresh (or dry) weight (Negri et al., 2021). The presence of the highest amounts of TAM in reproductive organs suggests that this molecule may play significant roles in reproductive development. The discovery of large quantities of tryptamine in the pollen of *Prosopis juliflora* (Al-Soqeer et al., 2017; Negri et al., 2021) further supports this hypothesis. Although TAM has been identified in various organs of known plant species, with higher accumulation in fruits and seeds, its biological role in plants has not been thoroughly investigated, leaving its functions largely unknown. The limited studies available suggest a potential defensive role of TAM against plant pests (Negri et al., 2021). The overexpression of *TDC* from *Catharanthus roseus* in tobacco (*Nicotiana tabacum*) resulted in a significant accumulation of TAM (Songstad et al., 1990). Interestingly, transgenic poplar (*Populus tremula* x *P. alba)* and tobacco expressing *TDC* from *Camptotheca acuminata* exhibited elevated TAM levels that correlated with a marked suppression of growth in herbivorous insects, such as *Malacosoma disstria* (forest tent caterpillar) and *Manduca sexta* (tobacco hornworm), which fed on TAM-hyperaccumulating leaves (Gill and Ellis, 2006; Gill, Ellis, and Isman, 2003). This observation suggests that TAM functions as an effective antifeedant, inhibiting feeding behavior and consequently reducing leaf consumption and limiting larval

growth. Further supporting this idea, studies on *Drosophila melanogaster* have shown that TAM administration negatively affects reproduction rates, likely due to depression-induced anti-oviposition effects (Thomas et al., 1998), suggesting that TAM may function as an anti-attractant in plants. Additionally, Chen & Luetje (2014) demonstrated that TAM inhibits odorant receptors in insects across three orders (*Diptera*, *Lepidoptera*, and *Coleoptera*), highlighting its role in altering insect behavior through the antagonism of co-receptor subunits (Luetje and Chen, 2014). Recently, increased resistance to root knot nematodes (RKNs) has been observed in tobacco plants overexpressing the *TDC* gene from *Ae. variabilis*. Interestingly, while TAM levels remained similar between these transgenic lines and wild-type tobacco plants, the concentrations of TAM derivatives – such as N-hydroxytryptamine, N-acetyltryptamine, and 5-methoxy-N-N-dimethyltryptamine – were increased in the most resistant line. Furthermore, in this genotype, SER accumulation was nearly eightfold higher compared to wild-type plants (Li et al., 2016). In *Setaria viridis* a strong induction of *TDC* expression and SER accumulation was observed in response to insect feeding (Dangol et al., 2022). These findings raise important questions about the distinct roles of TAM and SER in plant defense. While the mechanisms of action of TAM against plant pests remain unclear and warrant further investigation, all these results underscore the significance of *TDC* genes, TAM (along with its derivatives) in enhancing plant resistance to herbivores.

1.3.2 The multifunctional role of serotonin in plants

Since its discovery in the stinging hairs of cowage (*Macuna pruriens*) in 1954, SER has been found in over 70 plant families (Negri et al., 2021). Similarly to its role in animals, in plants SER acts as a multifunctional molecule involved in numerous physiological processes, ranging from the regulation of growth and morphogenesis, to the control of flowering and pollen germination, as well as defense against abiotic and biotic stress (Mishra and Sarkar, 2023; Mohammad-Zadeh, Moses, and Gwaltney-Brant, 2008). Despite the large number of studies

conducted over the past 20 years, in many cases the mechanisms of action of SER in these processes have not yet been fully elucidated.

1.3.3 Serotonin and its role in the regulation of plant growth and morphogenesis

Numerous studies have shown that SER is involved in regulating vegetative growth and root development, with one of the initial hypotheses suggesting auxin-like activities. However, subsequent research on *Arabidopsis thaliana* has demonstrated that SER acts as an auxin inhibitor, reducing the development of primary and adventitious roots by inhibiting the expression of auxin-responsive genes (Pelagio-Flores et al., 2011). Auxins are generally responsible for maintaining apical dominance and promoting root formation, while cytokinins work antagonistically to auxins to encourage lateral bud and shoot development. Studies conducted on *A. thaliana* following SER treatment have observed enhanced lateral root growth (Mishra and Sarkar, 2023). Furthermore, in vitro studies on *Mimosa pudica* revealed that SER promotes lateral root induction and shoot production by 60% and 70%, respectively. These findings — specifically, the inhibition of primary roots, the enhancement of lateral root growth, and the increase in the number of shoots — have led to the association of SER with cytokinin-like activity (Erland et al., 2015; Murch et al., 2001). The morphogenetic effects of SER have also been linked to calcium signaling and its cross-talk with MEL, which, in *in-vitro* studies on *Hypericum perforatum*, have shown to exhibit auxin-like effects (Danilovich, Alberto, and Juárez Tomás, 2021; Ramakrishna et al., 2016; Manchester et al., 2015). Some authors proposed that the balance between SER and MEL may function similarly to the auxin/cytokinin relationship, albeit to a lesser extent, in modulating plant morphogenesis (Sun et al., 2021). Interestingly, recent studies have indicated that auxin can modulate indoleamine biosynthesis and affect the SER/MEL ratio, thereby influencing plant growth and morphogenesis (Mishra and Sarkar, 2023).

1.3.4 Role as a mitigator of abiotic stress

SER has been associated with increased tolerance to various types of abiotic stress, particularly salt and water stress (Mishra and Sarkar, 2023). In tomato seedlings subjected to osmotic stress, serotonin application enhanced the detoxification of free radicals (O_2^-, and H_2O_2) by increasing FeSOD and CAT2 activity, provided a steady supply of reduced glutathione through increased *GR1* expression, and elevated osmolyte proline levels by enhancing *P5CS* transcript levels. Consequently, cell membrane degradation and ethylene synthesis were reduced under salt and drought stresses, demonstrating serotonin's stress-mitigating effects similar to MEL (Akcay and Okudan, 2023). In addition, it has been observed that SER accumulates in roots, cotyledons, and leaves of sunflower (*Helianthus annuus*) and rice seedlings subjected to saline conditions, indicating its potential involvement in mitigating salt stress (Gupta and De, 2017; Mukherjee et al., 2014). In *Paeonia lactiflora*, a strong induction of tryptophan decarboxylase (TDC), but not of tryptophan 5-hydroxylase (T5H), was observed during drought stress. However, SER levels were not evaluated, and the authors attributed the tolerance to this type of stress to MEL (Daqiu Zhao et al., 2019). In *A. thaliana*, SER and MEL treatment induce the expression of key genes such as *LBD16* and *XTR6*, which promote lateral root growth under salinity stress (Wan et al., 2018; Xu et al., 2020; Zhang et al., 2023). Under temperature stress, SER and MEL cooperate to enhance cell proliferation and regulate isoflavone production in *Glycine max* (soybean), as their ratio has been proven to modulate isoflavone content and biomass production (Kumar et al., 2021). Recently, Shan et al. (2025) demonstrated that mangrove seedlings (*Kandelia obovata*) sprayed with SER (200 $\mu mol \cdot L^{-1}$) exhibit increased resistance to cold stress, as evidenced by a reduced extent of leaf damage. (Shan et al., 2025).

1.3.5 Role of serotonin in biotic stress protection

SER plays a multifaceted role in biotic stress resistance in plants by acting as defensive chemical or by activating genetic responses (Erland et al., 2018). Furthermore, SER acts as a powerful antioxidant and ROS scavenger, protecting damaged and healthy tissues during hypersensitive response (Hayashi et al., 2016). Additionally, SER and its derivatives, such as N-acetylserotonin (NAS) and MEL, activate defense-related genes like *ICS1*, *PR1*, and *PR5*, and trigger MAPK signaling pathways to enhance stress tolerance (Mishra and Sarkar, 2023). In *Anabena variabilis*, *Camptotheca acuminata*, e *Capsicum annuum*, *TDC* genes are minimally expressed under normal physiological condition, but their expression was strongly induced by pathogen elicitors (Negri et al., 2021). In different members of the *Poaceae* family, an increase in SER content (and SER-derived phenylpropanoids amides) is observed following attacks by fungi and nematodes (Erland et al., 2015). In rice leaves, SER content is generally low, but following inoculation with the pathogenic fungus *Magnaporthe oryzae*, SER levels can rise up to 80-fold in necrotic areas at the infection site. The increased SER levels have been associated with the appearance of halo lesions (lesions with a brown ring) that can inhibit the progression of the infection (Ishihara et al., 2008). In the Sekiguchi rice mutant, which is unable to convert TAM into SER, the absence of halo lesions has been observed. This mutant exhibit increased susceptibility to infections by *Magnaporthe grisea* (Fujiwara et al., 2010; Ueno et al., 2003) and *Bipolaris oryzae* (Ishihara et al., 2008). Exogenous administration of SER not only restored plant resistance, but also restored the appearance of halo lesions, highlighting the role of SER in the hypersensitive response (Fujiwara et al. 2010). Furthermore, some authors have reported that SER contributes to herbivore deterrence by enhancing the stinging sensation caused by mechanical rupture of plant structures and the release of toxic compounds, such as oxalic and formic acids, in synergy with other biogenic amines like acetylcholine and histamine (Negri et al., 2021). These evidences suggest that SER may play an important role

in orchestrating plant defense against a wide range of biotic stresses, particularly in response to pathogenic fungi.

1.3.6 The mysterious role of SER in reproductive organs

Although SER has been found in various plant organs, some species tend to accumulate this indolamine in their reproductive organs, such as fruits and seeds. For example, in the seeds of *Juglans regia*, SER accumulates during embryo development, reaching up to 400 μg g^{-1} FW (Grosse, 1982; Grosse et al., 1983). Similar to *Juglans regia*, in tomato, SER accumulates in the seed during embryo development, peaking in the fully developed seed (Commisso et al., 2022). In many edible plant species, including kiwi (*Actinidia deliciosa*), banana (*Musa spp*), tomato, and pineapple (*Ananas comosus*), SER is primarily accumulated in the fruit. In these species, SER accumulation follows distinct patterns tied with fruit development and ripening. For instance, while in banana and tomato berries, SER peaks at later stages of maturation, in kiwi and pineapple fruits, SER reaches its highest concentrations during early development, with levels decreasing in ripe and overripe fruits (Negri et al., 2021). SER levels also fluctuate throughout various stages of flower development. For example, in *Juglans regia* (Lembeck and Skofitsch, 1984) and *Datura metel* (Erland et al., 2018), serotonin levels are higher during the early stages of flowering. While the exact mechanism behind this remains unclear, serotonin's known association with phytochrome suggests it may regulate flowering time through interactions with this photoreceptor (Erland et al., 2018). Taken together, these findings highlight the multifaceted and still unexplored roles of SER in the reproductive development of angiosperms.

1.4 Metabolic pathways for the biosynthesis of plant indolamines

1.4.1 The plant serotonin/melatonin biosynthetic pathway

The metabolic pathways underlying the biosynthesis of SER and MEL, have been extensively studied in various taxa, including plants, fungi, and mammals (Xie et al., 2022; Dake Zhao et al., 2019). Higher plants and certain species of ascomycete fungi share similar biosynthetic pathways, whereas in animals, the metabolic pathway diverges during the synthesis of SER (Mannino et al., 2021 b; Wang et al., 2021). However, although minor and alternative pathways exist, from this point onward, the biosynthetic pathways of plants and animals converge and proceed similarly toward MEL. In this section, the main metabolic pathways characterized to date in angiosperms will be described in detail. In all the aforementioned organisms, the biosynthetic pathway begins with the amino acid tryptophan. To date, five enzymes involved in the MEL biosynthetic pathway in plants have been characterized: L-tryptophan decarboxylase (TDC), tryptamine 5-hydroxylase (T5H), serotonin N-acetyltransferase (SNAT), acetylserotonin O-methyltransferase (ASMT), and caffeic acid 3-O-methyltransferase (COMT). Additionally, the existence of a tryptophan hydroxylase (TPH) with a function similar to that in humans has been hypothesized (Mannino et al., 2021 b). The first committed step in the plant MEL biosynthetic pathway is the conversion of tryptophan to TAM, catalyzed by the cytoplasmic TDC enzyme (Zhou et al., 2020). TAM is then rapidly converted to SER (5-hydroxytryptamine) by the enzyme T5H (Figure 2).

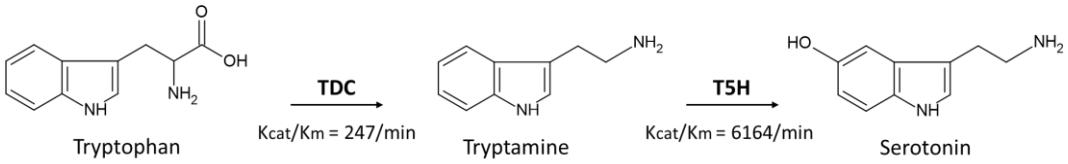

Figure 2. Plant tryptamine and serotonin biosynthetic pathway.

The T5H enzyme belongs to the cytochrome P450 monooxygenase family, and it is localized in the endoplasmic reticulum (Fujiwara et al., 2010). Given the low catalytic efficiency of TDC (Kcat/Km = 247/min) compared to T5H (Kcat/Km =

6164/min), the conversion of tryptophan to TAM represents one of the rate-limiting steps of this metabolic pathway. Interestingly, in the Sekiguchi rice mutant, despite the complete absence of T5H activity, the presence of MEL has been detected, albeit at lower levels compared to the wild type. As mentioned earlier, an alternative pathway analogous to that found in humans has been hypothesized in plants. According to this hypothesis, tryptophan is converted to 5-hydroxytryptophan by the enzyme TPH, and subsequently, through the action of TDC in plants (AADC in humans), 5-hydroxytryptophan is converted to SER. However, to date, the plant *TPH* gene has not yet been identified, and it has been widely demonstrated that the primary pathway for SER production in plants involves the decarboxylation of tryptophan followed by the hydroxylation of TAM (Back, Tan, and Reiter, 2016 a). The synthesis of MEL from SER occurs in two consecutive enzymatic reactions involving three different enzymes (SNATs, ASMTs, and COMT). In plants, SER is preferentially converted to N-acetylserotonin by SNAT in chloroplasts. Subsequently, N-acetylserotonin is rapidly converted to MEL by the enzymes ASMT or COMT in the cytoplasm. Since MEL levels do not appear to correlate with the much higher SER levels, it has been hypothesized that the production of N-acetylserotonin by SNAT may represent another rate-limiting step in this metabolic pathway. In plants, an alternative pathway has also been observed, involving the production of 5-methoxytryptamine from SER, catalyzed by ASMT/COMT in the cytoplasm, followed by the conversion of 5-methoxytryptamine into MEL by ASNT located in chloroplasts. It has been suggested that the shift between these two alternative pathways may depend on the physiological conditions and developmental stage of the plant (Ye et al., 2019). Specifically, the pathway proceeding from tryptophan through TAM, SER, and N-acetylserotonin to MEL has been associated with normal physiological conditions, which correspond with relatively low levels of SER (Ye et al., 2019). The alternative pathway, proceeding from tryptophan through the intermediates TAM, SER, and 5-methoxytryptamine to MEL, is instead associated with senescence or abiotic stress conditions, during which there is a higher accumulation of TAM and SER

(Arnao, 2014). However, the fact that an increase in TAM and SER content does not correspond to a proportional increase in MEL levels suggests that TAM and SER may play specific biological roles under these particular physiological conditions.

1.4.2 A model for the biosynthesis of tryptamine and serotonin in the model species Solanum lycopersicum

In 2022, Commisso et al. proposed a functional model for the biosynthesis of TAM and SER in the model species *S. lycopersicum* cv. Micro-Tom. Following homology-based screening using well-characterized plant TDCs and T5H amino acid sequences, a three-member *SlTDC* gene family and a unique *SlT5H* gene were identified: *SlTDC1* (Solyc07g054860), *SlTDC2* (Solyc07g054280), *SlTDC3* (Solyc09g064430), and *SlT5H* (Solyc09g014900). To confirm their identity, the candidate genes were functionally characterized through their transient expression in *Nicotiana benthamiana*, a species that does not produce detectable levels of TAM and SER in its aerial organs. Subsequently, a detailed analysis of the expression profiles of the three *SlTDC* genes and the *SlT5H* gene was performed on various organs of Micro-Tom collected at different developmental stages. The same organs were used to measure the levels of TAM and SER through HPLC-ESI-MS analysis. The three *SlTDC* genes were characterized by distinct expression profiles across the different analyzed organs. The *SlTDC1* gene was found to be exclusively expressed in the fruit, reaching the highest expression level at the mature green stage. Conversely, the *SlTDC2* gene was characterized by strong expression in leaves and flowers, with minimal activity in the fruit. The *SlTDC3* gene was expressed at different levels in all organs and was the only *SlTDC* gene active in the roots. However, it should be noted that among the three *SlTDC* genes, *SlTDC3* was the least efficient in converting tryptophan to TAM in the heterologous system in *N. benthamiana*. In contrast to the intricate regulation of the *SlTDC* genes, the *SlT5H* gene was found to be expressed in all Micro-Tom organs. From the analysis of TAM and SER levels, it emerged that the biosynthesis and the accumulation of these two indolamines are tightly regulated processes. In general,

in all analyzed organs, SER levels were consistently higher than those of TAM (except in fruits at the immature green stage), with total concentrations ranging from 27.19 to 9322.02 ng g^{-1} FW for serotonin and 1.60 to 337.60 ng g^{-1} FW for TAM. The lowest levels of both compounds were found in the roots, with opposite trends (TAM increasing, SER decreasing) moving from the primary embryonal root to the distal part of the secondary roots. In aerial vegetative organs, TAM levels increased along the stem axis, peaking in the youngest leaves near the apical meristem (up to 337.60 ng g^{-1} FW). In contrast, SER reached its highest concentration in the fourth true leaf (up to 9.3 µg g^{-1} FW) before decreasing in leaves closer to the vegetative apex. In reproductive organs, particularly in flowers at anthesis, SER levels (758.54 ng g^{-1} FW) were approximately six times higher than TAM levels. Notably, in fruits at the immature green stage, TAM levels (up to 1.1 µg g^{-1} FW) were ten times higher than those of SER. This was the only organ and developmental stage where TAM was more abundant than SER. In addition, TAM accumulates at high levels exclusively in the fruit mesocarp and in the seed (up to approximately 8 µg g^{-1} FW), where it reaches levels comparable to those of SER. By integrating the TAM and SER accumulation patterns with the spatiotemporal gene expression profile, Commisso and co-workers proposed a model to explain the dynamic regulation of indolamine biosynthesis in the model species *S. lycopersicum*. According to this model, the gene *SlTDC1* is involved in the production and accumulation of TAM in the early stages of fruit development. The gene *SlTDC2* is responsible for the production and accumulation of TAM in aerial vegetative organs and flowers, while the genes *SlTDC3* and *SlT5H* work together to regulate SER levels throughout the entire tomato plant. Interestingly, despite the roots being characterized by high levels of expression of the genes *SlTDC3* and *SlT5H*, the levels of SER are low, indicating its possible translocation to aerial vegetative organs or its conversion into downstream products. Figure 3, illustrates the biosynthetic pathway of TAM and SER in tomato, based on the expression profiles of the involved genes. The highly regulated spatiotemporal biosynthesis and accumulation of TAM and SER, combined with their high levels in certain

tissues and organs, suggest that these metabolites are not merely intermediates in the indolamine biosynthetic pathway. Instead, they likely play specific roles in plant development and physiology, potentially contributing to processes such as reproductive development, fruit ripening, and seed development.

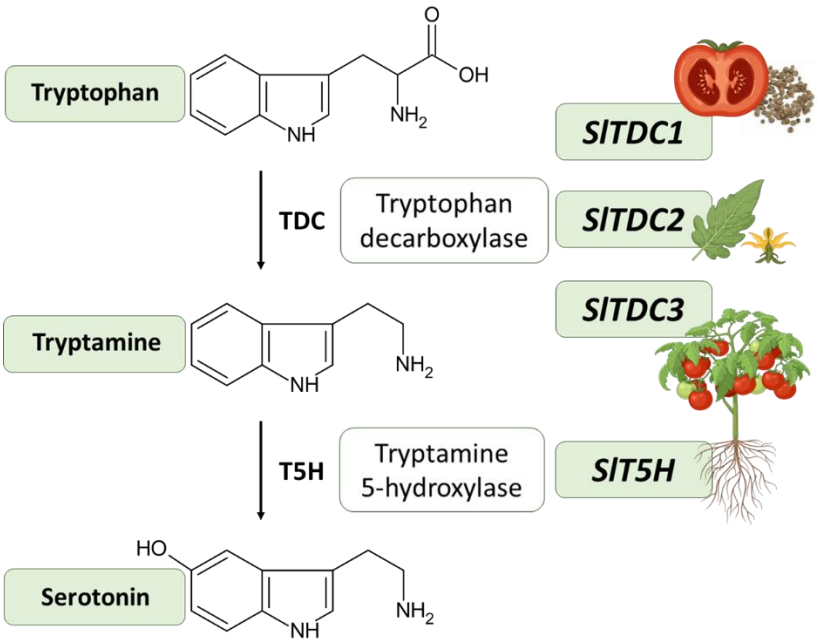

Figure 3. The tomato tryptamine and serotonin biosynthetic pathway: The gene SlTDC1 is involved in the biosynthesis of TAM in fruit and seed; the gene SlTDC2 drive the biosynthesis of TAM in aerial vegetative organs; the gene SlTDC3 is the active in all plant organs but is the least efficient among the three TDC isogenes; the gene SlT5H drive the conversion of TAM to SER and is active in all plant organs.

Chapter 2 - Materials and Methods

2.1 Plant material and management

2.1.1 Plant material

In this study, the wild-type cultivar Micro-Tom (ID:TOMJPF00001) was selected as genetic background for the stable genetic transformation of the model species *S. lycopersicum*. This cultivar was previously employed in our laboratory to generate three independent transgenic lines overexpressing the *SlTDC1* gene and three independent *SlTDC1*-knockout lines (Table 2.1.1). Consequently, Micro-Tom served as the reference genotype for all molecular and phenotypic characterization experiments performed on the engineered lines described in chapter 4, and 5.

Genetic background	Genotype	No. of lines	Progeny
Solanum lycopersicum cv. Micro-Tom ID:TOMJPF00001	*TDC1* overexpression *SlTDC1*-OE	3	T2/T3
	TDC1 knockout *SlTDC1*-KO	3	T2/T3

Table 2.1. List of Micro-Tom engineered genotypes available at the beginning of the research project.

2.1.2 Greenhouse growing conditions

Seeds were sown in seedbeds containing a 3:1:1 mixture of peat, perlite, and sand. Ten days after germination, the seedlings were transferred to their final 1-liter pots using the same soil mixture. Starting from the second week after the transfer to the final pots, the plants were fertigated every two weeks with an N-P-K 20-5-10 fertilizer until the end of flowering. The plants were grown under the following greenhouse conditions: a temperature range of 15–30°C, 50–70% relative humidity (RH), and a 16h/8h light/dark photoperiod. Under these environmental conditions, the plants were able to complete their life cycle within four months

after germination. At the end of each growing cycle, the plants were allowed to self-pollinate to collect seeds, which were stored at 4°C.

2.1.3 Growth chamber growing conditions

The plants were sown, germinated, and grown as described in the previous paragraph. Inside the growth chamber, the environmental conditions were as follows: a temperature range of 20–30°C, 30–65% relative humidity (RH), and a 16h/8h light/dark photoperiod. In this environment, the plants exhibited a life cycle similar to that observed in the greenhouse, lasting approximately 4 months from germination.

2.1.4. Hydroponic growing conditions

The plants used for the feeding experiments were sown in vitro on agar-solidified MS medium (Murashige & Skoog medium, Duchefa Biochemie) diluted 1:4 (MS ¼), and adjusted to pH 5.8 with 1N KOH. After 7 days in a growth chamber (25°C, 15 h light/9 h dark, dual fluorescent lamps 58W/840 and 58W/77), the seedlings were transferred to a hydroponic system. The nutrient solution, consisting of MS ¼ adjusted to pH 5.6, was renewed weekly. The plants were grown for three weeks under controlled conditions: 20–30°C, 30–60% relative humidity, and a photoperiod of 16 hours of light and 8 hours of dark, under LED lamps (120–277 VAC, 50/60 Hz, 150 W).

2.2 Assembly of plant gene expression vectors

2.2.1 The Golden Braid system

The assembly of plant gene expression vectors, which carry the T-DNA insert for the overexpression of *SlT5H* or the knockout of target genes (*SlTDC1*, *SlTDC2*, *SlTDC3*, and *SlT5H*), was performed using the Golden Braid (GB) cloning system (https://gbcloning.upv.es/). The GB system is a modular "cut and paste" cloning procedure based on the use of type IIS restriction enzymes. Through the GB system, DNA elements (GB modules) can be combined to create gene constructs composed of one or more transcriptional units (TUs). A TU typically consists of a promoter, a coding sequence (CDS), and a terminator. The GB system utilizes three different types of vectors: the entry vector pUPD2, used to adapt new DNA elements to the GB cloning procedure, and two series of expression vectors (pDGB3_α and pDGB3_Ω) which are used for both the assembly of TUs and stable genetic transformation of plants (Table 2.2). The expression vectors of the alpha (α) and omega (Ω) series are further divided into two levels: pDGB3_α1 and pDGB3_α2; pDGB3_Ω1 and pDGB3_Ω2. The alpha and omega series vectors differ in two fundamental elements: the enzyme used in the cloning procedure (BsaI for alpha vectors and BsmBI for omega vectors) and the antibiotic used for the selection of positive clones (kanamycin for alpha vectors and spectinomycin for omega vectors). These vectors are can be used to combine multiple TUs through an iterative cloning system.

GB vector	Vector function	Enzyme in	Enzyme out	Bacterial selection
pUPD2	DNA cloning	BsmBI	BsaI	Chloramphenicol
pDGB3α1	DNA cloning/plant genetic transformation	BsaI	BsmBI	Kanamycin
pDGB3α2	DNA cloning/plant genetic transformation	BsaI	BsmBI	Kanamycin
pDGB3Ω1	DNA cloning/plant genetic transformation	BsmBI	BsaI	Spectinomycin
pDGB3Ω2	DNA cloning/plant genetic transformation	BsmBI	BsaI	Spectinomycin

Table 2.2. List of Golden Braid vectors used in the assembly of gene constructs.

A GB vectors contain the cloning site within the LacZ gene in order to allow white/blue screening of positive clones on IPTG/X-Gal containing LB medium.

Any DNA sequence – including a promoter or a coding sequence (CDS) – can be adapted to the GB cloning system by adding specific 4-nucleotide overhangs (adapters) at the 5' and 3' ends. These adapters are designed *in-silico* using a dedicated tool available on the GB Cloning website. Following this step, the sequence of interest is synthesized by a commercial gene synthesis service. The sequence is then cloned into the pUPD2 entry vector via BsmBI. To assemble a TU, a promoter, a coding sequence (CDS), and a terminator — each individually pre-cloned into distinct pUPD2 vectors — are combined into an alpha vector (pDGB3_α1 or pDGB3_ α2) via BsaI. This initiates the iterative modular cloning procedure: two TUs, one cloned in pDGB3_α1, the other in pDGB3_α2, are merged into an omega vector (pDGB3_Ω1 or pDGB3_Ω2) via BsmBI. Similarly, TUs cloned in the two different omega vectors can be merged in an alpha vector using BsaI. This procedure can be repeated multiple times, enabling the assembly of complex genetic constructs composed by multiple TUs.

2.2.2 The GB vectors library

The GB platform offers a library of preassembled genetic modules designed to accelerate the cloning procedure. The GB modules used in this study include: the constitutive promoter 35s from *Cauliflower mosaic virus* used to induce a strong gene expression; the *Nopaline synthase* promoter (Pnos) and terminator (Tnos) commonly used as regulative elements in plant gene expression vectors; the U6-26 promoter form *A. thaliana,* required for the transcription of the single guide (sgRNA) within the plant cell nucleus mediated by the plant RNA polymerase III; the scaffold RNA (scRNA), a structural part of the CRISPR/Cas9 system which is essential for the formation of the active Cas9 ribonucleoprotein complex; the *NptII* TU (Pnos::*NptII*::Tnos), containing the plant optimized *Neomycin phosphotransferase* gene (kanamycin resistance gene) used for the selection of transgenic plants; and the multi-TUs GB module *NptII*::*hCas9* (Pnos::*NptII*::Tnos::P35S::*hCas9*::Tnos) containing the *NptII* cassette, and the *human Cas9* coding sequence (CDS) under the control of the 35S promoter and

the Tnos terminator. All these GB modules, along with brief description of their main features are listed in in Table 2.3.

Backbone	GB module	Module description	Enzyme out
pUPD2	P35S	Strong constitutive 35S promoter form *Cauliflower mosaic virus* (gene overexpression)	BsaI
pUPD2	PU626	U6-26 promoter from *Arabidopsis thaliana* (sgRNA transcription)	BsaI
pUPD2	Tnos	*Nopaline synthase* terminator (standard regulatory element)	BsaI
pUPD2	scRNA	Scaffold RNA (structural component of the CRISPR/Cas9 system)	BsaI
pDGB3α1	Pnos::*NptII*::Tnos	TU containing the plant optimized kanamycin resistance gene (*NptII* gene cassette)	BsmBI
pDGB3Ω1	*NptII*::*hCas9*	Multi-TU module containing the *NptII* cassette and the *human Cas9* CDS under the control of the 35S promoter	BsaI

Table 2.3. List of preassembled GB modules used in the assembly of plant gene expression vectors.

2.2.3 Cloning procedure

All cloning steps were performed according to developer's instructions by mixing the vectors, the proper restriction enzyme (BsaI or BsmBI), T4 DNA ligase and its buffer (Thermo Fisher Scientific) in a volume of 10 µL and performing 25 cycles of restriction/ligation reaction (37°C, 2 min / 16°C, 5 min). After each assembly, the ligation product was transformed into One Shot TOP10® *E. coli* cells via heat-shock, as specified by the manufacturer. These cells were then plated on low salt LB-agar *medium* (Duchefa Biochemie) supplemented with the appropriate selection antibiotic (50 µg ml^{-1} kanamycin for alpha vectors, 50 µg ml^{-1} spectinomycin for omega vectors, and 35 µg ml^{-1} chloramphenicol for pUPD2) and 40 mg/L of X-Gal (Duchefa Biochemie) to enable blue/white screening of positive clones. For each transformation event, three white colonies were propagated in liquid low salt LB *medium* supplemented with the appropriate antibiotic. Plasmid purification was conducted using the E.Z.N.A.® Plasmid Mini Kit I (Omega Bio-Tek), following the manufacturer's instructions. After each cloning step, the assembled vector was checked for the presence of the correct insert by digestion with two restriction enzymes and through PCR analysis using specific primers (Table 2.4). The identity

of the final constructs was confirmed by direct sequencing of the insert (Eurofins Genomics).

Target sequence	Primer name	5'- 3' sequence	Aim
Common primers			
pUPD2 vector	pUPD2-for	GCTTTCGCTAAGGATGATTTCTGG	a, b
	pUPD2-rev	CAGGGTGGTGACACCTTGCC	a, b
pDGB3 vector	pDGB3-for	GGTGGCAGGATATATTGTGG	a, b
	pDGB3-rev	GTTTTCAGATGACGGCTGCACT	a, b
KanR cassette	Kan-for	CAGAGTCCCGCTCAGAAGAACTCGTCA	a
	Kan-rev	GGAAGGGACTGGCTGCTATTGGGCGAA	a
Cas9 CDS	Cas9-for	CATCAGGGAGCAGGCAGAAA	a
	Cas9-rev	GGCTCAAAAGAACAGCA	a
CaMV 35S promoter	35S-for	AAGATGCCTCTGCCGACAGT	a
	35S-rev	TGACGCACAATCCCACTATC	a
Primers for SlTDC2 Knock-out			
SlTDC2 target1	target1-for	ATTGTACCACACGAATATTGCAT	a, c
	target1-rev	AAACATGCAATATTCGTGTGGTA	a, c
SlTDC2 target2	target2-for	ATTGCAGCGGAGCTAACAGTAGC	a, c
	target2-rev	AAACGCTACTGTTAGCTCCGCTG	a, c
Primers for SlTDC3 Knock-out			
SlTDC3 target1	target1-for	ATTGCTCAGTGCCGGGATTAACA	a, c
	target1-rev	AAACTGTTAATCCCGGCACTGAG	a, c
SlTDC3 target2	target2-for	ATTGTATCACATGACATGGCCAC	a, c
	target2-rev	AAACGTGGCCATGTCATGTGATA	a, c
Primers for SlT5H Knock-out			
SlT5H target1	target1-for	ATTGATGGAGGTGACCGATTATA	a, c
	target1-rev	AAACTATAATCGGTCACCTCCAT	a, c
SlT5H target2	target2-for	ATTGAGTGTACTGACGGAGACAC	a, c
	target2-rev	AAACGTGTCTCCGTCAGTACACT	a, c

Table 2.4. List of all primers used in the assembly of gene expression vectors. Legend: a, check of vector assembly by PCR; b, sequencing; c, cloning into pUPD2. All primers were purchased from Eurofins Genomics.

2.2.4. Agrobacterium tumefaciens transformation

Each assembled plant gene expression vector was used to transform *A. tumefaciens* EHA105 cells through the electroporation method. Putative transformed cells were plated on low salt LB-*agar medium* (Duchefa Biochemie) containing the appropriate selection antibiotic (50 mg L^{-1} rifampicin + 50 mg L^{-1} kanamycin or 50 mg L^{-1} spectinomycin for pDGB3_α or pDGB3_Ω vectors, respectively) and checked by colony-PCR to confirm the presence of the assembled vector using the primers listed in Table 2.4.

2.2.5 Assembly of the genetic construct to induce the overexpression of the gene SlT5H

The *SlT5H* CDS, previously isolated and functionally characterized by Commisso et al. (2022), was synthesized using the GenArt service from Thermo Fisher Scientific. According to the GB rules, after removing internal BsmBI recognition sites and adding the flanking adapter, the CDS was cloned into pUPD2 entry vector via BsmBI reaction. Subsequently, through a second cloning step using BsaI, the CDS was cloned into pDGB3_α2, together with the GB modules containing the 35S promoter, and the Tnos terminator (Table 2.3.). Finally, with a further cloning step using BsmBI, the assembled TU (P35S::SlT5H::Tnos) was cloned into pDGB3_Ω1 together with the GB module Pnos::*NptII*::Tnos (Table 2.3). The resulting plant expression vector pDGB3Ω1_Pnos::*NptII*::35S::*SlT5::*Tnos was then transformed into *A. tumefaciens* following the procedure described in the previous paragraph.

2.2.6 Design of single-guide RNAs for the CRISPR/Cas9 system

For each target gene, two single-guide RNAs (sgRNAs) were designed (Table 2.4), specifically targeting the upstream region of the coding sequence (CDS). The design of the guides used in this study was facilitated by the CRISPOR software (http://crispor.gi.ucsc.edu/). This tool supports over 150 genomes, including the latest tomato genome version (SL4.0), enabling the design of highly specific and efficient sgRNAs. The selection of the sgRNA was based on a series of criteria:

- The sgRNA should start with a G, which is a requirement associated with the use of the U6-26 *A. thaliana* promoter.
- The gene region targeted by Cas9 needs to be located in a structurally important region of the CDS.
- The chosen sgRNA should exhibit satisfactory on-target activity and ideally minimal off-target effects.

The on-target and off-target CFD score (Cutting Frequency Determination) available in CRISPOR when searching for gRNAs in a given sequence are calculated based on the algorithms developed by Doench et al. (2016). The CFD score considers the strength of the bond between the sgRNA and the target, the composition of the sgRNA, and the likelihood of off-target activity elsewhere in the genome. Furthermore, for each sgRNA, CRISPOR provides a list of potential off-targets, along with their coordinates within the tomato genome. In this study, only off-targets characterized by a high CFD score and those located within coding sequences or regulatory elements were selected for analysis.

2.2.7 Assembly of the genetic constructs for CRISPR/Cas9-mediated gene knockout

Selected sgRNAs were adapted to the GB cloning system using the "GB CRISPR domesticator" tool (https://gbcloning.upv.es/tools/crisprs/). This tool generates a 23-bp DNA sequence, corresponding to the sgRNA flanked by the GB adapters, that can be synthesized as complementary oligonucleotides and directly used in a cloning reaction (Figure 2.1). Briefly, the oligonucleotides corresponding to a sgRNA were diluted to a final concentration of 1 µM. Subsequently, 5 µl of each strand were mixed and let anneal at room temperature for 30 minutes before setting up the restriction-ligation reaction.

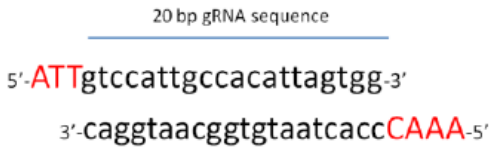

Figure 2.1. Schematic representation of the annealed 20 bp oligonucleotides containing the sgRNA sequence flanked by the GB adapters (in red).

The first cloning step involves the assembly of the U6-26 promoter from *A. thaliana* (GB part pUPD2_U626), one sgRNA (sgRNA1 or sgRNA2), and the scaffold RNA (GB part pUPD2_scRNA) to form a sgRNA transcriptional unit (sgRNA_TU). These elements were combined into an α-level pDGB3 vector through a single *BsaI* reaction. For each target gene, this procedure was repeated two times, creating two sgRNA_TUs: U626::sgRNA1::scRNA in pDGB3_α1, and U626::sgRNA2::scRNA in pDGB3_α2. Subsequently, through a BsmBI reaction these two modules were cloned together into pDGB3_Ω2 with the creation of the following construct pDGB3_Ω2-sgRNA1::sgRNA2. Concurrently, the GB parts PNos::*NptII*::TNos (pDGB3_α1), and P35S::*Cas9*::TNos (pDGB3_α2) were combined into pDGB3_Ω1 using *BsmBI*. Finally, the resulting vector pDGB3_Ω1-*NptII*::*Cas9* was combined with pDGB3_Ω2-sgRNA1::sgRNA2 using BsaI and pDGB3_α1 as destination vector. The final vector pDGB3_α1-*NptII*::*Cas9::* sgRNA1::sgRNA2 was transformed into *A. tumefaciens* as described in Section 2.2.4.

2.2.6. Preparation of CRISPR/Cas9 genetic construct for the simultaneous knockout of the three SlTDC iso-genes

By exploiting the modularity of the *Golden Braid* system, the vectors described in the previous paragraph were used to assemble the genetic constructs to obtain the simultaneous knockout of the three *SlTDC* genes. Briefly, the vectors pDGB3_Ω1-sgRNA1::sgRNA2-TDC2 and pDGB3_Ω2-sgRNA1::sgRNA2-TDC3 were clone together into pDGB3_α2 via BsaI reaction. The resulting vector pDGB3_α2-sgRNA1::sgRNA2-TDC2::sgRNA1::sgRNA2-TDC3 was combined with the vector pDGB3_α1-*NptII*::*Cas9*::sgRNA1::sgRNA2-*TDC1* using BsmBI and pDGB3_ Ω1 as destination vector. The final construct pDGB3_Ω1-*NptII*::*Cas9::sgRNAs-TDC1::sgRNAs-TDC2::sgRNA-TDC3* was transformed into *A. tumefaciens* as described in Section 2.2.4.

2.3. Plant stable genetic transformation and in-vitro regeneration

2.3.1 Agrobacterium tumefaciens-mediated stable genetic transformation of Micro-Tom and in-vitro regeneration of transgenic plants

All media used for the genetic transformation of Micro-Tom and for the *in-vitro* plant regeneration process were listed in Table 2.5. Wild-type Micro-Tom seeds (ID:TOMJPF00001) were sterilized, sowed on germination medium (Table 2.5) and placed in a growth chamber a 25°C for 8-10 days. The day before the transformation, 5 mm long hypocotyl and cotyledons explants obtained from germinated seedlings, were placed in Petri dishes containing solid KCMS *medium* (Table 2.5), and maintained in the dark at 25°C for 24 hours. Concurrently, a single colony of *A. tumefaciens* carrying the plasmid of interest was inoculated in 5 mL of liquid low salt LB *medium* and incubated for 24 hours in the dark at 28°C with horizontal shaking (210 rpm) until an OD_{600} of 1.2-1.5. The day after, the bacterial suspension was centrifuged at 3000 rpm for 15 minutes, and the pellet was resuspended in liquid KCMS (Table 2.5) to reach the optimal OD_{600} of 0.1. This infectant solution was sprinkled on the explants, previously moved from the KCMS-containing plates into empty Petry dishes. After 15 minutes, the solution was removed and the explants were placed back into the plates containing solid KCMS, and incubated for 48 hours in the dark at 25°C. Subsequently, the explants were transferred into new plates containing the RM1 *medium* (Table 2.5) supplemented with kanamycin (100 mgL^{-1}). After 2 weeks, only the callus-forming explants were moved to RM2 *medium* (Table 2.5) maintaining the kanamycin selective agent (100 mgL^{-1}); the RM2 *medium* was replaced every two weeks, until shoot emergence. Properly formed shoots were removed from the original callus and transferred into Magenta® boxes containing rooting *medium* (Table 2.5) supplemented with 75 mg L^{-1} kanamycin. After 3-4 weeks, rooted plantlets were moved into pots containing a mixture of soil, perlite, and sand (3:1:1) and maintained in acclimatation for one week at 25°C. After acclimatation, plants were grown in a growth chamber at 25°C with a 15h/9h light/dark photoperiod and let to set fruits.

	Germination medium	Solid KCMS	Liquid KCMS	Regeneration A	Regeneration B	Rooting medium
MS powder mix	2.2 g/L	4.4 g/L	4.4 g/L	4.4 g/L	4.4 g/L	2.2 g/L
Sucrose	15 g/L	20 g/L	21 g/L	30 g/L	31 g/L	10 g/L
Biotin	-	-	-	0,05 mg/L	0,05 mg/L	0,05 mg/L
Folic acid	-	-	-	0,5 mg/L	0,5 mg/L	0,5 mg/L
Glycine	-	-	-	2 mg/L	2 mg/L	2 mg/L
Myo-inositol	-	-	-	100 mg/L	100 mg/L	100 mg/L
Nicotinic acid	0,25 mg/L	-	-	5 mg/L	5 mg/L	5 mg/L
Pyridoxine	0,25 mg/L	-	-	0,5 mg/L	0,5 mg/L	0,5 mg/L
Thiamine	0,5 mg/L	0,9 mg/L	0,9 mg/L	0,5 mg/L	0,5 mg/L	0,5 mg/L
KH2PO4	-	200 mg/L	200 mg/L	-	-	-
Acetosyringone	-	40 mg/L	0,2 mg/L	-	-	-
Kinetin	-	0,1 mg/L	-	-	-	-
Zeatin riboside	-	-	-	2 mg/L	2 mg/L	-
Naftaleneacetic acid	-	-	-	0,01 mg/L	0,01 mg/L	-
Augmentin *	-			9 ml/L	5 ml/L	2,5 ml/L
Kanamycin	-	-	-	100 mg/L	101 mg/L	75 mg/L
Plant agar	7,5 g/L	7,5 g/L	-	8 g/L	8 g/L	4 g/L
Phytagel	-	-	-	-	-	3 g/L

*Table 2.5 Composition of the plant culture media used for genetic transformation of Micro-Tom and for in-vitro plant regeneration. * Augmentin (Glaxo Smith Kline, Brentford, UK) was prepared by dissolving the antibiotic powder (1g Amoxicillin/200mg Clavulanic acid) in 10 mL sterile water. All materials for in-vitro plant cultures were purchased by Duchefa (Haarlem, The Netherlands). All culture media were prepared at a pH of 5.8.*

2.3.2. Identification and selection of transgenic plants

Putative T_0 transgenic plants were tested by PCR analysis on their genomic DNA (gDNA) using primers designed to amplify the 5', and 3' regions of the T-DNA (Table 2.4). T1 seeds produced by confirmed transgenic plants were sowed in seeds trays containing a 3:1:1 mixture of soil, perlite, and sand. In order to select transgenic individuals, two weeks old plants underwent 5-day kanamycin spray treatment (300 mg L^{-1} kanamycin). Kanamycin resistant T_1 plants were checked for the presence of the T-DNA (as described for T_0 plants) and positive plants were selected for further molecular analysis.

2.4 Molecular biology

2.4.1 Extraction of genomic DNA

Genomic DNA (gDNA) was extracted from 100 mg of fresh leaf using the PureLink™ Plant Total DNA Purification Kit following the instructions provided by the manufacturer (Thermo Fisher Scientific).

2.4.2 Sequencing of putative knockout mutants

To characterize the editing events and the putative off-target sites T1 plants underwent sequencing analysis. For each target gene, specific primers (Tab 2.6) were designed to amplify the region targeted by the CRISPR/Cas9 system. The PCR reactions were performed using the Phusion™ High-Fidelity DNA Polymerases (Thermo Fisher Scientific) as specified by the manufacturer. Amplicons were checked by 2% agarose gel electrophoresis and purified using the GeneJET Gel Extraction and DNA Cleanup Micro Kit (Thermo Fisher Scientific) as specified by the manufacturer. Purified amplicons were sent to Eurofins genomics for SANGER sequencing analysis.

Target sequence	Primer name	5'- 3' sequence
Primers for the sequencing of the CRISPR/Cas9 target region		
SlTDC1 CDS	TDC1_Seq_F	AGCCCAACAAAATTGGCTGCT
	TDC1_Seq_R	TTAAAACACACTTTTTCTCAGCAAAC
SlTDC2 CDS	TDC2_Seq_F	TCCGTACCCAAGCCCATCAAAT
	TDC2_Seq_F	CAACCGAGTCGTATTCAGATCG
SlT5H CDS	T5H_Seq_F	GCACCGAACAGATTTTCACC
	T5H_Seq_R	CCTACCTTGTTGCATATGAACC
Primers for the sequencing of the off-target region		
SlT5H off-target site Solyc10g081240	Off-T_T5H_F	TGCAGTGCTCGGTCAAGTC
	Off-T_T5H_R	TCCCTTGCACTCCAGCAATAG

Table 2.6. List of primers used for the sequencing of the genes targeted by the CRISPR/Cas9 system, and for the characterization of the putative off-target sites.

2.4.3. RNA extraction and first strand cDNA synthesis

Total RNA was extracted from 100 mg of fresh tissue using the Spectrum™ Plant Total RNA Kit (Sigma-Aldrich). Purity of the extracted RNA was determined using the NanoDrop OneC spectrometer (Thermo Fisher Scientific), considering the following absorbance ratios: 1.8-2.2 (Abs_{260}/Abs_{280}); 1.7-2.2 (Abs_{260}/Abs_{230}). All RNA samples were treated with the Ambion® TURBO DNase (Life Technologies, Carlsbad, USA) to eliminate genomic DNA (gDNA) contamination. For each sample, 2 µg of total RNA were used for cDNA synthesis, using SuperScript III Reverse Transcriptase (Thermo Fisher Scientific) and oligo(dT)18 as primer (Eurofins Genomics). cDNA was tested by PCR using a primers pair designed to amplify a 100 bp region of the housekeeping *SlCAC* gene (*Solyc08g006960.2.1*) (González-Aguilera et al. 2016), and the resulting amplicons were visualized in 2% agarose gel electrophoresis. All reagents and kit were used according to the instructions provided by the manufacturers.

2.4.4. Gene expression analysis by quantitative real time-PCR

First strand cDNA was diluted 1:10 and used as template in quantitative Real-Time PCR (qRT-PCR) analysis to assess the expression levels of the *SlT5H* and *SlTDC1* genes using the constitutive *SlCAC* gene as calibrator. The primer used in this analysis were taken from the work of Commisso et al., (2022) and are listed in Table 2.7. Quantitative RT-PCR was performed with the StepOnePlus system (Applied Biosystems, Foster City - CA, USA) using the GoTaq®qPCR Master Mix (Promega, Madison-WI, USA) as specified by the manufacturer. The amplification conditions were set as follow: initial denaturation step of 95°C for 2 min followed by 40 cycles of denaturation at 95°C for 15 s, annealing at 60°C for 30 s and extension at 60°C for 30 s. The amplification process was followed by a melting curve analysis, ranging from 55°C to 95°C, with temperature increasing steps of 0.3°C every 15 s. The qRT-PCR analysis was carried out using the StepOnePlus system (Applied Biosystems, Foster City - CA, USA). To determine baseline and threshold cycles (Ct) values, raw data were processed through the LinRegPCR software. For each sample, transcript levels were expressed as MNE (mean

normalized expression) ± SD of three technical replicates, determined by comparing relative Ct values against the *SlCAC* reference gene, following the method described by Muller et al. (2002).

GOI	Primer name	5'-3' sequence	Tm (°C)	Amplicon (bp)
SlTDC1	RT-SlTDC1-for	CCACTTCCACTACAGCCGTCG	62.99	104
	RT-SlTDC1-rev	ACATGCGCTCCCTCCATAAGC	62.85	
SlT5H	RT-SlT5H-for	GGCCAAATTCCGACTCTAA	59.88	105
	RT-SlT5H-rev	TGAGCTGCAATGATTTGTGGA	59.24	
SlCAC	RT-SlCAC-for	GGGTTCGTTACATCACCAAAGC	62.48	121
	RT-SlCAC-rev	GTGCTGGTGTGATTGCATCC	62.85	

Table 2.7. List of primers used in quantitative Real-Time PCR analysis for the evaluation of gene expression levels.

2.5 Metabolomics

2.5.1 Metabolite extraction and sample preparation metabolomics analysis

For each sample, polar and medium polar metabolites extraction was performed on 100 mg of frozen powder with a variable volume of 100% methanol (LC-MS grade, Honeywell, Seezle, Germany): 0.5 mL (5:1 v/w) of 100% methanol for ripe fruits, leaves and roots; 1 mL of 100% methanol (10:1 v/w) for seeds. Briefly, after adding methanol the samples were mixed vigorously for 30 sec, sonicated at 40 KHz in an ultrasonic bath at 4° C for 15 min (Sonica® Ultrasonic Cleaner, SOLTEC) and centrifuged at 16000 rcf at 4°C for 15 min. The methanolic extracts were then recovered and stored at -80°C until the analysis. To ensure the generation of a proper signal for mass spectrometer detection, the optimal sample dilution and injection volume, for each type of tissue, were chosen through a preliminary UPLC-ESI-MS analysis, and were listed in Table 2.8. All the samples were differentially diluted in ultrapure water (LC-MS grade, Honeywell) according to the type of original matrix, filtered through 0.2 µm Minisart RC4 filters and introduced into the UPLC system.

Type of organ	Dilution	Injection volume (µl)
Root	2:3	10
Leaf	1:5	1
Ripe fruit (pulp + skin)	1:10	1
Seed	1:20	1

Figure 2.8. Dilutions and injection volume used in targeted metabolomics analysis.

2.5.2 Detection and relative quantification of tryptophan, tryptamine and serotonin by UPLC-ESI-MS

Samples were analyzed through an Acquity I Class UPLC system connected to a Xevo G2 Q-Tof mass spectrometer featuring an electrospray ionization (ESI) source operating in positive ionization mode and controlled by MassLynx v4.1 (Waters, Milford, MA, USA). Extracts were injected into a Waters Acquity UPLC BEH C18 column (2.1 mm x 100 mm, 1.7 µm) kept a 30°C. The mobile phase consisted of

0.1% formic acid in 100% ultrapure water as solvent A, and 100% acetonitrile as solvent B (LC-MS grade, Honeywell). The initial conditions were 99% A and 1% B, and the following elution profile was applied: 0-1 min., 1% B; 1-10 min., 1-40% B; 10-13.50 min., 40-70% B; 13.50-14.00 min., 70-99% B; 14.00-16.00 min., 99% B; 16.00-16.10 min., 99-1% B (initial conditions). Subsequently, the system was equilibrated in 99% A and the elution ended after 20 min. The flow rate was set to 0.350 mL/min. Samples were randomized and kept at 8°C for the entire analysis. In order of monitoring the UPLC-Q-ToF performance throughout the entire experiments, a quality control (QC) sample and a mix of authentic standards (MoS) were used. The QC was prepared by mixing each sample in equal volume, while the standards mix was made by mixing each standard at a known concentration. The list of authentic standards and their final concentration is reported in Table 2.9. QC and MoS were injected and analyzed every 9 samples. The ion flow parameters were set as follow: capillary voltage 0.8 kV, sampling cone voltage 40 V, source offset voltage 80 V, source temperature 120 °C, desolvation temperature 500 °C, cone gas flow rate 50 L/h and desolvation gas flow rate 1000 L/h. Nitrogen gas was used for the nebulizer and in desolvation whereas argon was used to induce collision-induced dissociation. An MS method was created to acquire data in continuum mode using a fixed collision energy in two scan functions. In function 1, the low energy was disabled, whereas in function 2 the high energy was set to 35 V. In both functions, the Xevo G2-XS was set to perform the analysis within the range 50–2000 *m/z* and with a scan time of 0.3 s. The lock mass solution used as "calibrator" to verify the accuracy of the mass spectrometer consisted of a 100 pg/µL leucine-enkephalin solution (Waters) injected with a flow rate of 10 µL/min, and generating a signal of 556.2771 in positive mode and 554.2615 in negative mode. Peak areas relative to tryptophan, TAM and SER signals were manually extrapolated using MassLynx, on the basis of the following m/z values, previously chosen after the analysis of commercial standards: 188.0699 for tryptophan; 160.0762 for serotonin; 144.0813 for tryptamine. These *m/z* values corresponded

to the highest in-source generated fragments detected in positive ionization mode.

Standard	Injected amount (ng)
Chlorogenic acid	1
Daidzein	
Naringenin	
Gallic acid	3
Quercetin	
dihydroartemisinic acid	
Phenylalanine	2

Table 2.9. List of commercial standards included in the standard mixture. For each molecule, the amount injected into the mass spectrometer is specified.

2.6 Statistical analysis

2.6.1 Statistical analysis of phenotypic data

The data obtained from phenotypic analyses were analyzed using two different types of statistical tests: the two-tailed Student's t-test and the one-way ANOVA test with multiple comparisons. In both tests, statistical significance was considered reliable for P values < 0.05. The two-tailed Student's t-test was performed in cases where the data collected from the analyzed genotypes were compared only with the negative control represented by the wild-type Micro-Tom genotype. Comparisons among genotypes (overexpressing, knockout, and wild-type) were performed using one-way ANOVA followed by Tukey's multiple comparisons test.

2.6.2 Statistical analysis of qRT-PCR analysis and metabolomics data

Gene expression and metabolite level data were analyzed using a two-tailed Student's t-test. Statistical significance was defined at P values < 0.05.

Chapter 3 – Results of Gene Expression Vector Assembly and Plant Stable Genetic Transformation

3.1 The CRISPR/Cas9 genome editing tool

The CRISPR/Cas9 system is a powerful genome editing tool that relies on the coordinated action of two main components: the Cas9 protein, a nuclease capable of introducing double-strand breaks (DSBs) into the genome, and a 20-nucleotides (20-nt) single-guide RNA (sgRNA), which directs Cas9 to a specific target sequence (Figure 3.1). Target recognition is achieved through the complementary pairing of the sgRNA with its target DNA sequence, along with the binding of Cas9 to a short, adjacent sequence known as the Protospacer Adjacent Motif (PAM). The PAM sequence is essential for the system's activity, and the Cas9 protein derived from *Streptococcus pyogenes* specifically recognizes the "NGG" PAM sequence.

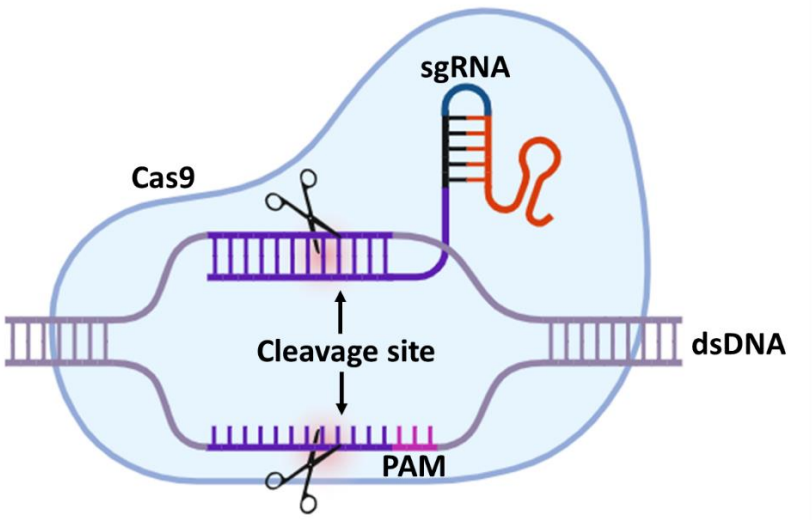

Figure 3.1. Schematic representation of the active Cas9/sgRNA ribonucleoprotein complex bound to a target sequence of genomic DNA (dsDNA). The image clearly shows the Cas9 protein, the sgRNA, and the cutting site on the genome, located 4 nucleotides away from the PAM sequence.

Following the introduction of a DSB, the cell predominantly repairs the damage via the Non-Homologous End Joining (NHEJ) pathway, an error-prone repair mechanism. This process often results in small insertions or deletions (Indels), which can induce frameshift mutations leading to the emergence of premature stop codons, ultimately resulting in the inactivation of the target gene (gene

knock-out). Consequently, when designing a gene knockout experiment using the CRISPR/Cas9 system, it is crucial for the sgRNA to target the 5' region of the gene of interest (GOI), ideally near the start codon (ATG), or at least within the first exons (Figure 3.2). This approach increases the chances of producing a truncated, non-functional protein following the introduction of a premature stop codon. Furthermore, to enhance the efficiency of genome editing, the simultaneous use of multiple sgRNAs targeting the same gene has been widely adopted (Figure 3.2). This strategy not only increases the likelihood of generating knockout mutations but also mitigates potential inefficiencies associated with individual sgRNAs.

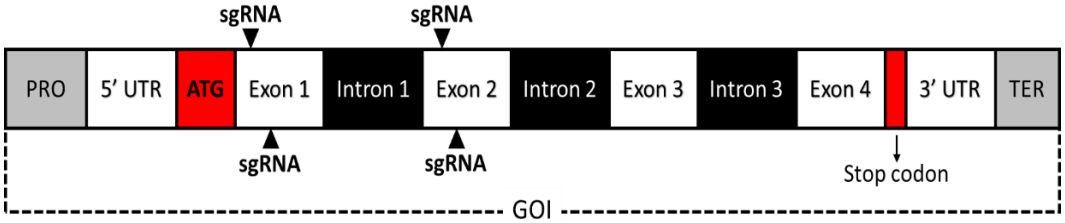

Figure 3.2. Schematic representation of a eukaryotic gene highlighting the first two exons as optimal regions for designing sgRNAs to knockout the gene of interest (GOI). Image legend: PRO, promoter; 5' UTR, 5' untranslated region; ATG, translation start codon; sgRNA, single guide RNA; 3' UTR, 3' untranslated region; TER, terminator.

3.2 CRISPOR software facilitates the identification of multiple RNA guides for each target gene

The CRISPOR software was used to design the sgRNAs necessary for inducing knockouts of the genes *SlTDC1* (Solyc07g054860), *SlTDC2* (Solyc07g054280), *SlTDC3* (Solyc09g064430), and *SlT5H* (Solyc09g014900). For each gene, two sgRNAs targeting the upstream region of the coding sequence (CDS) were selected based on the CFD score (Cutting Frequency Determination) assigned by the software, with higher scores indicating greater specificity and efficiency. The CFD score ranges from 0 to 100, where values above 50 are considered indicative of an efficient and highly specific guide. This score is calculated using an algorithm developed by Doench et al. (2016), which takes into account various parameters, including the number of potential off-target sites and the theoretical cutting efficiency associated with each guide. The selected guides, along with their corresponding target genes and CFD scores, are detailed in Table 3.1.

Target gene	Gene ID	Guide RNA (5'- 3' sequence)	CFD score
SlTDC1	Solyc07g054860	GGTTCTAAGCCAAGTCGAAC	98
		GTTAGTTCCGCAGCGTTCAT	99
SlTDC2	Solyc07g054280	GCAGCGGAGCTAACAGTAGC	99
		GTACCACACGAATATTGCAT	97
SlTDC3	Solyc09g064430	GCTCAGTGCCGGGATTAACA	99
		GTATCACATGACATGGCCAC	99
SlT5H	Solyc09g014900	GATGGAGGTGACCGATTATA	99
		GAGTGTACTGACGGAGACAC	100

Table 3.1. List of target genes for the CRISPR/Cas9 system. For each gene, two sgRNAs selected via CRISPOR software are listed, together with their corresponding CFD scores indicating predicted cleavage efficiency.

For each guide, the software provides a list of potential off-target sites along with their positions in the genome. Each off-target site is associated with a CFD off-target score, calculated using the same algorithm employed for guide design. The

CFD off-target scores range from 0 to 1, where a lower score indicates a reduced likelihood of the off-target event occurring. Only off-target sites corresponding to coding sequences or regulatory regions with a CFD off-target score of 0.1 or higher were annotated. Table 3.2 lists the putative off-target sites identified for each guide, along with their genomic reference (gene ID) and CFD off-target scores. As shown in Tables 3.1 and 3.2, one of the off-targets associated with the sgRNA 1 targeting the *SlTDC2* gene (Solyc07g054280) is the *SlTDC1* gene (Solyc07g054860). This was expected, as both genes belong to the same family and share a high degree of homology, complicating the design of highly specific guides. All off-target sites listed in the table have been selected in order to proceed with their characterization through sequencing analysis.

Target gene	Guide RNA	Off-target ID	Genetic element	CFD off-target score
SlTDC1	1	Solyc03g093620	exon	0.1
SlTDC2	1	Solyc07g054860	exon	0.45
		Solyc06g008850	exon	0.12
	2	Solyc04g072170	exon	0.18
		Solyc10g018500	exon	0.15
SlTDC3	2	Solyc06g005860	exon	0.24
SlT5H	1	Solyc10g081240	exon	0.24

Table 3.2. List of potential off-target sites associated with the sgRNAs selected to knockout the target genes. The off-target site Solyc07g054860, associated with sgRNA1 targeting the SlTDC2 gene, corresponds to the SlTDC1 gene.

3.3 Assembly of the plant gene expression vectors

A total of four plant gene expression vectors were assembled using the *Golden Braid* cloning system (Table 3.3).

GB backbone	Assembled T-DNA	Vector aim
pDGB3Ω1	*NptII*::*SlT5H*	*SlT5H* overexpression
pDGB3α1	*NptII*::*hCas9*::sgRNA1/2-*SlT5H*	Knockout of *SlT5H*
pDGB3α1	*NptII*::*hCas9*::sgRNA1/2-*SlTDC2*	Knockout of *SlTDC2*
pDGB3Ω1	*NptII*::*hCas9*::*SlTDC1*::*SlTDC2*::*SlTDC3*	Knockout of *SlTDC1*, *SlTDC2*, and *SlTDC3*

Table 3.3. List of the assembled plant gene expression vectors with a brief description of their function.

In Figure 3.3, the T-DNA of the genetic construct assembled to induce the overexpression of the *SlT5H* gene is represented. This construct consists of two elements: the kanamycin resistance gene *NptII* (*neomycin phosphotransferase*), which is necessary for the selection of transformed plants, and the *SlT5H* CDS under the control of the constitutive 35S promoter.

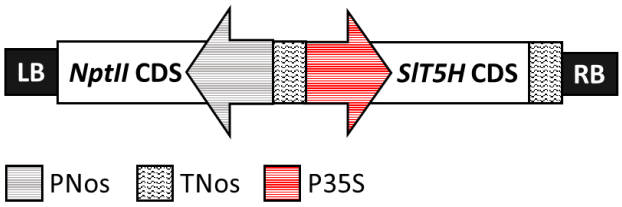

Figure 3.3. Schematic representation of the T-DNA assembled to induce overexpression of the SlT5H gene. Image legend: LB, left T-DNA border; RB, right T-DNA border; Pnos, nopaline synthase promoter; Tnos, nopaline synthase terminator; P35S, cauliflower mosaic virus 35S promoter; NptII, neomycin phosphotransferase CDS conferring kanamycin resistance in plants; SlT5H, S. lycopersicum tryptamine 5-hydroxylase gene.

In Figure 3.4, the T-DNAs assembled to induce the knockout of the *SlT5H* gene, the *SlTDC2* gene, and the three *SlTDC* isogenes are represented. Each construct contains the kanamycin resistance gene *NptII*, the coding sequence of *human Cas9* under the control of the constitutive 35S promoter, and the transcriptional units necessary for the synthesis of the sgRNAs. The construct designed to induce the simultaneous knockout of the three *SlTDC* genes contains six transcriptional units

for the synthesis of sgRNAs targeting the *SlTDC1*, *SlTDC2*, and *SlTDC3* genes, respectively.

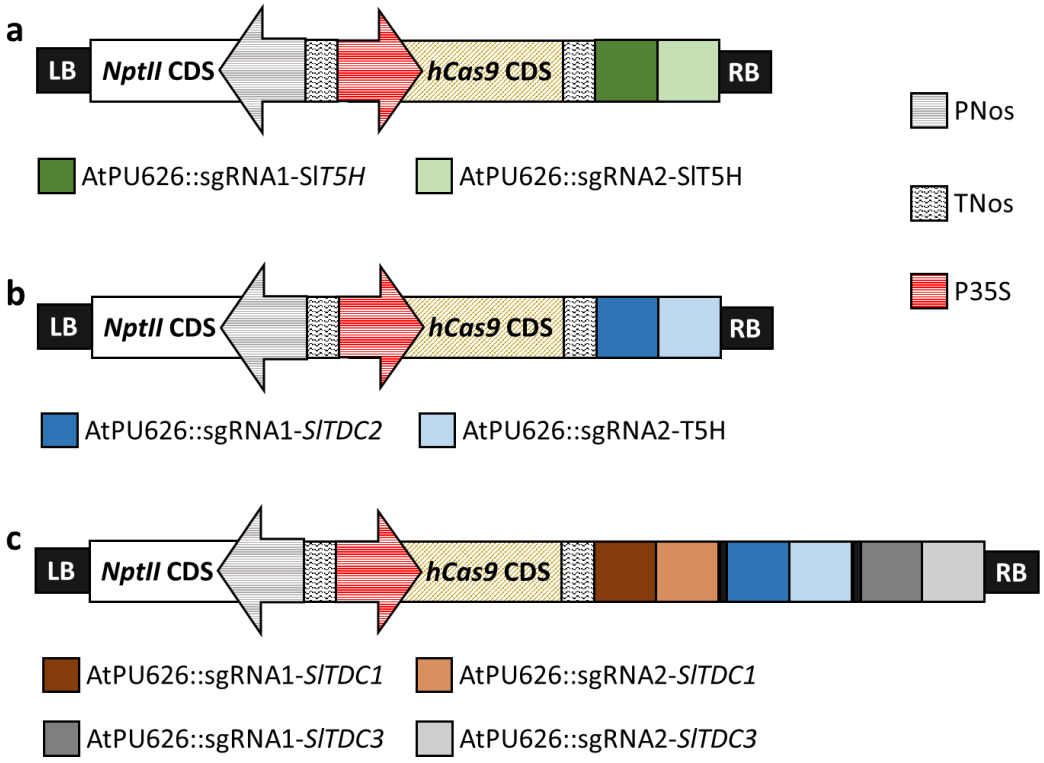

Figure 3.4. Schematic representation of the CRISPR/Cas9 genetic constructs assembled to knockout the SlT5H gene (a), the SlTDC2 gene (b), and the three SlTDC isogenes (c), respectively. Vector legend: LB, left T-DNA border; RB, right T-DNA border; NptII, plant optimized neomycin phosphotranspherase gene conferring resistance to kanamycin; Pnos, Nopaline synthase promoter; Tnos, Nopaline synthase terminator; P35S, CaMV 35S promoter; AtU626, A. thaliana U6-26 promoter; hCas9, human cas9 CDS; sgRNA, single-guide RNA. Each colored square represents a sgRNA transcriptional unit (TU).

3.4 Genetic transformation of Micro-Tom results in the generation of multiple transgenic lines for each genetic construct

All assembled plant gene expression vectors were used to perform stable genetic transformation of *S. lycopersicum* cv. Micro-Tom plants via *A. tumefaciens*. Explants, including both cotyledons and hypocotyls, were *in-vitro* regenerated via callus formation followed by direct organogenesis to produce T0 plants. Following the regeneration process on kanamycin-selective media, the plants were transferred to rooting medium containing kanamycin, where they were maintained until a proper root system was developed. The rooted seedlings were then transferred to a growth chamber where they remained until the end of their life cycle. The following putative T0 lines were obtained: 45 plants putatively transformed with the construct for the overexpression of the *SlT5H* gene; 20 plants putatively transformed with the construct for the knockout of the *SlT5H* gene; 35 plants putatively transformed with the construct for knockout of the *SlTDC2* gene; and 53 plant putatively transformed with the construct for simultaneous knockout of the three *SlTDC* genes. The transgenic state of T0 plants was evaluated by PCR on their gDNA using the same primer pairs employed to confirm the identity of the assembled plant gene expression vectors (Chapter 2, Table 2.4). These primers were specifically designed to amplify the 5' and 3' regions of the T-DNA adjacent to the left border (LB) and right border (RB), respectively, as depicted in Figure 3.5. After the PCR analysis, the following transgenic lines were identified: 28 T0 lines transformed with the construct for overexpressing the *SlT5H* gene; five T0 lines harboring the construct to induce the knockout of the *SlT5H* gene; 18 T0 lines transformed with the construct to obtain the knockout of the *SlTDC2* gene. The screening of the T0 lines transformed with the construct to induce the simultaneous knockout of the three *SlTDC*s, is currently ongoing; however, 18 T0 lines have been identified so far.

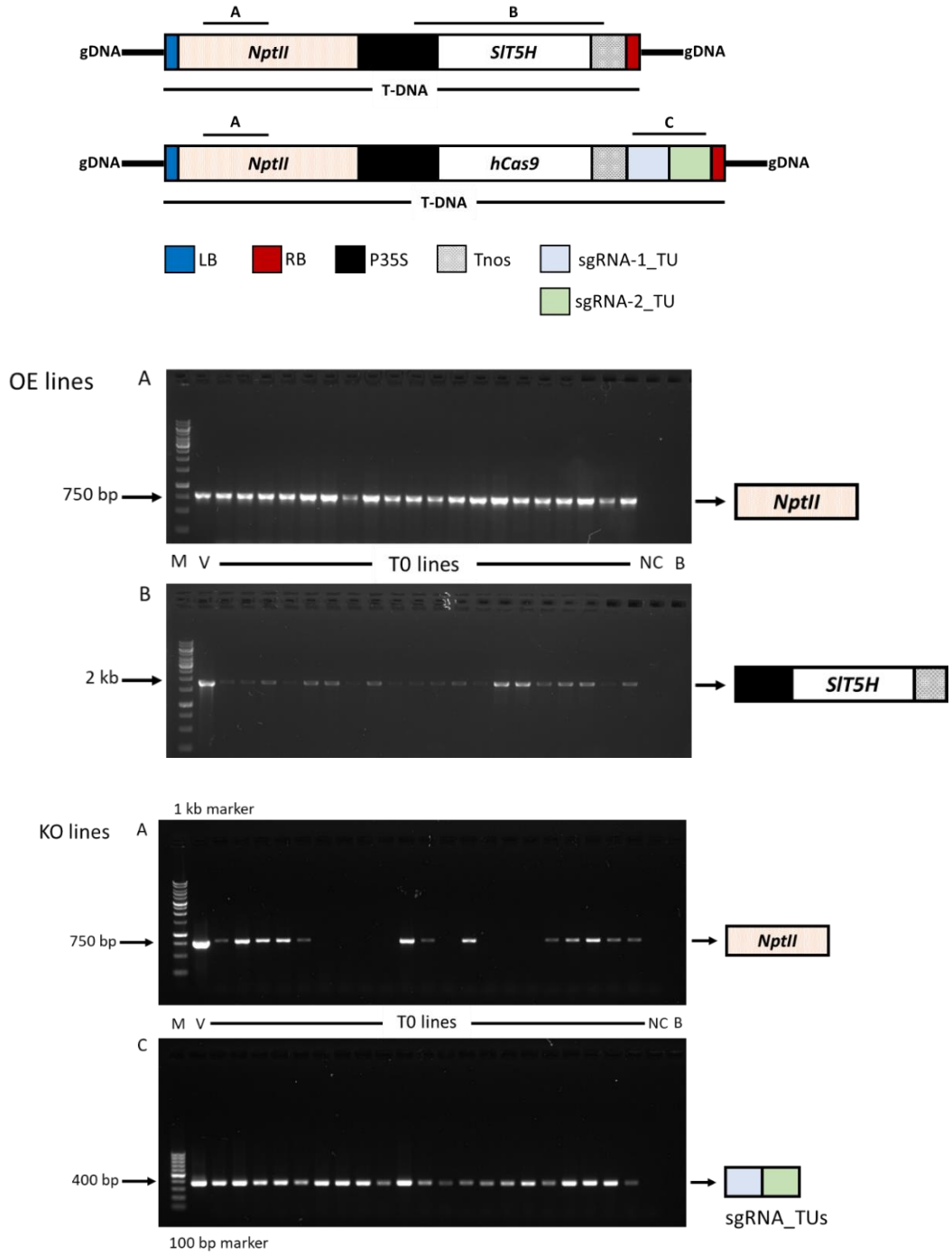

Figure 3.5. Schematic representation of the T-DNA regions assembled to perform the overexpression of the SlT5H gene (top) and the single knockout of the target genes (bottom). The letters A-C represent the T-DNA regions amplified via PCR using specific primers (Chapter 2, Table 2.4) to check for the presence of the T-DNA insert in the genome of the T0 plants: A: NptII-for/NptII-rev, 795 bp; B: 35S-for/Tnos-rev, 2 kb; C: sgRNA1-for/sgRNA2-rev, 372 bp. Vector legend: LB and RB, left and right T-DNA borders; NptII, plant-optimized Neomycin phosphotransferase gene conferring resistance to kanamycin; P35S, CaMV 35S promoter; Tnos, Nopaline synthase terminator; sgRNA_TU, single-guide RNA transcriptional units. PCR legend: M, molecular marker; V, assembled vector used as positive control; NC, negative control (gDNA from wild-type Micro-Tom); B, blank.

3.5 Selection of *SlTDC2* knockout mutants

The T1 progeny, derived from the 18 T0 lines positively transformed with the construct designed to knock out the *SlTDC2* gene, were analyzed to characterize editing events at the *SlTDC2* locus through sequencing analysis. Genomic DNA from two-week-old T1 plantlets was amplified using a pair of primers specifically designed to target the region of the *SlTDC2* gene encompassing the recognition sites of the two sgRNAs (Figure 3.6).

ATGGGAACCCTTAATTCAAATAACAACCCTCAAACCCAATCCAACTTCCCAAAATTCAACCCGCTTGA
CCCGGAAGAATTCCGTACCCAAGCCCATCAAATGGTGGACTTCATTGCTGATTACTACAAGAATATTG
AGTCCTACCCGGTTCTAAGTCAAGTCGAACCCGGTTATCTTCGTACCCAATTACCCGAAAACGCCCCT
AATCGACCCGAATCATTCGATTTAATTATGAAAGATGTCCAAAACCATATTATCCCGGGTATGACCCA
TTGGCTAAGCCCGAATTTCTTCGCATTTTTTCCAGCTACTGTTAGCTCCGCTGCGTTTCTAGGTGAAA
TGCTTTGCAATTGTTTCAACTCCGTCGGATTTAATTGGCTGGCTTCGCCAGCCATGACGGAGTTGGAA
ATGGTAGTCATGGACTGGCTTGCTAATACGTTGAAATTACCAAAAACTTTCATGTTTTCTGGCACGGG
TGGTGGTGTACTACAAAGTACAACTAGTGAAGCTATACTGTGTACGTTAATCGCTGCGCGTGATCATA
AGATCGAGAATATAGGTGTTGATGAGATAGGAAAATTTGTAGTCTACGGTTCTGATCAAACTCACTCT
ACTTATAGCAAAGCCTGCAAGGTAGCTGGTATTTTCCCATGCAATATTCGTGTGGTACCAACTTGTAT
TGAAAGCGATTTCGCTTTATCTCCTCTAGCACTACGTGGAATTATTGAAGCTGATGTTGCTGCTGGAC
TGGTCCCACTTTTCCTCTGTGCTACCGTTGGGACCACTTCCACAACAGCAGTTGATCCTCTCAGCCAG
CTGGGTCAGCTGGCTGAGGAATTCAATATTTGGTTCCACGTGGACGCTGCTTATGGAGGTAGCGCGTG
TATATGTCCAGAGTTTAGACAATATCTGGACGGAGTCGAACTAGCGGACTCGTTAAGCCTAAGCCCAC
ATAAGTGGCTATTAAGTTACTTAGATTGTTGTTGTATGTGGGTGAAAGAACCAAACGTGTTAGTGAAG
ACATTGAGCACGAATCCCGAGTACTTACGTAATAAACGATCTGAATACGACTCGGTTGTTGATTATAA
AGACTGGCAAATCGGTACGGGACGAAAGTTCAAGTCTCTCCGATTATGGTTCGTCATGCGTACTTATG
GCGTAGACAATC

Figure 3.6. Sequence of the SlTDC2 gene. The start codon for translation, ATG, is highlighted in red; the pair of primers used for amplifying the gene region containing the guides is highlighted in green; and sgRNA1 and sgRNA2 are highlighted in blue and gray, respectively.

The resulting amplicons were subsequently purified and sent to Eurofins Genomics for SANGER sequencing. Of the 12 lines analyzed so far, five were found to lack mutations in the regions associated with either sgRNA1 or sgRNA2 (Figure 3.7). Conversely, the remaining six lines exhibited various editing events at the sgRNA1 target site, while only four of these lines also displayed mutations at the sgRNA2 target site.

Regarding the editing events at the sgRNA1 target site:

- Line 28: Homozygous mutant with a 1 bp insertion (thymine, T).
- Line 10: Heterozygous biallelic mutant with a 1 bp insertion (adenine, A) in one allele and a 3 bp deletion in the other.
- Line 13: Heterozygous biallelic mutant with two different 1 bp insertions, a T in one allele and a C (cytosine) in the other.
- Line 30: Heterozygous biallelic mutant with two different 1 bp insertions (A and T).
- Line 12: Heterozygous mutant with a 1 bp insertion (thymine, T) in one allele and no mutation in the other.
- Line 35: Heterozygous mutant with a 1 bp deletion (adenine, A) in one allele and no mutation in the other.

Regarding the editing events at the sgRNA2 target site:

- Line 13: Homozygous mutant with a 1 bp insertion (adenine, A) in both alleles.
- Line 28: Homozygous mutant with a 1 bp insertion (thymine, T) in both alleles.
- Line 12: Heterozygous mutant with a 3 bp deletion in one allele and no mutation in the other.
- Line 30: Heterozygous biallelic mutant with two different 1 bp insertions, an adenine (A) in one allele and a cytosine (C) in the other.

The nucleotide sequences obtained from the homozygous mutant (line 28) and the biallelic mutants (lines 13 and 30) were subjected to in silico translation. The analysis revealed that the mutations at the *SlTDC2* locus, corresponding to the sgRNA1 target site, resulted in the formation of a premature stop codon in all three genotypes. Alignment with the wild-type amino acid sequence confirmed premature termination of the SlTDC2 protein in all three genotypes (Figure 3.8). The sequencing of the theoretical off-target sites for the three confirmed knockout lines (lines 13, 28, and 30) is currently underway.

```
SlTDC2_WT          GGCTAAGCCCGAATTTCTTCGCATTTTTTCCAGCT-ACTGTTAGCTCCGCTGCGTTTCTAGGTGAAA  340
KO_10-allele1      GGCTAAGCCCGAATTTCTTCGCATTTTTTCCAGCTAACTGTTAGCTCCGCTGCGTTTCTAGGTGAAA  341
KO_10-allele1      GGCTAAGCCCGAATTTCTTCGCATTTTTTCCAGCT----GTTAGCTCCGCTGCGTTTCTAGGTGAAA  338
KO_12-allele1      GGCTAAGCCCGAATTTCTTCGCATTTTTTCCAGCT-ACTGTTAGCTCCGCTGCGTTTCTAGGTGAAA  340
KO_12-allele2      GGCTAAGCCCGAATTTCTTCGCATTTTTTCCAGCTTACTGTTAGCTCCGCTGCGTTTCTAGGTGAAA  341
KO_13-allele1      GGCTAAGCCCGAATTTCTTCGCATTTTTTCCAGCTTACTGTTAGCTCCGCTGCGTTTCTAGGTGAAA  341
KO_13-allele2      GGCTAAGCCCGAATTTCTTCGCATTTTTTCCAGCTCACTGTTAGCTCCGCTGCGTTTCTAGGTGAAA  341
KO_28-homozygous   GGCTAAGCCCGAATTTCTTCGCATTTTTTCCAGCTTACTGTTAGCTCCGCTGCGTTTCTAGGTGAAA  341
KO_30-allele1      GGCTAAGCCCGAATTTCTTCGCATTTTTTCCAGCTAACTGTTAGCTCCGCTGCGTTTCTAGGTGAAA  341
KO_30-allele1      GGCTAAGCCCGAATTTCTTCGCATTTTTTCCAGCTTACTGTTAGCTCCGCTGCGTTTCTAGGTGAAA  341
KO_35-allele1      GGCTAAGCCCGAATTTCTTCGCATTTTTTCCAGCTAACTGTTAGCTCCGCTGCGTTTCTAGGTGAAA  341
KO_35-allele1      GGCTAAGCCCGAATTTCTTCGCATTTTTTCCAGCT-ACTGTTAGCTCCGCTGCGTTTCTAGGTGAAA  340
                   **********************************    ****************************
```

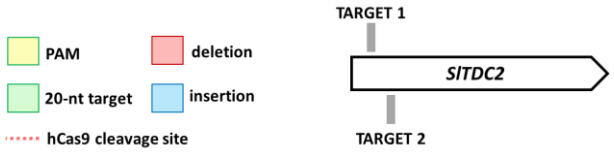


```
SlTDC2_WT          CAAAGCCTGCAAGGTAGCTGGTATTTTCCCATG-CAATATTCGTGTGGTACCAACTTGTATTGAA  729
KO_12-allele1      CAAAGCCTGCAAGGTAGCTGGTATTTTCCCATG-CAATATTCGTGTGGTACCAACTTGTATTGAA  729
KO_12-allele2      CAAAGCCTGCAAGGTAGCTGGTATTTTCCCATG----TATTCGTGTGGTACCAACTTGTATTGAA  726
KO_13-homozygous   CAAAGCCTGCAAGGTAGCTGGTATTTTCCCATGACAATATTCGTGTGGTACCAACTTGTATTGAA  730
KO_28-homozygous   CAAAGCCTGCAAGGTAGCTGGTATTTTCCCATGTCAATATTCGTGTGGTACCAACTTGTATTGAA  730
KO_30-allele1      CAAAGCCTGCAAGGTAGCTGGTATTTTCCCATGACAATATTCGTGTGGTACCAACTTGTATTGAA  730
KO_30-allele2      CAAAGCCTGCAAGGTAGCTGGTATTTTCCCATGCCAATATTCGTGTGGTACCAACTTGTATTGAA  730
                   **********************************    ****************************
```

Figure 3.7. The top image shows the results of the alignments of the sequences obtained from the T1 SlTDC2-knockout mutants against the SlTDC2 sequence of the wild-type Micro-Tom genotype, related to the site recognized by sgRNA1 (target 1); the bottom image presents the alignments related to the site of the SlTDC2 gene recognized by sgRNA2 (target 2). Legend: the PAM (protospacer adjacent motif) sequence is highlighted in yellow; the sequence of the SlTDC2 gene recognized by the sgRNAs is highlighted in green; deletions resulting from the editing event are highlighted in red; and insertions occurring as a result of the editing event are shown in blue

```
SlTDC2             MGTLNSNNNPQTQSNFPKFNPLDPEEFRTQAHQMVDFIADYYKNIESYPVLSQVEPGYLR   60
SlTDC2_KO13        MGTLNSNNNPQTQSNFPKFNPLDPEEFRTQAHQMVDFIADYYKNIESYPVLSQVEPGYLR   60
SlTDC2_KO28        MGTLNSNNNPQTQSNFPKFNPLDPEEFRTQAHQMVDFIADYYKNIESYPVLSQVEPGYLR   60
SlTDC2_KO30        MGTLNSNNNPQTQSNFPKFNPLDPEEFRTQAHQMVDFIADYYKNIESYPVLSQVEPGYLR   60
                   ************************************************************

SlTDC2             TQLPENAPNRPESFDLIMKDVQNHIIPGMTHWLSPNFFAFFPATVSSAAFLGEMLCNCFN  120
SlTDC2_KO13        TQLPENAPNRPESFDLIMKDVQNHIIPGMTHWLSPNFFAFFPAHC---------------  105
SlTDC2_KO28        TQLPENAPNRPESFDLIMKDVQNHIIPGMTHWLSPNFFAFFPAYC---------------  105
SlTDC2_KO30        TQLPENAPNRPESFDLIMKDVQNHIIPGMTHWLSPNFFAFFPLLA---------------  105
                   ****************************************
```

Figure 3.8. Alignment of the amino acid sequences of SlTDC2 protein with the truncated products derived from in-silico translation of the selected SlTD2-knockout mutants.

3.6 Selection of *SlT5H* knockout mutants

Among the five T0 plants transformed with the construct designed to knock out the *SlT5H* gene, two produced parthenocarpic fruits, making it impossible to obtain the seeds of T1 progeny. The remaining three lines successfully generated T1 progeny, which were subsequently used to characterize the editing events through sequencing analysis, as described in the previous paragraph for the *SlTDC2*-knockout mutants. Briefly, gDNA from two-week-old T1 plantlets was PCR-amplified with a primer pair designed to amplify the region of the *SlT5H* gene encompassing the sites recognized by the two sgRNAs. The resulting amplicons were purified and sent to Eurofins Genomics for sequencing. All three analyzed lines were identified as homozygous mutants, each exhibiting different types of mutations at the site targeted by sgRNA1 (Figure 3.9). Specifically, line 1 displayed a 1 bp insertion (adenine, A), while line 2 showed a 3 bp deletion. No editing events were detected at the sgRNA2 target site for these two lines. Interestingly, line 3 exhibited a 496 bp deletion, corresponding precisely to the region of the gene located between the two sgRNAs. The *in-silico* translation of the nucleotide sequences corresponding to the three mutated versions of the *SlT5H* gene revealed the presence of a premature stop codon, resulting in truncation of the amino acid sequence (Figure 3.10). This finding was confirmed by aligning the wild-type amino acid sequence of the SlT5H enzyme with those derived from the three edited *SlT5H*-knockout mutants. Sequencing of the off-target region Solyc10g081240, identified using the CRISPOR software during the sgRNA design, revealed the absence of off-target events in all three analyzed lines (data not shown). These three *SlT5H*-knockout lines (*slt5h*-1, *slt5h*-2, and *slt5h*-3) were then selected for subsequent phenotypic and molecular analyses.

Figure 3.9. The alignments of the wild-type SlT5H sequence with the mutated versions identified in the SlT5H-KO_1 and SlT5H-KO_2 mutants are shown in image (a). For these two lines, no mutations were detected at the site recognized by sgRNA2 (target 2). Image (b) presents the alignment of the wild-type SlT5H sequence with the mutated version found in the SlT5H-KO_3 line. In this case, a deletion of 496 bp occurred, extending from the site recognized by sgRNA1 (target 1) to the recognition site of sgRNA2 (target 2). Legend: the PAM (protospacer adjacent motif) sequence is highlighted in yellow; the sequence of the SlTDC2 gene recognized by the sgRNAs is highlighted in green; deletions resulting from the editing event are highlighted in red; and insertions occurring as a result of the editing event are shown in blue.

```
SlT5H          MEASILQLLLLLSLTSCTILFYKIRGRWRRRPPSPPSLPIIGHLHLLNQMPHHTFFNLSQ   60
SlT5H_KO1      MEASILQLLLLLSLTSCTILFYKIRGRWRRRPPSPPSLPIN-------------------   41
SlT5H_KO2      MEASILQLLLLLSLTSCTILFYKIRGRWRRRPPSPPSLPIV-------------------   41
SlT5H_KO3      MEASILQLLLLLSLTSCTILFYKIRGRWRRRPPSPPSLPIT-------------------   41

SlT5H          KLGKIIYLQLGQIPTLIISSPRLAELILKTNDHIFCSRPQIIAAQYLSFGCSDITFSPYG  120
SlT5H_KO1      ---------RSPPSPQPNASSHLLQSISKTRKNYLSSTRPNSDSNHLISSSS--------   84
SlT5H_KO2      ---------TSISSTKCLITPSSIYLKNSEKLSIFNSAKFRL------------------   74
SlT5H_KO3      ---------GVVSWVLFWGFFSRF-----------------------------------   56
```

Figure 3.10. Alignment of the amino acid sequences of SlT5H protein with the truncated products derived from the in-silico translation of the selected SlT5H-knockout mutants.

3.7 Selection of *SlT5H*-overexpressing genotypes characterized by the highest levels of *SlT5H* expression

The T1 progeny, from the confirmed transgenic plants transformed with the construct to induce the overexpression of the *SlT5H* gene was used to determine the expression levels of the *SlT5H* gene. Two-week-old plantlets were subjected to a five-day treatment with kanamycin (300 mg L^{-1}) administered as foliar spray. At the end of the treatment, nine T1 kanamycin-resistant plants, each representing and independent T0 genotype, were selected. For each of these lines, total RNA was extracted from a pool of basal, medial, and apical leaves. The RNA was used to produce cDNA, which served as a template in qRT-PCR analysis to assess the relative transcript levels of *SlT5H* and *SlCAC*. The latter is the tomato housekeeping gene used as a calibrator to calculate the Mean Normalized Expression (MNE). The qRT-PCR analysis revealed that, compared to the control, the expression levels of *SlT5H* were higher in all nine analyzed lines (Figure 3.11). Subsequently, lines 2, 3, 7, and 9 were selected for further phenotypic and molecular analyses.

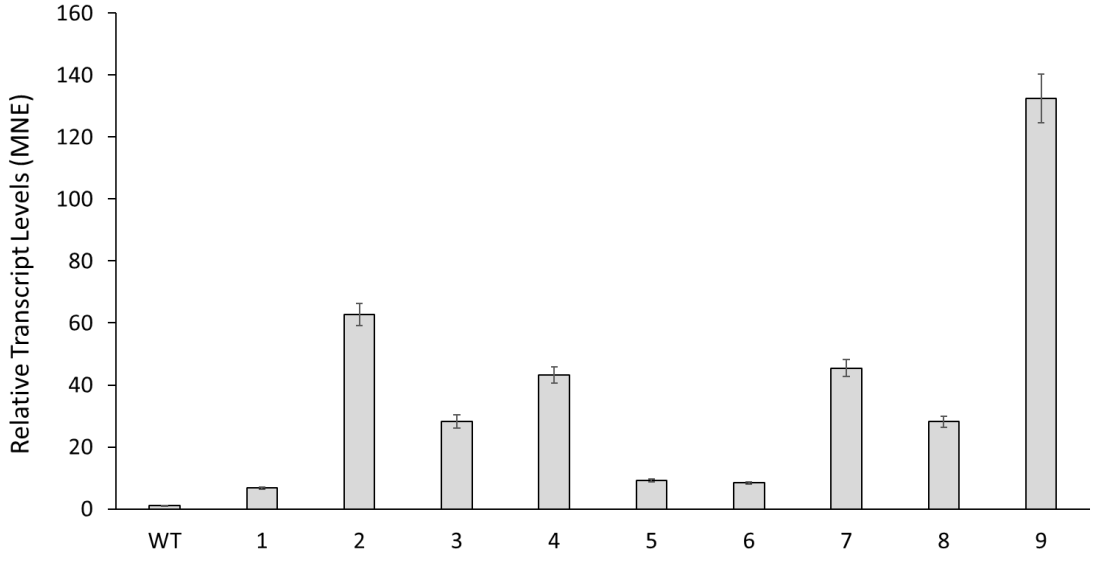

Figure 3.11. Expression levels of SlT5H in Micro-Tom transgenic overexpressing lines (T1) detected by qRT-PCR analysis. Bars represent standard error (n=3; technical replicates).

Chapter 4 - Phenotypic and Molecular Characterization of *SlTDC1*-overexpressing and *SlTDC1*-knockout Lines

4.1. Experimental workflow of phenotypic and molecular analysis

To investigate the biological roles of tryptamine (TAM) and serotonin (SER) in *S. lycopersicum* cv. Micro-Tom, three independent *SlTDC1*-overexpressing lines (*SlTDC1*-OE) and three independent *SlTDC1*-knockout lines (*sltdc1*) were generated in our laboratory (Negri et al., 2020). This chapter presents the results of the phenotypic and molecular characterization of these engineered tomato lines. Sections 4.2 and 4.3 describe the results of two independent phenotyping experiments conducted on the *SlTDC1*-OE and s*ltdc1* lines, respectively. The phenotypic traits related to vegetative and reproductive development described in table 4.1 were assessed by analyzing 9–16 plants per genotype. At the end of these experiments, roots, true leaves, and deseeded ripe fruits were subjected to LC-MS analysis to quantify the relative levels of tryptophan, TAM, and SER. For the *SlTDC1*-OE lines, these organs were also used to measure the expression levels of *SlTDC1* and *SlT5H* genes via qRT-PCR. While no significant differences were observed in vegetative development, notable variations were detected in the reproductive performance of the s*ltdc1* lines compared to the wild-type control. Consequently, a third phenotyping experiment, described in Section 4.4, was conducted to examine in more detail the reproductive phase in both *SlTDC1*-OE and s*ltdc1* lines. In this experiment, overexpressing and knockout lines were analyzed together. To ensure proper plant management and robust data collection, the number of individuals per genotype was reduced to five. The three phenotyping experiments described in Section 4.2, 4.3, and 4.4 were carried out in a greenhouse under consistent environmental conditions, using the same filial generation (T2). Finally, a germination test was performed on T3 seeds derived from *SlTDC1*-OE and *sltdc1* lines. The results of this test, along with LC-MS data quantifying tryptophan, TAM, and SER levels in the seeds, are detailed in Section 4.6 and 4.7.

4.2 *SlTDC1*-OE lines with altered TAM and SER levels are characterized by a reduced seed germinability

The *SlTDC1*-OE lines were evaluated based on the parameters listed in Table 4.1 and compared to the wild-type Micro-Tom genotype.

Measured phenotypic parameter
Vegetative phase
Number of germinated plants (germination percentage)
Number of true leaves before the inflorescence meristem
Epicotyl length measured at 60 days post germination (dpg)
Length of the first six internodes at 60 dpg
Length (longitudinal axis) of the first seven true leaves at 60 dpg
Leaf morphology
Flower morphology (at anthesis)
Reproductive phase
Number of flowers of the main inflorescences
Number of ripe fruits collected from the main inflorescences
Fresh weight of ripe fruits at harvest (collected from the main inflorescences)
Ripe fruit morphology
Total number of seeds collected from ripe fruits of the main inflorescences

Table 4.1 List of parameters measured in the phenotypic characterization of SlTDC1-OE lines and Sltdc1 lines. Legend: dpg, days post germination.

All three analyzed lines were characterized by reduced germinability compared to the control. Specifically, the OE-1 and OE-2 lines exhibited germination rates of approximately 60% and 64%, respectively. Among the analyzed genotypes, the highest germination rate was observed in the control (92%), followed by the OE-3 line, which displayed a germination rate of approximately 80%. Additionally, the other measured parameters did not show statistically significant differences between the three *SlTDC1*-OE lines and the control. Furthermore, leaves, fruits, and flowers did not exhibit evident morphological differences. At the end of the phenotypic characterization, roots, leaves (from the first to the last node before the inflorescence meristem), and deseeded ripe fruits were collected and used for

metabolomic and gene expression analysis. Metabolomic analysis revealed that overexpressing lines, compared to the wild-type genotype, exhibited 5- to 10-fold higher SER levels in both roots and leaves, respectively (Figures 4.1a and 4.1c), while TAM levels remained similar to those found in the wild type. In these organs, the slight increase in *TDC1* expression (0.5- to 1.5-fold compared to wild type) led to a strong increase in *T5H* expression (2- to 20-fold higher than wild type), which explains the increased SER levels (Figures 4.1b and 4.1d). Thus, *TDC1* overexpression failed to increase TAM in roots and leaves, as TAM was probably converted to SER by the T5H enzyme. The expression levels of *TDC1* in ripe fruits were significantly higher (15- to 25-fold) than those found in the leaves and roots. This is likely due to the presence of the endogenous *sltdc1*, which is characterized by fruit-specific activity; consequently, the observed result reflects both the expression levels of the endogenous gene and those of the transgene. However, the elevated *TDC1* expression levels in ripe fruits did not result in the strong *T5H* expression observed in the roots and leaves (Figure 4.1f). Surprisingly, despite these high levels of *TDC1* expression, ripe fruits produced by the overexpressing lines exhibited a significant decrease in both TAM and SER compared to the control (Figure 4.1e). While the decrease in SER is likely dependent on the reduction in TAM, the significant reduction of TAM following the increased expression of *TDC1*, which encodes the enzyme that converts tryptophan into TAM, could derive from more complex feedback control processes that need to be investigated and elucidated. Tryptophan levels were also checked in all three organs, and they were comparable to those of the wild type across all three overexpressing lines (data not shown).

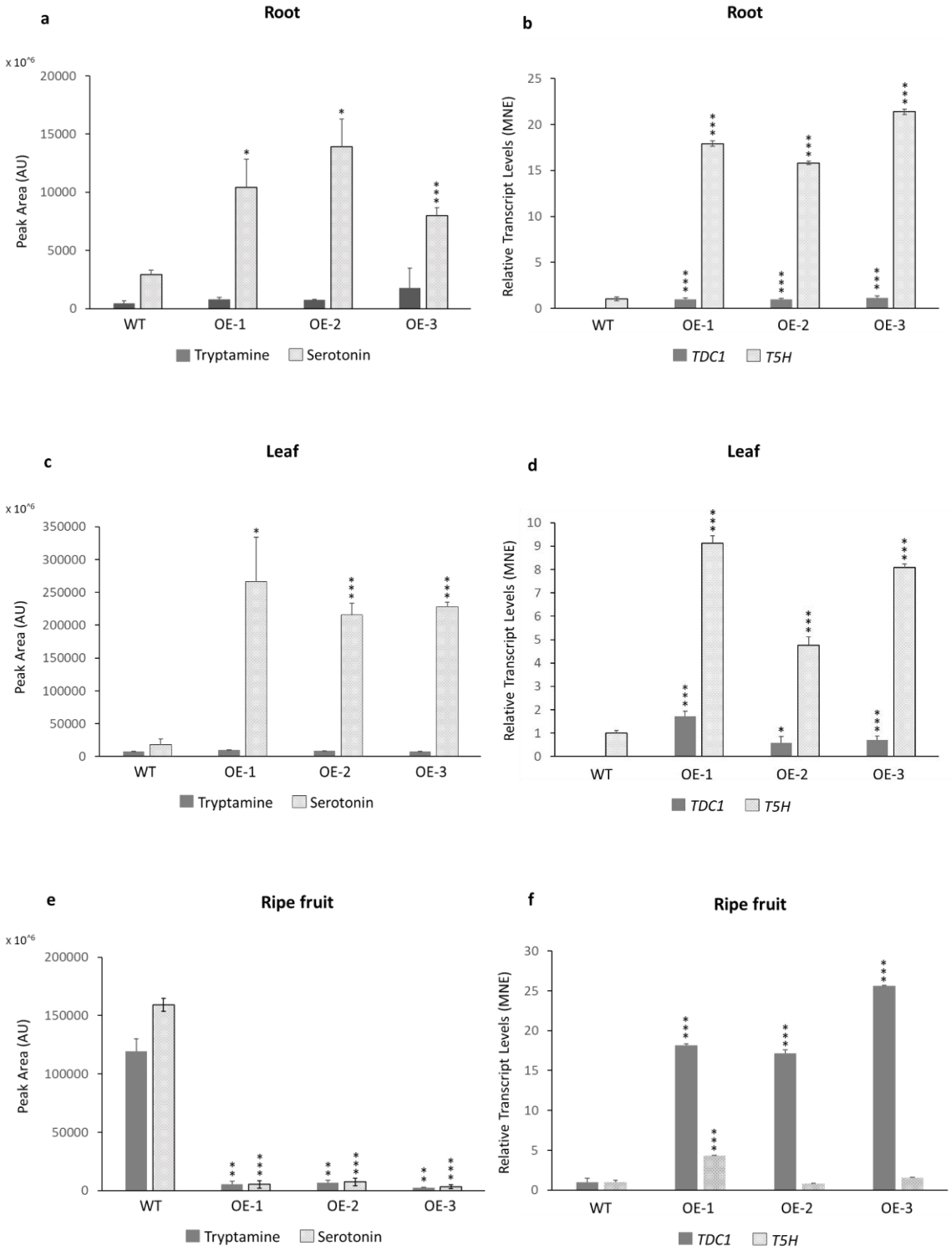

*Figure 4.1. Molecular analysis of roots, leaves, and deseeded ripe fruits from T2 SlTDC1-OE lines. Relative levels of TAM and SER in the leaf (a), root (b) and deseeded ripe fruit (e). Tryptamine and serotonin levels were detected by LC-ESI-MS analysis and are expressed as peak area (arbitrary units - AU), bars indicate standard deviations (n=3; biological replicates). Relative expression levels of sltdc1 and SlT5H in the leaf (b), root (d) and deseeded ripe fruit were detected by qRT-PCR. Bars represent standard error (n=3; technical replicates). Student's t-test was used for the statistical analysis (*P < 0.05; **P < 0.01; ***P < 0.001).*

4.3 *sltdc1* lines with depleted levels of TAM and SER in ripe fruits exhibited a reduced number of flowers and ripe fruits from the main inflorescences

Like the *SlTDC1*-OE lines, *sltdc1* lines were characterized by measuring the phenotypic parameters listed in Table 4.1. Similar to the three *Sltdc1*-overexpressing lines, the three *sltdc1* lines exhibited reduced germinability compared to the control. Specifically, the germination rates were 52% for the KO-1 line, 56% for the KO-2 line, and only 20% for the KO-3 line, while the wild-type line displayed a rate of approximately 96%. The KO-3 line was excluded from the analysis due to its low germinability. As observed for the *SlTDC1*-OE lines, the analysis of vegetative development and the overall leaf and flower morphology showed no significant differences between the two *sltdc1* lines and the control. However, the analysis of reproductive development revealed that the two knockout lines produced, on average, fewer flowers and ripe fruits from the main inflorescences, while exhibiting a higher average weight of ripe fruit (Figures 4.2a, 4.2b, and 4.2c).

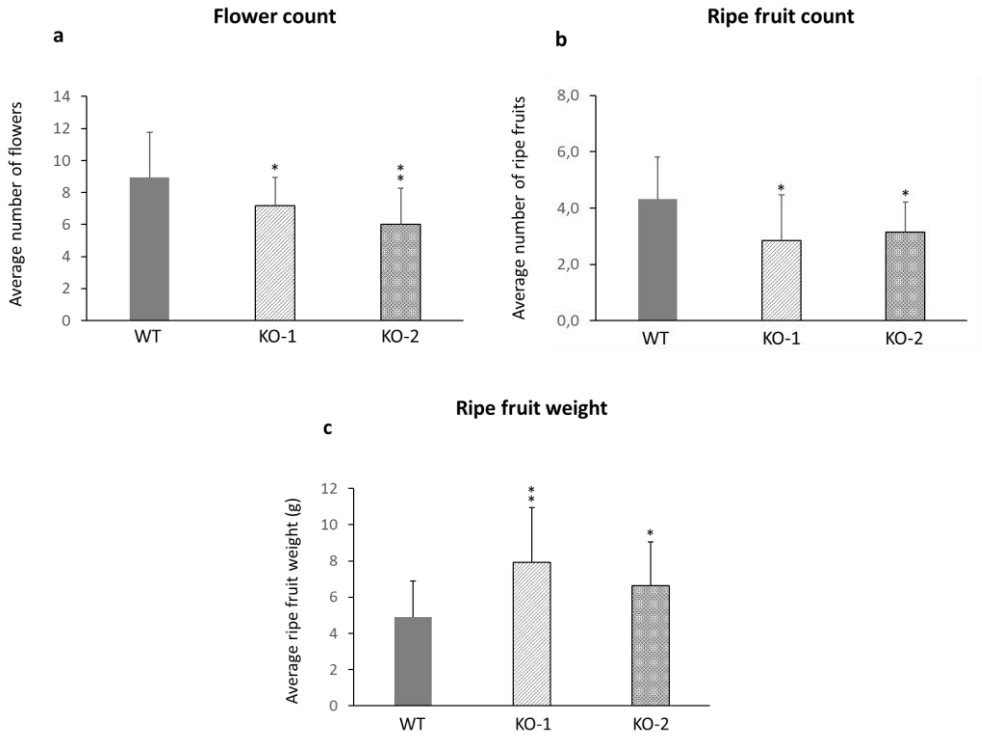

*Figure 4.2. Phenotypic analysis of T2 sltdc1 lines. a) number of flowers produced by the main inflorescences; b) number of fruits produced by the main inflorescences; c) fresh weight of ripe fruit at harvest in grams (g). Phenotypic values are reports as means ± standard deviation. Student's t-test was used for the statistical analysis (*P < 0.05; **P < 0.01; ***P < 0.001).*

As done for the overexpressing lines, at the end of the phenotyping experiment, roots, leaves, and deseeded ripe fruits were collected to determine the relative levels of tryptophan, TAM, and SER. Metabolomic profiling of the root from the two knockout (KO) lines revealed a slight increase in tryptophan levels (Figure 4.3a), accompanied by a decrease in tryptamine and serotonin levels compared to the control (Figure 4.3b). However, these variations were not statistically significant.

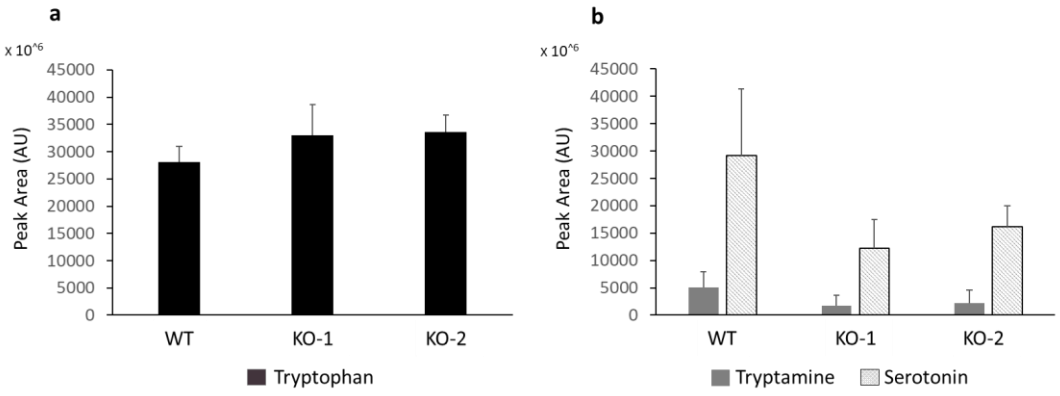

Figure 4.3. Metabolomic analysis of roots from T2 sltdc1 lines. Relative levels of tryptophan (a), tryptamine and serotonin (b). Tryptamine and serotonin levels were detected by LC-ESI-MS analysis and are expressed as peak area (arbitrary units - AU), bars indicate standard deviations (n=3; biological replicates). Values are reports as means ± standard deviation. Student's t-test was used for the statistical analysis (P < 0.05).

In the leaves (Figure 4.4a, 4.4b), the only significant change was observed in the KO-2 line, which exhibited an approximate 0.3-fold increase in tryptamine levels compared to the levels found in the control, while tryptophan and serotonin levels remained comparable to those of the control. No notable variations in the levels of the three metabolites were observed in the leaves of the KO-1 line.

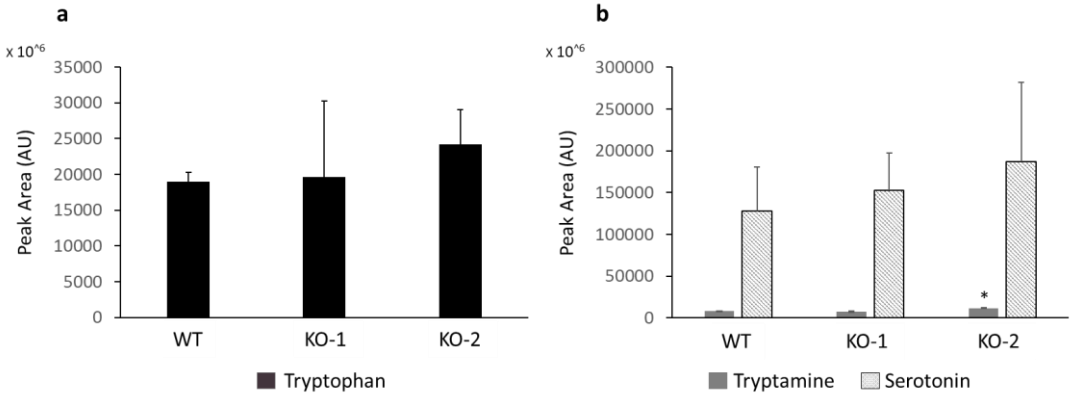

*Figure 4.4. Metabolomic analysis of leaves from T2 sltdc1 lines. Relative levels of tryptophan (a), tryptamine and serotonin (b). Tryptamine and serotonin levels were detected by LC-ESI-MS analysis and are expressed as peak area (arbitrary units - AU), bars indicate standard deviations (n=3; biological replicates). values are reports as means ± standard deviation. Student's t-test was used for the statistical analysis (*P < 0.05).*

Metabolomic analysis of deseeded ripe fruits revealed that both *sltdc1* lines exhibited a complete depletion of TAM and SER (Figure 4.5b). Additionally, a moderate increase in tryptophan content, which was significant only in the KO-1 line, was also observed (Figure 4.5a). These results, combined with the reduction in the number of flowers and fruits produced by the two *sltdc1* lines, suggest a possible role of serotonin and/or tryptamine in the reproductive development of tomato plants.

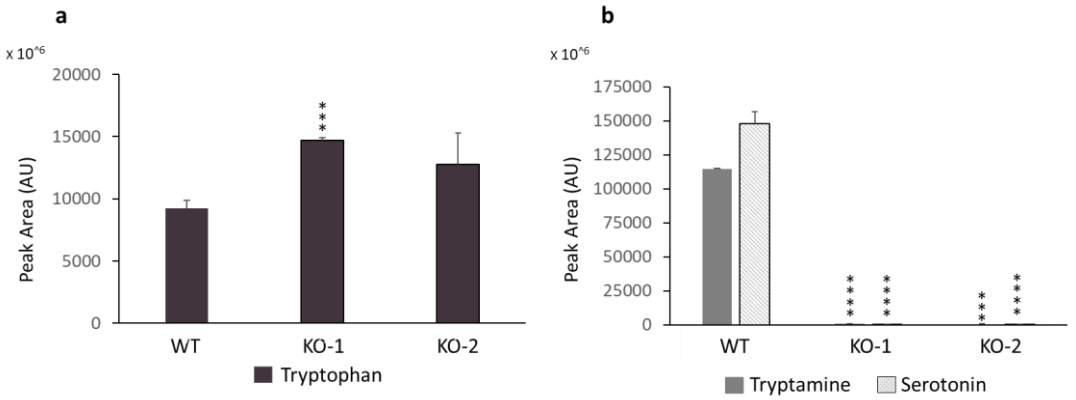

*Figure 4.5. Metabolomic and phenotypic analysis of deseeded ripe fruits from T2 sltdc1 lines. Relative levels of tryptophan (a), tryptamine and serotonin (b). Tryptamine and serotonin levels were detected by LC-ESI-MS analysis and are expressed as peak area (arbitrary units - AU), bars indicate standard deviations (n=3; biological replicates). values are reports as means ± standard deviation. Student's t-test was used for the statistical analysis (*P < 0.05; **P < 0.01; ***P < 0.001).*

4.4 Experimental design for the comparative phenotyping of *sltdc1* and *SlTDC1*-OE lines

Since the early phenotyping experiment indicated a potential role of TAM and SER in reproductive biology (variation in the number of flowers and ripe fruits) a further more detailed phenotyping experiment was conducted on the same Micro-tom lines described in Sections 4.2 and 4.3, to thoroughly investigate the reproductive performance of tomato plants with altered TAM and SER levels. This study included three *sltdc1* lines (KO-1, KO-2, KO-3), three *SlTDC1*-OE lines (OE-1, OE-2, OE-3), and the wild-type Micro-Tom genotype serving as a control. Within each line, five T2 generation plants underwent detailed phenotypic analysis, focusing on critical developmental transitions, including the shift from vegetative to reproductive stages, fruit development throughout maturation, and overall reproductive performance. The transition to flowering was quantified by tracking the time interval from germination to first floral bud emergence and from floral bud emergence to first flower anthesis, expressed as days post-germination (dpg), and days post floral bud emergence (dpbe), respectively. Additionally, also the number of true leaves preceding the inflorescence meristem was recorded. The reproductive phase was further characterized by recording the daily anthesis counts from the start of flowering to the end of the plant's life cycle. Moreover, the first 14 flowers on the main inflorescences of each plant were tagged and monitored from anthesis through fruit maturation. This process included documenting six fruit distinct ripening stages: immature green (IG), mature green (MG), breaker (B), turning (T), orange (O), and ripe (R). The intervals between flower anthesis and the onset of each ripening stage were calculated and expressed as days post-anthesis (dpa). At the conclusion of the experiments, the total number of fruits and seeds produced per genotype were counted. Additionally, the dry weight of 100 seeds was determined by weighing three independent seed pools as biological replicates for each line. All the measured parameters are summarized in Table 4.2. At the end of the phenotyping experiment, T3 seeds were collected and subjected to a germination test to

validate the reduction in germinability observed in the phenotyping experiments of T2 seeds described in Sections 4.2 and 4.3 for both the *SlTDC1*-OE and *sltdc1* lines. To complement these results, the levels of tryptophan, TAM, and SER in the seeds were quantified through LC-MS analysis.

Measured phenotypic parameter
Transition from vegetative to reproductive phase
Number of true leaves before the inflorescence meristem
Time interval between germination and floral bud emergence (dpg)
Time interval between floral bud emergence and first anthesis (dpbe)
Reproductive phase
Daily anthesis count until the 65th day after germination
Time interval between anthesis and onset of immature green stage (IG)
Time interval between anthesis and onset of mature green stage (MG)
Time interval between anthesis and onset of breaker stage (B)
Time interval between anthesis and onset of turning stage (T)
Time interval between anthesis and onset of orange stage (O)
Time interval between anthesis and onset of ripe stage (R)
Total fruit count
Total seed count
Dry weight of 100 seeds

Table 4.2. List of phenotypic parameters measured to study the transition from vegetative to reproductive phase, and to evaluate the reproductive performance of the sltdc1 and SlTDC1-OE lines. Legend: dpg, days post germination; dpbe, days post floral bud emergence.

4.5 Comparative phenotyping of *sltdc1* and *SlTDC1*-OE lines revealed significant differences in reproductive performances

The analysis of phenotypic data revealed that floral buds emerged on average 2-4 days earlier in all three *SlTDC1*-OE lines compared to the *sltdc1* lines (Figure 4.6b). In addition, in the overexpressing lines OE-1 and OE-2, the first anthesis occurred on average 2-3 days earlier than in the knockout lines (Figure 4.6c). Consistent with this finding, these lines (OE-1 and OE-2) exhibited a lower number of true leaves preceding the inflorescence meristem compared to the three knockout lines, indicating a shortening of the vegetative phase (Figure 4.6a).

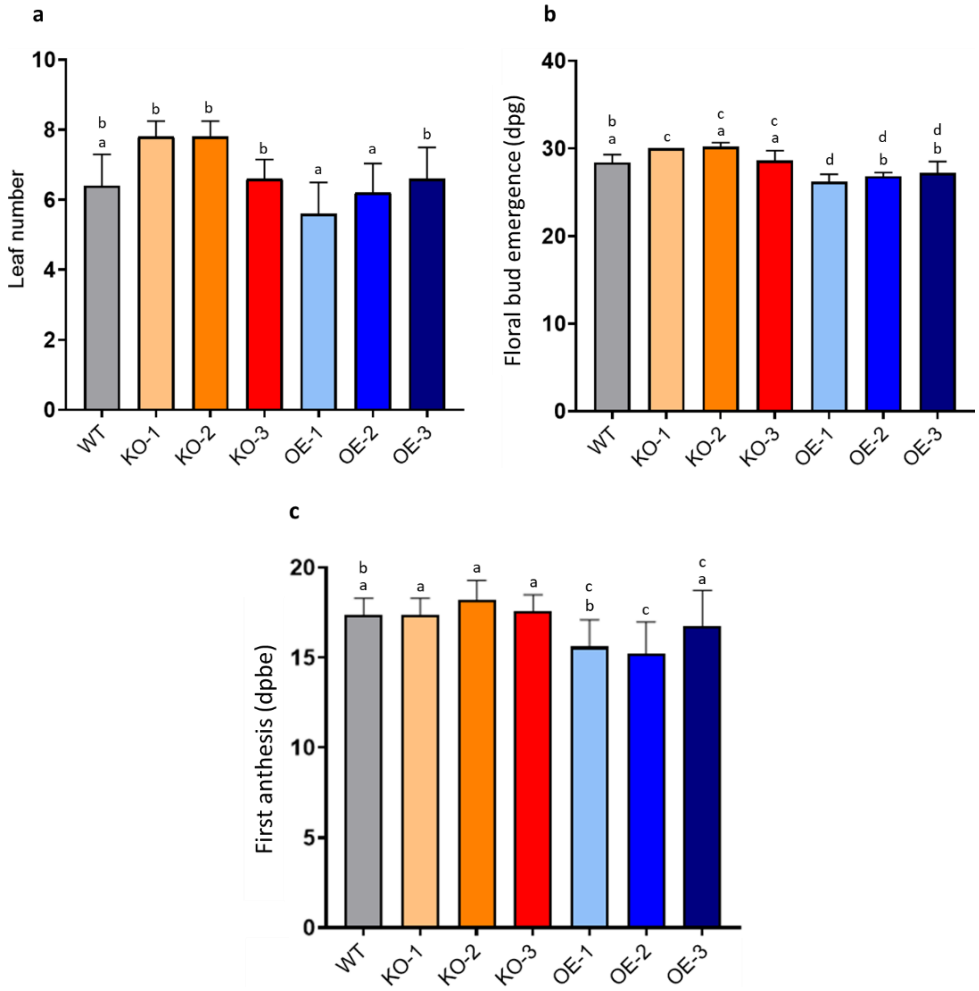

Figure 4.6. Phenotypic analysis of T2 sltdc1 and T2 SlTDC1-OE lines: a) number of leaves before the first inflorescence; b) floral bud emergence; c) First anthesis (dpbe); The values reported are means ± standard deviation. For the statistical analysis, an ordinary one-way ANOVA with multiple

comparisons was performed (P < 0.05). Legend: dpg, days post germination; dpfb, days post floral bud emergence.

Furthermore, the *SlTDC1-OE* lines were characterized by a significant increase in the number of anthesis recorded at 50-, and 55-days post germination (dpg) when compared to both the wild-type genotype and the *sltdc1* lines (Figure 4.7a, 4.7b, and 4.7c).

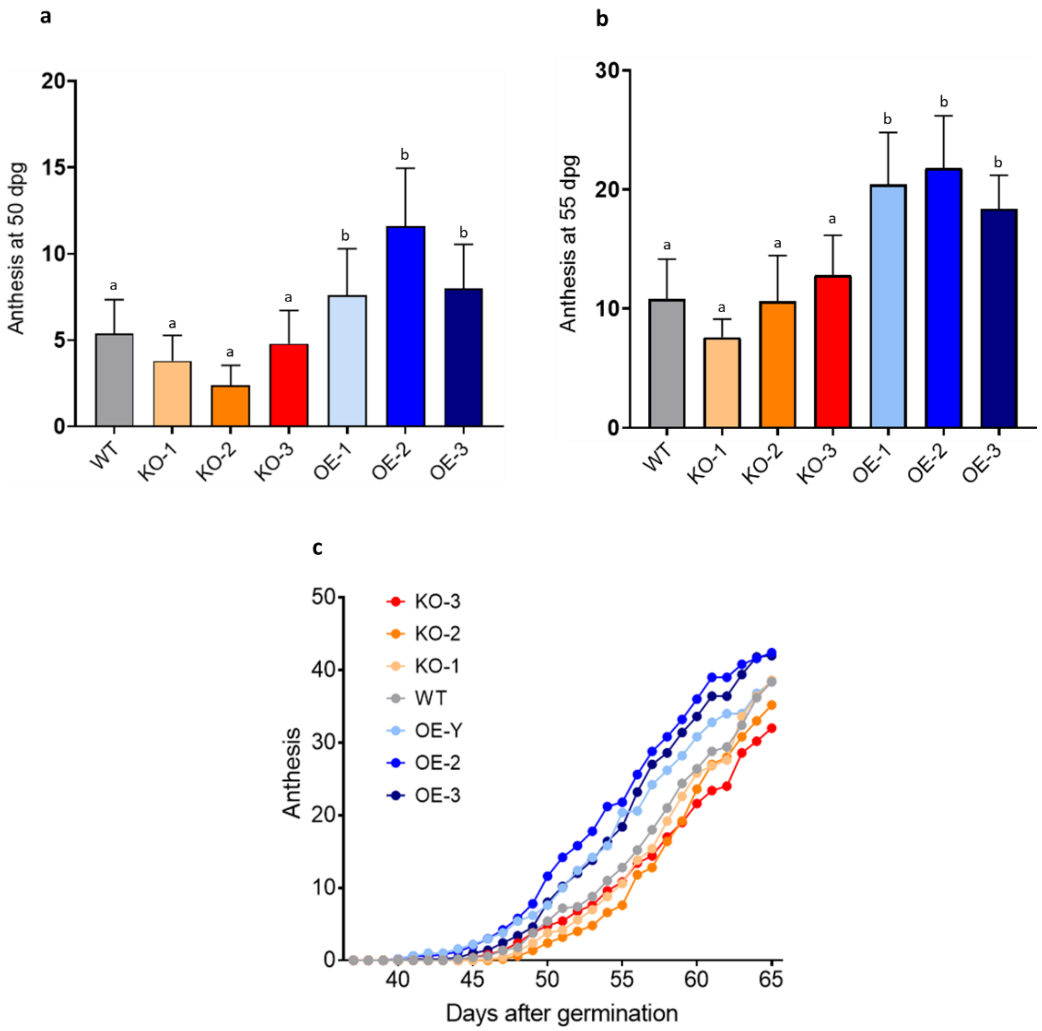

Figure 4.7. Phenotypic analysis of T2 sltdc1 and T2 SlTDC1-OE lines: a) anthesis number at 50 dpg; b) anthesis number at 55 dpg; c) anthesis progression. The values reported are means ± standard deviation. For the statistical analysis, an ordinary one-way ANOVA with multiple comparisons was performed (P < 0.05).

Regarding fruit development and progression through various ripening stages, no significant differences were observed among the different genotypes, although the overexpressing lines 2 and 3 were exhibited a delay in the appearance of the

MG stage compared to the *sltdc1* lines (Figure 4.8a). All three *sltdc1* lines showed a significant reduction in the number of fruits produced (Figure 4.8b).

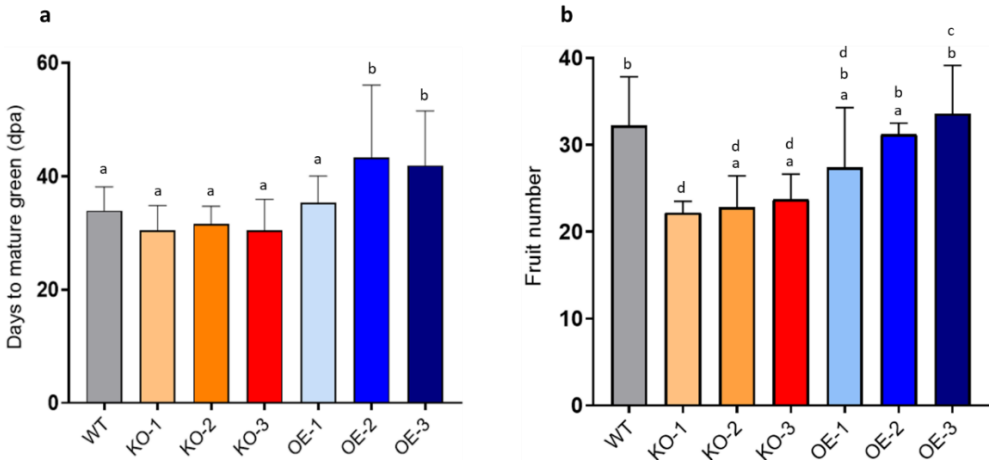

Figure 4.8. Phenotypic analysis of T2 sltdc1 and T2 SlTDC1-OE lines: a) time interval between the anthesis and the onset of mature green stage of fruit; b) number of ripe fruits; The values reported are means ± standard deviation. For the statistical analysis, an ordinary one-way ANOVA with multiple comparisons was performed (P < 0.05).

Quantitative determination of mature dry seed weight revealed significant differences among genotypes, with the seeds of overexpressing lines OE-2 and OE-3 (264 ± 15 and 223 ± 9 mg per 100 seeds, respectively) significantly lighter than the control (303 ± 7 mg per 100 seeds) and the *sltdc1* lines. No differences were observed in seed weight between the knockout lines and the control (Figure 4.9).

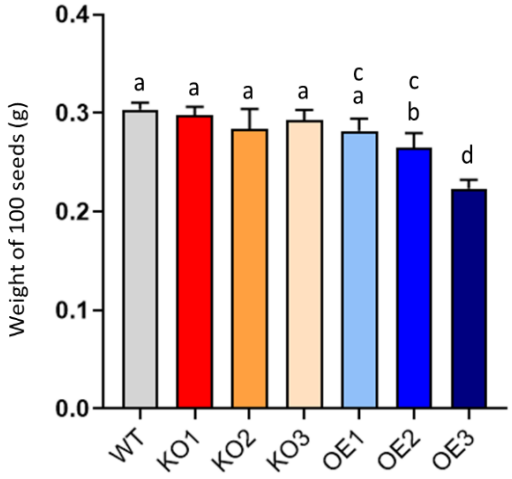

Figure 4.9. Seed weight measured on dried seeds (T3) produced by T2 sltdc1 and T2 SlTDC1-OE lines. Weight of 100 of seeds expressed in grams (g). Values are reported as the mean of three biological replicates ± standard deviation. For the statistical analysis, an ordinary one-way ANOVA with multiple comparisons was performed (P < 0.05).

Interestingly, while seed weight remained comparable to that of wild-type plants, seeds from all three knockout lines, but not those from overexpressing lines, exhibited a distinctive phenotype characterized by a dark pigmentation of the seed coat (Figure 4.10).

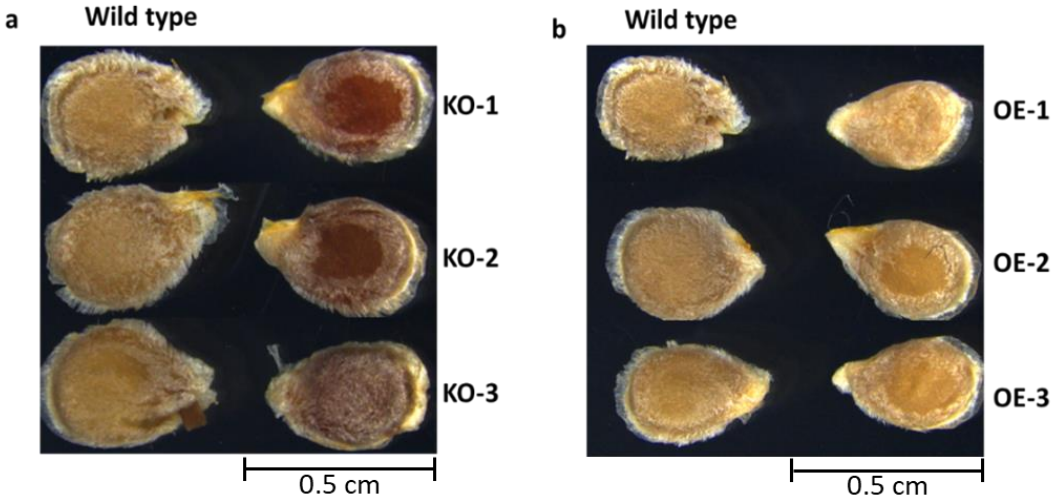

Figure 4.10. Images acquired with the Leica MZ10 F stereomicroscope: a) dark pigmentation observed in T3 seeds from the three sltdc1 lines. b) T3 seeds from the three SlTDC2-OE lines exhibit a seed pigmentation similar to that of the wild-type genotype.

4.6 Seeds produced by *sltdc1* and *SlTDC1*-OE lines are characterized by a reduced germinability

T3 seeds from both s*ltdc1* lines and *SlTDC1*-OE lines underwent a germination trial to evaluate their germinability and overall viability. The germination test was conducted on a total of 75 seeds per line, divided into three replicates of 25 seeds each. Seeds were sown in vitro and monitored for 15 days, recording both the number of germinated seeds per day and the total number of germinated seeds at the end of the experiment, and this latter parameter was used to calculate the total germination percentage. The daily germination counts were utilized to calculate the Mean Days to Germination (MDG) parameter. This parameter not only expresses the speed of germination progression, but also provides insights into the uniformity of germination and the overall seed viability. All three *sltdc1* lines exhibited a significant increase of the MDG compared to the control, requiring between 9 and 12 days for germination, compared to 5-6 days for the

wild-type Micro-Tom genotype. The overexpressing lines OE-2 and OE-3 behaved similarly to the control, with only the OE-1 line showing a significant increase in MDG, albeit to a lesser extent than the knockout lines (Figure 4.11).

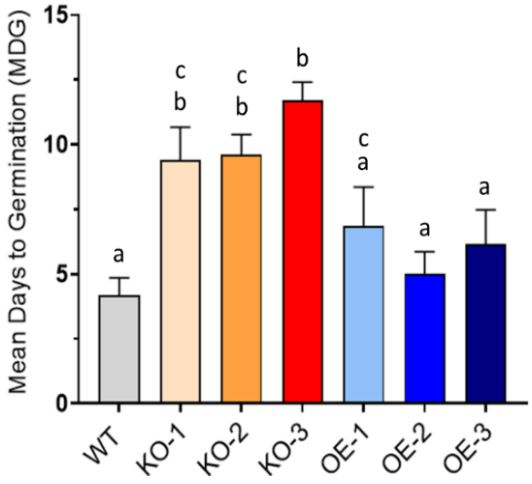

Figure 4.11. Mean days to germination (MDG) of T3 seeds from sltdc1 and SlTDC1-OE lines calculated using the formula of Gerson and Honma (1978). For statistical analysis an ordinary one-way ANOVA with multiple comparisons was performed (P < 0.05).

All analyzed lines, except for the overexpressing line 4, showed a reduction in germination rate. In particular, the three knockout lines were characterized by a drastic decrease in germination percentage, ranging from 20% for line KO-3 to 35% for line KO-2, while the control showed a germinability close to 100% (Figure 4.12).

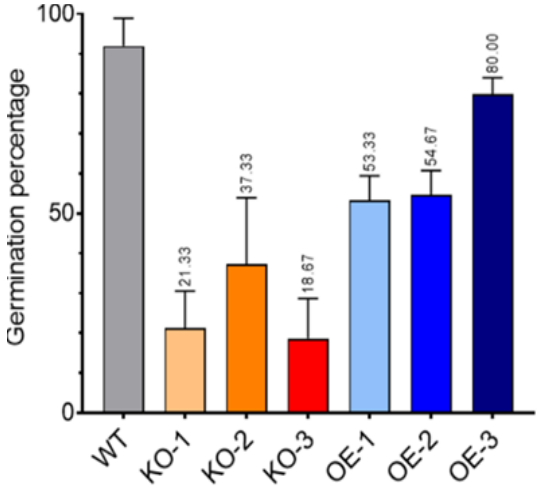

Figure 4.12. Germination percentage of T3 seeds from sltdc1 and SlTDC1-OE lines. For statistical analysis an ordinary one-way ANOVA with multiple comparisons was performed (P < 0.05).

4.7 Targeted metabolomic analysis revealed a strong depletion of TAM and SER in the seeds produced by *sltdc1* and *SlTDC1*-OE lines

The knockout of *sltdc1* resulted in a 5-fold reduction in TAM levels compared to the control, along with the almost complete depletion of SER (Figure 4.13b and 4.13c, respectively). With the exception of the KO-1 line, which exhibited higher tryptophan levels than the control, the reductions in TAM and SER levels in KO-2 and KO-3 lines did not affect tryptophan levels. As observed in ripe fruits, the overexpression of *SlTDC1* did not lead to increased production of TAM and SER in the seeds of the *SlTDC1*-OE lines. Specifically, the levels of these two metabolites were significantly lower than those found in the seeds of the wild-type genotype. Compared to the control, TAM levels were reduced by 4- to 5-fold, while SER levels decreased by approximately 2-fold (Figures 4.13b, and 4.13c). As hypothesized for ripe fruit, a complex feedback regulation mechanism may also be active in the seed, preventing or limiting the accumulation of TAM and SER in this organ. This aspect clearly warrants further investigation. Notably, as observed in the knockout lines KO-2 and KO-3, the reduction in TAM and SER levels in fruits was not accompanied by an increase in tryptophan (Figure 4.13a), whose levels remained comparable to those of the control. In summary, in Micro-Tom seeds, similar to the other analysed organs, *TDC1* expression does not necessarily correlate positively with TAM accumulation. This suggests the existence of regulatory mechanisms controlling TAM levels, one of which is the *TDC1*-induced activation of *T5H* transcription observed in leaves and roots, leading to the conversion of TAM into SER. Conversely, SER levels in seeds positively correlates with seed germinability: the OE lines, which unexpectedly exhibit decreased TAM and SER levels, show a reduced germination percentage and increased mean germination day (MDG), while the KO lines, displaying TAM levels comparable to those of the OE lines but significantly lower SER levels, exhibit an even further reduction in germination percentage and an increased MDG.

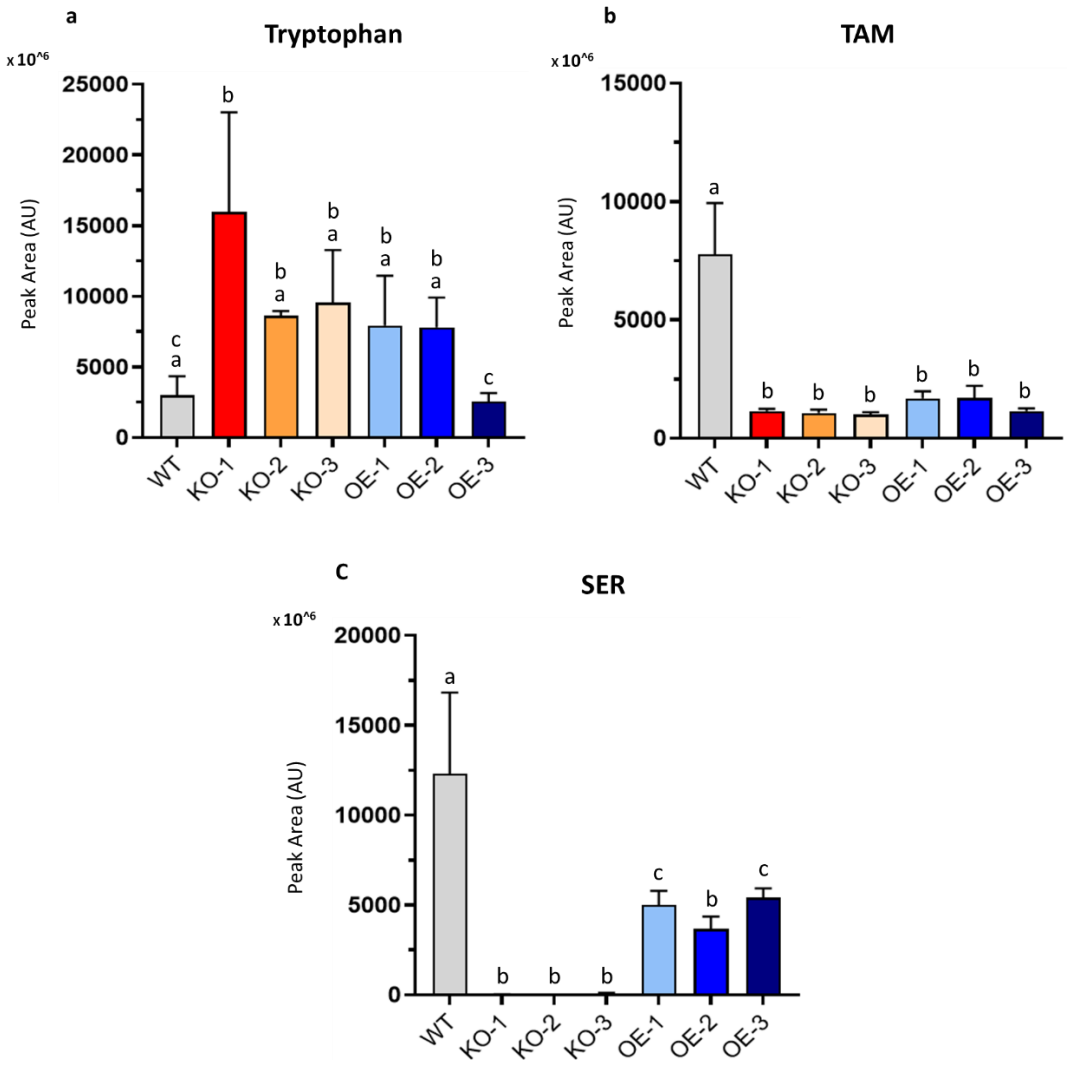

Figure 4.13. Metabolomic analysis of T3 seeds from sltdc1 and SlTDC1-OE lines. Relative levels of tryptophan (a), tryptamine (b) and serotonin (c). Tryptophan, tryptamine and serotonin levels were detected by LC-ESI-MS analysis and are expressed as peak area (arbitrary units - AU), bars indicate standard deviations (n=3; biological replicates). For the statistical analysis, an ordinary one-way ANOVA with multiple comparisons was performed (P < 0.05).

Chapter 5 – Phenotypic and Molecular Characterization of *SlT5H*-overexpressing and *slt5h*-knockout Lines

5.1 A preliminary phenotypic and molecular characterization of *SlT5H*-OE and *slt5h* lines

To evaluate the effect of overexpression and knockout of the *SlT5H* gene on vegetative and reproductive development in *S. lycopersicum* (cv. Micro-Tom), a comparative phenotypic analysis was conducted on *SlT5H*-OE lines and *slt5h* lines (Table 5.1). The experiment included four T1 *SlT5H*-OE lines, three T2 homozygous T2 *slt5h* lines, and the wild-type Micro-Tom genotype serving as a control. To select only transgenic individuals, two-week-old plantlets from the *SlT5H*-OE lines underwent a five-day treatment with kanamycin (100 mg/ml) administered as foliar spray.

Line ID	Parental (T0)	Genotype	Characterized progeny
SlT5H-OE1 (OE-1)	Line 1	*SlT5H*-overexpression	T1
SlT5H-OE2 (OE-2)	Line 3	*SlT5H*-overexpression	
SlT5H-OE3 (OE-3)	Line 7	*SlT5H*-overexpression	
SlT5H-OE4 (OE-4)	Line 9	*SlT5H*-overexpression	
slt5h-1 (KO-1)	Line 1	*SlT5H*-knockout	T2
slt5h-1 (KO-2)	Line 2	*SlT5H*-knockout	
slt5h-1 (KO-3)	Line 3	*SlT5H*-knockout	

Table 5.1. List of SlT5H-OE and slt5h lines used in the phenotypic and molecular characterization.

The phenotypic characterization was conducted by measuring quantitative parameters associated with vegetative development and reproductive performances, along with temporal metrics to evaluate the transition from the vegetative to reproductive phase (Table 5.2). The transition from vegetative to reproductive development was evaluated by counting the number of true leaves before the inflorescence meristem (as a lower number of true leaves is an indicator of early flowering), and by measuring the time intervals between

germination and the emergence of floral buds, while the onset of flowering was evaluated by measuring the time interval between the appearance of floral buds and the first anthesis.

Measured phenotypic parameter
Vegetative phase
Number of germinated plants (germination percentage)
Number of true leaves before the inflorescence meristem
Stem length (from the first true leaf up to the last true leaf before the inflorescence meristem)
Leaf morphology
Flower morphology (at anthesis)
Transition from vegetative to reproductive phase
Number of true leaves before the inflorescence meristem
Time interval between germination and floral bud emergence (dpg)
Time interval between floral bud emergence and first anthesis (dpbe)
Reproductive phase
Daily anthesis count until the 65th day after germination
Total fruit number
Total ripe fruit number
Ripe fruit morphology
Ripe fruit weight (grams of fresh weight – g of FW)
Total seed count
Weight of 100 seeds (grams of dry weight – g of DW)

Table 5.2. List of parameters measured in the phenotypic characterization of SlT5H-OE and slt5h lines

For each genotype, 12 plants were grown in a long-day growth chamber, with randomized spatial arrangement to minimize positional effects. Under these conditions, plants completed their life cycle in approximately three months from germination. At the end of the phenotyping experiment, roots, leaves, deseeded ripe fruits, and seeds were collected and used to determine the relative levels of tryptamine and serotonin through LC-ESI-MS analysis. Furthermore, leaves from the three overexpressing lines were used to determine the expression levels of *SlT5H* via qRT-PCR analysis.

5.2 All genotypes are characterized by a reduced size compared to the control

Among the overexpressing genotypes, the OE-4 lines exhibited the highest levels of *SlT5H* expression. However, due to its poor germination rate, it was excluded from the analysis. The other genotypes were characterized by a germinability ranging from 52% in the KO-3 line to 90% in the OE-2 line (Table 5.3).

Germination percentage (%)							
WT	OE-1	OE-2	OE-3	OE-4	KO-1	KO-2	KO-3
76	64	90	58	18	74	58	52

Table 5.3. Percentage of germinated seeds from SlT5H-OE (T1) and slt5h (T2) lines. For each line, 50 seeds were sown.

In all analyzed lines, reduction in stem length compared to the control was observed (Figures 5.1). Notably, both the *SlT5H*-OE lines and the s*lt5h* lines exhibited a similar phenotype for this parameter, although the statistical significance was greater for the three OE lines.

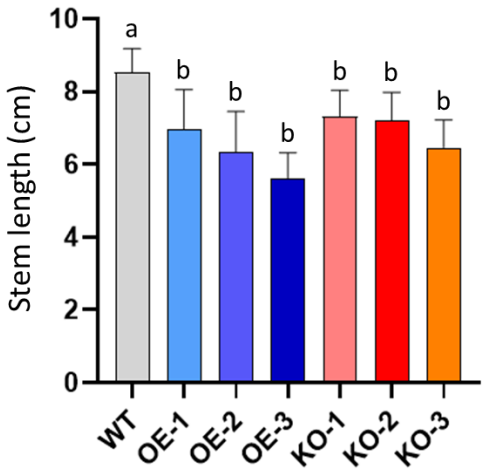

Figure 5.1. Phenotypic analysis of T1 SlT5H-OE and T2 slt5h lines. Stem length (cm) measured from the first true leaf up to the last true leaf before the inflorescence meristem. The values reported are means ± standard deviation. For the statistical analysis, an ordinary one-way ANOVA with multiple comparisons was performed (P < 0.05).

Regarding the morphology of leaves and flowers at anthesis, no differences were observed among the *SlT5H1*-OE lines, the *slt5h* lines, and the control.

5.3 The *SlT5H*-OE lines are characterized by a faster transition from vegetative to reproductive phases

The OE-1 and OE-2 lines are characterized by a reduced number of true leaves before the inflorescence meristem compared to the control and the three *Slt5h* lines. Furthermore, in all three *SlT5H*-OE lines, the development of the floral buds occurred on average approximately 2-3 days earlier than in the control and the knockout lines (Figure 5.2a, 5.2b).

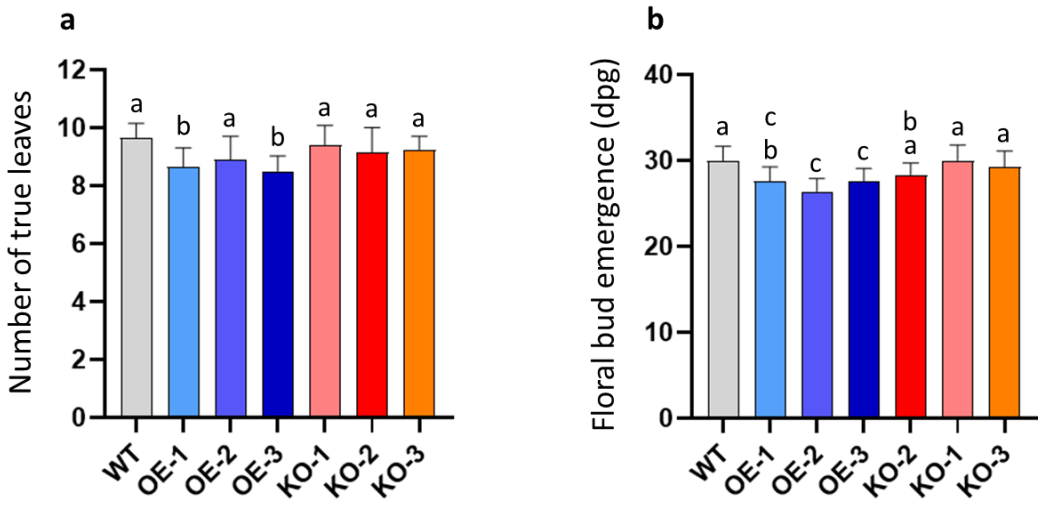

Figure 5.2. Phenotypic analysis of T1 SlT5H-OE and T2 slt5h lines. Number of true leaves before the inflorescence meristem (a). Floral bud emergence expressed as days post germination (dpg) (b). Values reported are means ± standard deviation. For statistical analysis, an ordinary one-way ANOVA with multiple comparisons was performed ($P < 0.05$).

Although the *SlT5H*-OE lines exhibited a shorter time interval between germination and the emergence of floral buds, no significant differences were found in the time interval between the emergence of floral buds and the first anthesis (Figure 5.3).

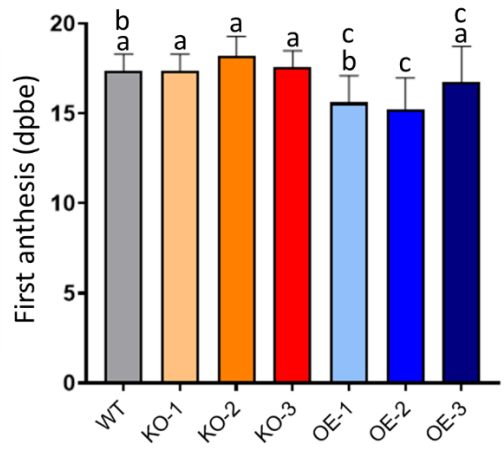

Figure 5.3. Phenotypic analysis of T1 SlT5H-OE and T2 slt5h lines. Time interval between floral bud emergence and first anthesis expressed as days post floral bud emergence (dpbe). Values reported are means ± standard deviation. For the statistical analysis, an ordinary one-way ANOVA with multiple comparisons was performed (P < 0.05).

This result indicates that although the overexpressing lines exhibited a faster development of flower buds compared to the control and knockout lines, this difference did not correspond to a statistically significant changes in the timing of the first anthesis.

Regarding the other measured parameters related to reproductive development (number of ripe fruits, average weight of ripe fruit, etc.), no significant differences were found among the analyzed genotypes (data not shown). Similarly, no differences in the morphology of ripe fruits were observed among the genotypes under study

5.4 Metabolomic analysis revealed strong TAM accumulation and SER depletion in all three *slt5h* lines

Metabolomic analysis confirmed the knockout of the *SlT5H* gene in all three *slt5h* lines. These lines are characterized by a significant accumulation of TAM in all analyzed organs, accompanied by the complete depletion of SER. In the leaves SER was not completely depleted, even though the levels were still much lower than in the control (Figure 5.4 a-d). This result may indicate, as suggested in other studies, the existence of an alternative pathway for SER biosynthesis that does not rely on T5H. However, in plants the specific gene involved in this alternative pathway still needs to be identified.

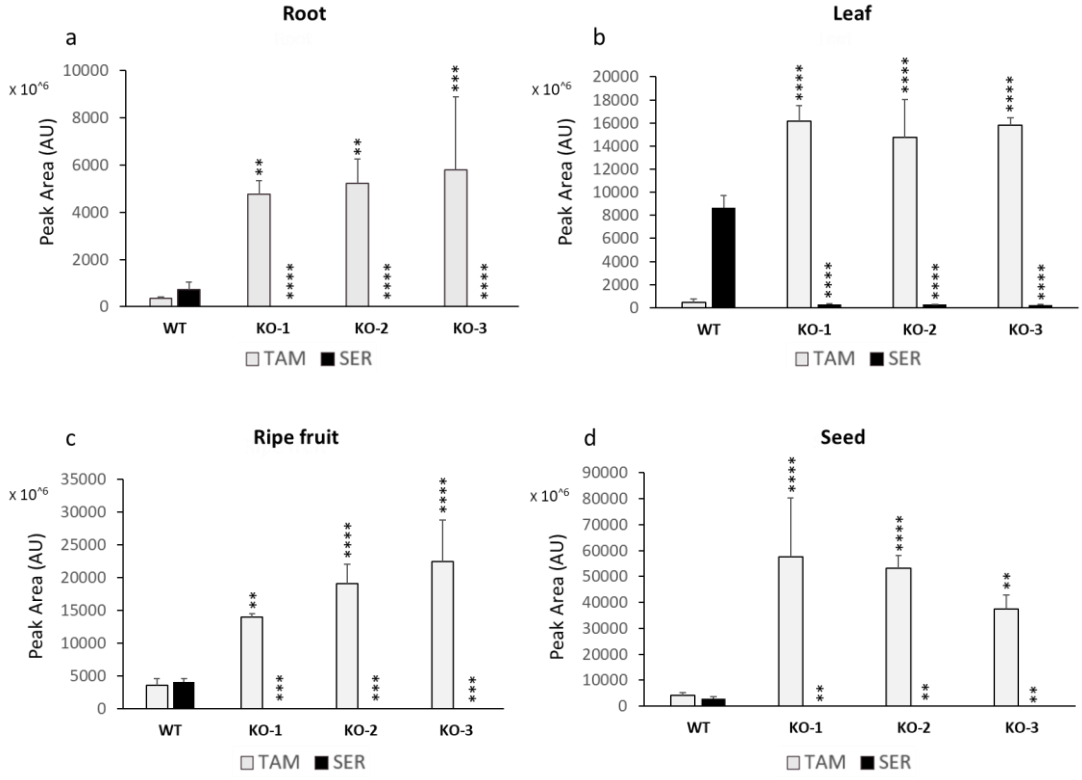

*Figure 5.4. Metabolomic analysis of roots, leaves, deseeded ripe fruits and seeds from T2 slt5h lines. Relative levels of TAM and SER in the leaf (a), root (b), deseeded ripe fruit (c), and seed (d). Tryptamine and serotonin levels were detected by LC-ESI-MS analysis and are expressed as peak area (arbitrary units - AU), bars indicate standard deviations (n=3; biological replicates). Student's t-test was used for the statistical analysis (*P < 0.05; **P < 0.01; ***P < 0.001).*

5.5 Variable outcomes of *SlT5H* overexpression on TAM and SER Levels by organ type and genotype

The LC-ESI-MS analysis of TAM and SER levels across the different organs revealed, in most cases, no significant differences between the control and the three *SlT5H*-OE lines. Specifically, TAM levels in the roots of the overexpressing lines were comparable to those detected in the control (Figure 5.5). Concerning SER levels, although a decreasing trend was observed in the three *SlT5H*-OE lines compared to the control, the differences were not statistically significant (Figure 5.5).

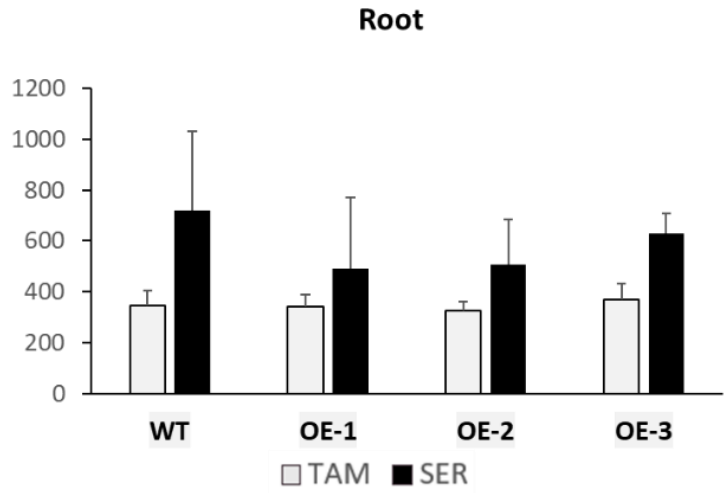

*Figure 5.5. Metabolomic analysis of roots from T1 SlT5H-OE lines (relative levels of TAM and SER). Tryptamine and serotonin levels were detected by LC-ESI-MS analysis and are expressed as peak area (arbitrary units - AU), bars indicate standard deviations (n=3; biological replicates). Student's t-test was used for the statistical analysis (*P < 0.05; **P < 0.01; ***P < 0.001).*

Similarly, to what was observed in the roots, TAM levels detected in the leaves were comparable to those in the control (Figure 5.6). Likewise, SER levels showed a decreasing trend in the three overexpressing lines compared to the control, although the differences were not statistically significant (Figure 5.6).

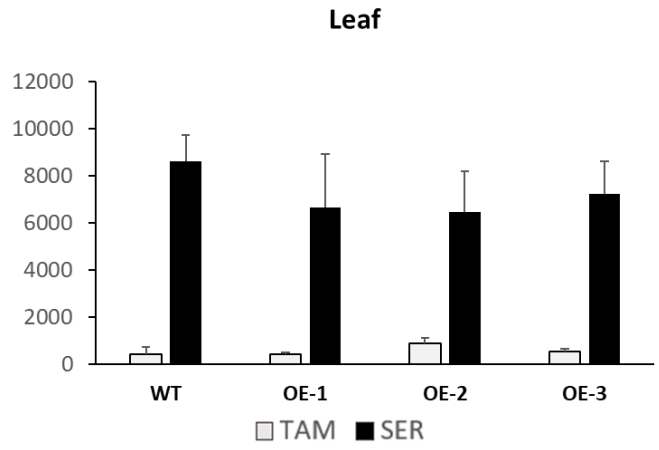

*Figure 5.6. Metabolomic analysis of leaves from T1 SlT5H-OE lines (relative levels of TAM and SER). Tryptamine and serotonin levels were detected by LC-ESI-MS analysis and are expressed as peak area (arbitrary units - AU), bars indicate standard deviations (n=3; biological replicates). Student's t-test was used for the statistical analysis (*P < 0.05; **P < 0.01; ***P < 0.001).*

With respect to ripe fruits, no significant differences in TAM levels were observed between the control and the three *SlT5H*-OE lines (Figure 5.7). A different pattern was observed for SER levels, with the OE-2 and OE-3 lines showing a significant increase compared to the control (Figure 5.7).

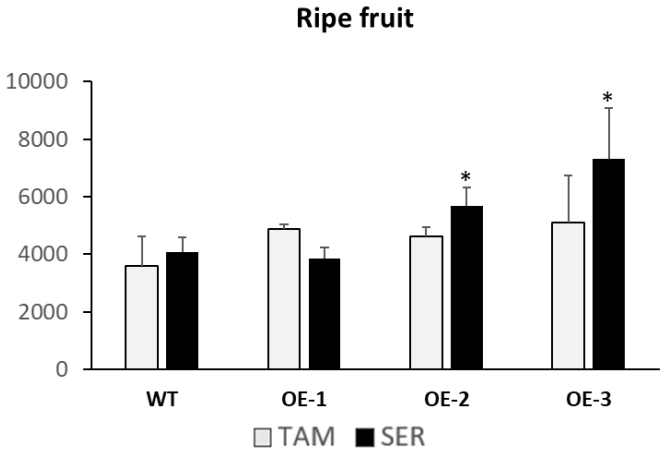

*Figure 5.7. Metabolomic analysis of deseeded ripe fruits from T1 SlT5H-OE lines (relative levels of TAM and SER). Tryptamine and serotonin levels were detected by LC-ESI-MS analysis and are expressed as peak area (arbitrary units - AU), bars indicate standard deviations (n=3; biological replicates). Student's t-test was used for the statistical analysis (*P < 0.05; **P < 0.01; ***P < 0.001).*

The analysis of TAM levels in seeds revealed an increasing trend in all three *SlT5H*-OE lines, but the increase was statistically significant only in the OE-1 line.

Concerning SER levels, no statistically significant differences were observed between the overexpressing lines and the control, although a slight decrease in SER levels was noted in the OE-1 line (Figure 5.8).

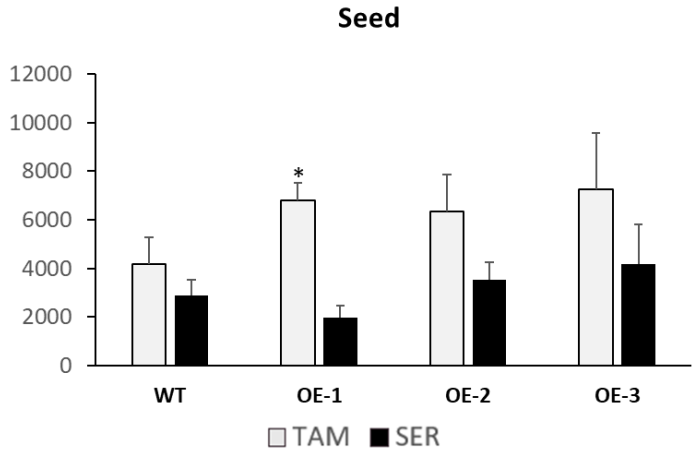

*Figure 5.8. Metabolomic analysis of seeds from T1 SlT5H-OE lines (relative levels of TAM and SER). Tryptamine and serotonin levels were detected by LC-ESI-MS analysis and are expressed as peak area (arbitrary units - AU), bars indicate standard deviations (n=3; biological replicates). Student's t-test was used for the statistical analysis (*P < 0.05; **P < 0.01; ***P < 0.001).*

qRT-PCR conducted on the leaves of the *SlT5H*-OE lines confirmed the overexpression of the *SlT5H* gene in all three genotypes (Figure 5.9). In the OE-1 line, *SlT5H* expression was approximately four times higher than in the control, whereas in the OE-2 and OE-3 lines, expression levels increased approximately 100- to 150-fold.

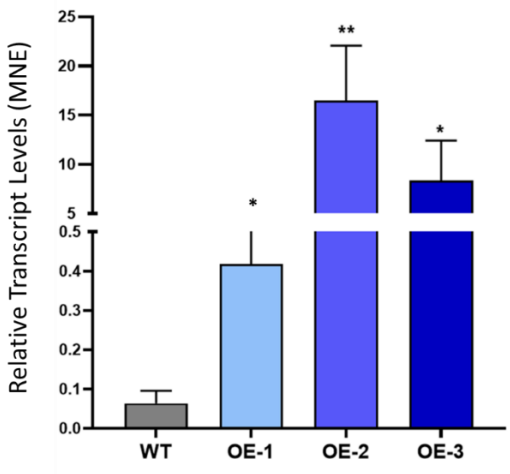

*Figure 5.9. Relative expression levels of SlT5H in leaves from T1 SlT5H-OE lines detected by qRT-PCR. Bars represent standard error (n=3; technical replicates). Student's t-test was used for the statistical analysis (*P < 0.05; **P < 0.01; ***P < 0.001).*

Chapter 6 – Development of an Exogenous Administration Method of Tryptamine at the Root Level

6.1 A preliminary implementation of a hydroponic growth system for the exogenous administration of tryptamine in Micro-Tom

The exogenous administration of precursors or metabolic intermediates serves as a useful tool for both reverse genetics and metabolomics studies. In reverse genetics, this administration can be utilized as a complementation method to restore a specific phenotype without the need to restore gene functionality through genetic engineering techniques, which are often laborious and time-consuming. In metabolomics, the use of deuterated precursors or intermediates, coupled with mass spectrometry, represents a powerful tool for tracking the fate of a molecule within biological systems. This approach enables the study of the molecule's movement within the organism, identifying both derived metabolites and potential degradation products, while also facilitating the identification of new metabolic pathways.

6.1.1 Experimental design and analysis workflow

The purpose of this experiment is to establish a protocol for the exogenous administration of tryptamine (TAM) to the model species *S. lycopersicum* (cv. Micro-Tom), through its solubilization in the growth medium. To this aim, wild-type Micro-Tom plants were cultivated hydroponically for approximately three weeks. On the day of treatment, the basic nutrient solution (MS 1/4, pH 5.7) was replaced with a TAM-supplemented solution at varying concentrations. Four experimental conditions were set up, including a control with the unmodified base medium:

- MS 1/4, pH 5.7 (control, no TAM);
- MS 1/4, pH 5.7 + TAM 2.5 mM;
- MS 1/4, pH 5.7 + TAM 5 mM;
- MS 1/4, pH 5.7 + TAM 10 mM;

Nine plants were used per condition, for a total of 36 plants. The experiment was conducted in duplicate with two independent batches of 36 plants, allowing sampling at 24- and 48-hours post-treatment.

a

Batch 1 (36 plants)			
C-	1 mM	5 mM	10 mM
9 plants	9 plants	9 plants	9 plants
Sampling 24 hours after treatment			

b

Batch 2 (36 plants)			
C-	1 mM	5 mM	10 mM
9 plants	9 plants	9 plants	9 plants
Sampling 48 hours after treatment			

Figure 6.1. Schematic representation of the two groups of plants used in the experiment: Batch 1 (a) represents the group of plants sampled 24 hours after treatment with TAM; Batch 2 (b) represents the group of plants sampled 48 hours after treatment with TAM.

The treatment lasted 12 hours, after which the roots were thoroughly rinsed with Milli-Q water. The nutrient solution containing TAM (or only MS 1/4 for the control) was then replaced with a TAM-free base medium. One batch of plants was sampled 24 hours after the end of the treatment, and the second batch was sampled 48. In both cases, during sampling the plants were divided into three sections: (1) roots; (2) basal leaves (first and second true leaves) along with the stem section between them; and (3) apical leaves (fifth and sixth true leaves), including the stem section and vegetative apices. The collected plant material was analyzed to quantify TAM and serotonin (SER) levels using HPLC-ESI-MS.

6.1.2 Micro-Tom plants can adsorb exogenous TAM from roots, convert it to SER or translocate it to aerial vegetative organs

As illustrated in Figures 6.2, the concentration of tryptamine (TAM) in the roots increased in proportion to the concentration of TAM in the growth medium, peaking at the 10 mM TAM treatment in plants sampled 24 hours post-treatment. In plants sampled at 48 hours, the levels of TAM decreased but remained significantly higher than in the control across all three treatments (Figure 6.2a) Similarly, the concentration of serotonin (SER) in the roots increased in relation to the concentration of TAM in the medium, suggesting that absorbed TAM could be metabolized and converted into SER (Figure 6.2b). However, the increase in SER levels was statistically significant only in plants sampled 48 hours post-treatment. The most substantial increase in SER was observed in plants treated with 10 mM of TAM, which may also explain the lower TAM levels in the roots sampled at 48 hours compared to those sampled after 24 hours.

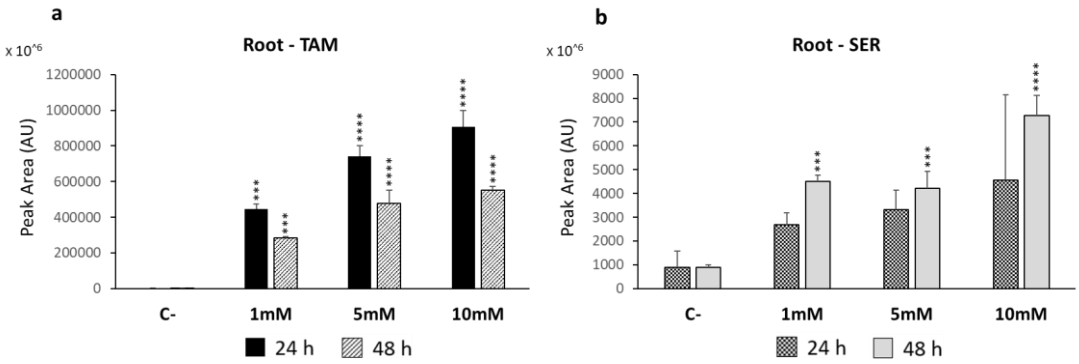

*Figure 6.2. Relative levels of TAM (a) and SER (b) in the roots of plant treated with different concentration of TAM and sampled at 24- and 48-hours post-treatment. Tryptamine and serotonin levels were detected by LC-ESI-MS analysis and are expressed as peak area (arbitrary units - AU), bars indicate standard deviations (n=3; biological replicates). Values are reports as means ± standard deviation. Student's t-test was used for the statistical analysis (*P < 0.05; **P < 0.01; ***P < 0.001).*

Analysis of the levels of the two metabolites in the basal leaves revealed that TAM levels increased significantly compared to the control in both the 5 mM and 10 mM TAM treatments for plants sampled at 24 hours. For plants sampled at 48 hours, the increase was significant only in the 10 mM treatment (Figure 6.3a). In contrast to the findings in the roots, the levels of serotonin (SER) in the basal

leaves were comparable to those in the untreated control (Figure 6.3b). This indicates that, at least in this part of the plant, the absorbed TAM is not converted into SER.

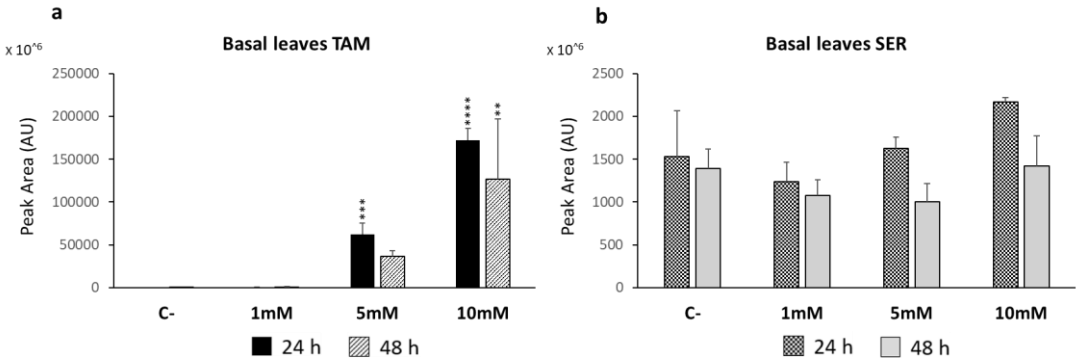

*Figure 6.3. Relative levels of TAM (a) and SER (b) in the basal leaves of plant treated with different concentration of TAM and sampled at 24- and 48-hours post-treatment. Tryptamine and serotonin levels were detected by LC-ESI-MS analysis and are expressed as peak area (arbitrary units - AU), bars indicate standard deviations (n=3; biological replicates). Values are reports as means ± standard deviation. Student's t-test was used for the statistical analysis (*P < 0.05; **P < 0.01; ***P < 0.001).*

The apical leaves exhibited the highest levels of TAM, which were significantly greater than the control in the 10 mM treatment sampled at 24 hours, as well as in the 5 mM and 10 mM treatments sampled at 48 hours (Figure 6.4a). Notably, in these organs — particularly those from plants treated with 10 mM of TAM — the levels of serotonin (SER) were found to be 5-6 times higher than those in the control (Figure 6.4b)

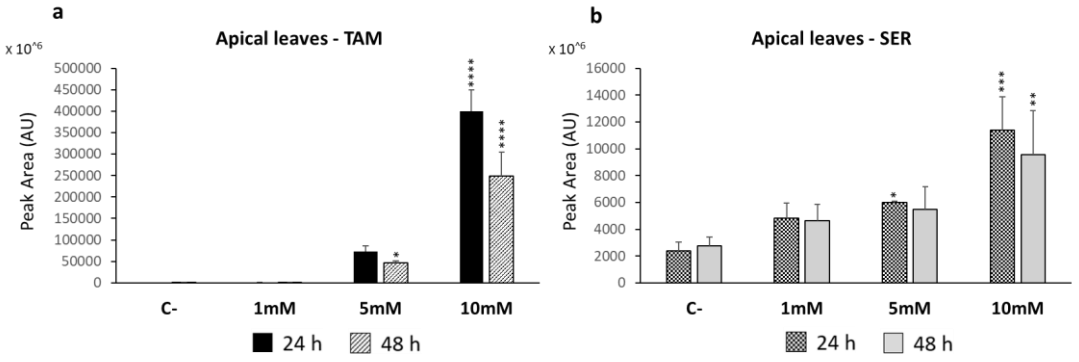

Figure 6.4. Relative levels of TAM (a) and SER (b) in the apical leaves of plant treated with different concentration of TAM and sampled at 24- and 48-hours post-treatment. Tryptamine and serotonin levels were detected by LC-ESI-MS analysis and are expressed as peak area (arbitrary units - AU), bars indicate standard deviations (n=3; biological replicates). Values are reports as means ±

*standard deviation. Student's t-test was used for the statistical analysis (*P < 0.05; **P < 0.01; ***P < 0.001).*

Based on these results, it can be hypothesized that the TAM absorbed in the roots is not only taken up and translocated to the aerial vegetative organs, with the higher leaves that represents the final site of accumulation along the stem, but is also converted into SER. This conversion is particularly evident in the roots and apical leaves. In the case of the basal leaves, where SER levels are comparable to those in the control, two hypotheses can be proposed: either SER is translocated toward the vegetative apex, contributing to the increased SER levels observed in the apical leaves and vegetative apex, or it is converted into another metabolite that has yet to be identified.

Although the system requires further optimization, the results obtained offer valuable insights for refining both the administration protocol and the experimental design. Implementing a more detailed sampling approach — analyzing various sections of the plant instead of solely focusing on the basal and apical leaves — could enhance resolution and yield clearer information regarding the fate of the absorbed TAM.

Chapter 7 - Discussion

7.1 Complex networks in metabolic regulation of tryptamine and serotonin biosynthesis emerge from the analysis of *SlTDC1*- and *SlT5H*-overexpressing lines

7.1.1 Two distinct hypothetical models for the regulation of TAM and SER biosynthesis in roots and leaves, and in fruits and seeds of tomato plant

The comparative analysis of *SlTDC1* and *SlT5H* expression profiles with the levels of TAM and SER in roots, leaves, ripe fruits, and seeds of the *SlTDC1*-OE lines revealed both expected and unexpected outcomes. The aim of *SlTDC1* overexpression was to enhance the production of TAM and SER throughout the tomato plant, to shed light on the roles of these two metabolites. Metabolomic analysis revealed that only SER levels increased, specifically in roots and leaves. In contrast, ripe fruits and seeds exhibited a strong depletion of both SER and TAM. Consistent with metabolomics data, in the roots and leaves of *SlTDC1*-OE lines, a 0.5- to 1.5-fold increase in *SlTDC1* expression led to a significant upregulation of *SlT5H* expression, with levels being 2- to 20-fold higher than in the control. The heightened *SlT5H* activity explains the marked increase in SER levels (5- to 10-fold), while TAM levels remained comparable to those of the control. These findings suggest that the excess of TAM is readily converted into SER by T5H, whose activity is enhanced due to the increased *SlT5H* expression. It can be hypothesized that *SlT5H* expression might be regulated by TAM levels (Figure 7.1). In line with this observation, also Tsunoda et al. (2021) reported that *SlTDC1* overexpression is associated with increased *SlT5H* activity and higher SER levels (Tsunoda et al., 2021). Further evidence supporting the correlation between TAM levels, T5H activity, and SER biosynthesis was provided by results from the exogenous application of TAM at the root level (described in Chapter 6). These experiments revealed that increasing TAM concentrations in the medium correlated with higher SER levels in roots and apical leaves. Similarly, Kang et al., (2007) reported a dose-dependent increase in SER levels in rice following exogenous TAM application, accompanied by a parallel increase in T5H activity (Kang et al., 2007a).

Unexpectedly, despite the high levels of *SlTDC1* expression compared to the control, ripe fruits from the three *SlTDC1*-OE lines exhibited a strong depletion of both TAM and SER. Interestingly, *SlT5H* expression levels varied among the lines: it increased in one line but decreased in the other two. The mechanism underlying this unexpected result remains unclear and requires further investigation. However, some speculative hypothesis can be proposed (see the model in Figure 7.2): TAM might inhibit *TDC1* mRNA translation or enzyme activity, and/or SER could be promptly removed by the activation of downstream enzymes (Back, Tan, and Reiter, 2016b; Wegner et al., 2015). Nevertheless, this hypothesis also implies that the mechanism responsible for *TDC1* inhibition should not be active in leaves and roots, where *TDC1* overexpression led to increased SER levels. Notably, seeds produced by these lines also showed a strong reduction in TAM and SER, indicating that, among the analyzed organs, the mechanism responsible for this phenotype occurred exclusively in fruits and seeds. The depletion observed in the three *SlTDC1*-OE lines suggests the presence of a regulatory mechanism, such as the one proposed in the model in Figure 7.2, which prevented the overaccumulation of TAM or SER in fruits and seeds.

The analysis of TAM and SER levels in various organs of the *SlT5H*-OE lines, which were designed to produce higher levels of SER at the expense of TAM, revealed that SER levels increased exclusively in the ripe fruits of two overexpressing lines (OE-2 and OE-3). Notably, this increase – approximately 1.3- to 1.7-fold compared to the control – was not accompanied by a reduction in TAM. Additionally, TAM levels were noted to rise only in the seeds of line OE-1, while no significant differences in the levels of these two metabolites were detected in the roots and leaves of the three *SlT5H*-OE lines. Based on these findings, and considering that *TDC* acts as the rate-limiting step in this pathway (Mannino et al., 2021), it can be proposed that, without an upregulation of *TDC* — and therefore an adequate supply of TAM — *SlT5H* overexpression alone is insufficient to further enhance SER production. This hypothesis is supported by the results obtained from the exogenous application of 10 mM TAM, which led to a significant increase in SER

production, with levels in the apical leaves being 5- to 6-fold higher than in untreated controls. On the other hand, considering the low catalytic efficiency of TDC compared to T5H (Mannino et al., 2021b), it was expected that the overexpression of *SlT5H* would result in the complete depletion of TAM in favor of SER. However, at least in the analyzed organs, this did not occur. These findings suggest the existence of a regulatory mechanism that ensures the maintenance of basal TAM levels, regardless of *SlT5H* activity. For instance, Kang et al. (2007) described a negative feedback mechanism in rice, where SER suppresses *TDC* expression. It is therefore plausible that, also in tomato, the activity of the genes responsible for TAM and SER biosynthesis may be modulated by the relative abundance of these metabolites. In the model proposed in Figure 7.2, decreased TAM levels would promote TAM production through increased *TDC1* mRNA translation and/or TDC1 enzyme activity, thereby maintaining TAM levels within a certain range. Interestingly, as reported by Commisso et al. (2022), in the wild-type Micro-Tom genotype, TAM tends to accumulate in specific organs, such as fruits and seeds. This suggests that not all TAM is converted into SER by T5H, despite its high catalytic efficiency. Organ-specific control of TAM levels in tomato may depend not only on the organ-specific expression of the three different tomato *TDCs*, as observed by Commisso et al. (2022), but also on unidentified mechanisms regulating *TDC* mRNA translation and/or enzyme activity. These mechanisms likely allow for the fine-tuned accumulation of TAM and/or SER depending on the organ and developmental stage. By integrating findings from our research with existing literature, we proposed two different models for the regulation of TAM and SER biosynthesis in root/leaf (Figure 7.1), and fruit/seed (Figure 7.2) in tomato plant. According to the first model (Figure 7.1), in root and leaf *SlT5H* is upregulated by high levels of TAM, which are promptly converted into SER. In this way, the ratio between TAM and SER in these organs is maintained in favor of SER, as observed in the work published by Commisso et al. (2022).

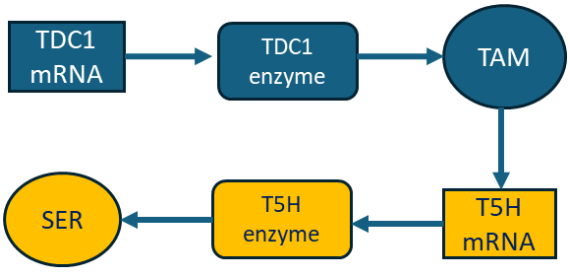

Figure 7.1. Hypothetical model for the regulation of TAM and SER biosynthesis in root and leaf of Solanum lycopersicum cv. Micro-Tom.

Regarding the regulatory model proposed for fruits and seeds (Figure 7.2), low TAM levels, induced by its efficient conversion into SER by T5H, promote *TDC1* transcription, resulting in increased TAM and SER levels. However, when TAM exceeds a certain threshold, it self-inhibits its production (product inhibition), acting either at the level of *TDC1* transcript or enzyme activity, thereby maintaining stable TAM and SER levels. Additionally, the excess of SER may be redirected toward the production of downstream metabolites. To validate this model, further analyses will be necessary, and additional insights may be obtained by exploring the expression levels of genes downstream in the serotonin pathway, particularly *SNAT* and *ASMT/COMT*, which are involved in the conversion of SER into melatonin.

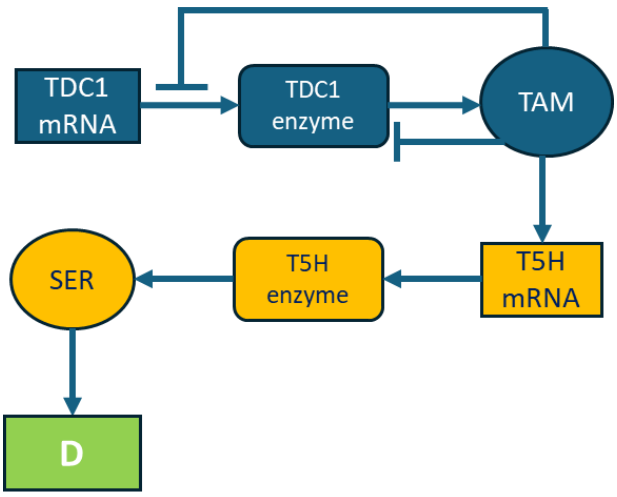

Figure 7.2. Hypothetical model for the regulation of TAM and SER biosynthesis in fruit and seed of Solanum lycopersicum cv. Micro-Tom.

7.1.2 The knockout of SlTDC1 and SlT5H genes confirm their role in the biosynthesis of TAM and SER in tomato

The metabolomic analysis conducted on various organs of the *sltdc1* and *slt5h* mutants definitively demonstrated the role proposed by Commisso et al. (2022) regarding the *SlTDC1* and *SlT5H* genes in the biosynthesis of tryptamine (TAM) and serotonin (SER) in tomato. This analysis specifically addressed the fruit- and seed-specific activity of the *SlTDC1* gene and the ubiquitous expression pattern of the *SlT5H* gene. In the *sltdc1* mutants, the knockout of the *SlTDC1* gene resulted in a complete depletion of TAM and SER in fruits and seeds, whereas in other analyzed organs (leaves and roots), the levels of these two metabolites did not show statistically significant variations compared to the wild-type Micro-Tom genotype, that can be explained with the expression of the other *TDCs* in these organs, as shown by Commisso et al. (2022). As for the *slt5h* mutants, the knockout of the unique *SlT5H* gene induced a substantial accumulation of TAM in all analyzed organs (roots, leaves, mature fruits, and seeds) and a complete depletion of SER in roots, mature fruits, and seeds. Interestingly, in the leaves of these lines, a complete depletion of SER was not observed, although its levels were still drastically lower compared to the control. This result may suggest, as particularly observed in rice, the existence of an alternative pathway for SER production, similar to that present in vertebrates, based on the hydroxylation of TAM by a tryptophan-5-hydroxylase or a plant enzyme with similar activity, which has not yet been identified (Park et al. 2012). In Sekiguchi rice mutants, characterized by the lack of *SlT5H* gene activity, low SER levels were detected, analogous to what was observed in the leaves of our *slt5h* mutants.

7.2 Phenotypic analysis of *SlTDC1*-OE and *slt5h* lines revealed a potential role of TAM and SER in tomato reproductive development

As discussed in the introductory chapter, serotonin (SER) is crucial for various biological processes in plants, including protection against biotic and abiotic stresses, regulation of root and shoot organogenesis, promotion of somatic embryogenesis *in-vitro*, seed germination, and chrono-regulation. Several mechanisms have been proposed to explain SER's activity. These include cross-talk with phytohormones such as auxin, jasmonic acid, and abscisic acid, as well as interaction with intracellular signaling pathways, particularly those mediated by calcium/calmodulin (Erland et al., 2015). Additionally, SER exhibits antioxidant activity by scavenging reactive oxygen species (ROS) and modulating gene expression within primary metabolic networks (Erland et al., 2015; Erland, Turi, and Saxena, 2016). While receptors for SER have been identified in vertebrates and invertebrates, none have been found in plants. It is hypothesized that, due to structural similarities between auxin, SER, and melatonin (MEL), these indolamines may interact with auxin receptors, which also applies to tryptamine (TAM), the precursor of both SER and MEL. Recent findings indicate that auxin can modulate the SER/MEL ratio, influencing plant growth and morphogenesis. This balance may resemble the auxin/cytokinin interplay, which regulates root and shoot development (Mishra and Sarkar, 2023b). However, many hypotheses rely on exogenous applications of SER (and MEL) at unnatural concentrations, leading to contradictory results. These observations underscore the necessity for reliable systems to study indolamines in vivo, such as transgenic or CRISPR-edited plants. The primary goal of this thesis is to engineer tomato plants to produce mutants with altered TAM and SER levels to investigate their biological roles, since the mechanisms through which TAM, and SER exert their functions in plants remain largely unclear (and this is especially true for TAM), representing a significant area of interest in plant biology. Due to time constraints, not all the possible metabolomic analyses on key organs, such as apical leaves during pre-flowering, floral buds, flowers at anthesis, were performed, being the work mainly focused

on leaves during the vegetative growth phase, roots, seeds and ripe fruits. These analyses, along with the determination of MEL, and auxin levels, will be conducted in the coming months to better interpret the obtained phenotypic and molecular findings.

7.2.1. The overexpression and knockout of the SlTDC1 gene resulted in distinct effects on the reproductive development of Micro-Tom

Following the characterization of the *SlTDC1*-OE and *sltdc1* lines, no significant phenotypes related to vegetative development were observed. For the *sltdc1* lines, this result was expected, as the *SlTDC1* gene, as confirmed by metabolomic analyses, is characterized by seed- and fruit-specific expression, while leaves and root express *SlTDC2/SlTDC3* (Commisso et al., 2022). In the *SlTDC1-OE* lines, which are characterized by higher SER accumulation in roots and leaves, the absence of phenotypes related to vegetative development aligns with the findings of Tsunoda et al. (2021), who reported that overexpression of the *SlTDC1* in Micro-Tom does not affect vegetative growth. Although the literature suggests a link between SER and shoot growth and development (Erland et al., 2015), this molecule has never been clearly established as a determining factor for the final size of the plant. Concerning reproductive development, interesting phenotypes were observed in both *SlTDC1*-OE and *sltdc1* lines. The *SlTDC1*-OE lines, characterized by elevated SER levels in leaves, showed a faster transition from the vegetative to the reproductive stage. These lines exhibited a reduction in the number of true leaves, averaging one leaf less than the *sltdc1* lines. This was accompanied by an earlier appearance of flower buds, which occurred 2 to 4 days earlier than those in the *sltdc1* lines, as well as an early onset of first anthesis, which occurred 2 to 3 days earlier than in the *sltdc1* lines. Additionally, these lines exhibited a higher number of daily anthesis throughout the entire flowering period, compared to both the control and the *sltdc1* lines. In plants, phytochromes are involved in physiological processes such as photomorphogenesis, seed germination, and the regulation of flowering time. The ability of SER to interact with phytochrome and modulate its activity has led some authors to hypothesize a role for SER in flowering time

regulation, although this theory is not currently supported by convincing experimental data (Anon, 2017; Negri et al., 2021). The earlier onset of flowering observed in the *SlTDC1*-OE lines could be linked to increased MEL levels (not yet determined in our lines). Recently, in *sant* mutants of *A. thaliana*, a reduced MEL content was associated with a slight delay in flowering, which the authors attributed to decreased GA biosynthesis and the consequent downregulation of the *FT* (*FLOWERING LOCUS T*) gene (Arnao and Hernández-Ruiz, 2020; Lee and Back, 2019). It is possible to speculate that, in the *SlTDC1*-OE lines, an increase in MEL levels could have exerted the opposite effect, thereby resulting in the observed earlier onset of flowering. Concerning the *sltdc1* lines, which exhibited a reduction in the number of flowers produced by the main inflorescence (and consequently in the number of ripe fruits), this phenotype is particularly challenging to interpret, especially considering that *SlTDC1* is mainly expressed in the fruit and seed, with very low expression levels in floral buds, where instead the activities of *SlTDC2* and *SlTDC3* predominate. However, it cannot be ruled out that the knockout of the *SlTDC1* gene may have induced imbalances in the levels of TAM and SER (or MEL as well) in the flowers, interfering with floral induction and inflorescence meristem differentiation. In various plant species, fluctuations in SER levels have been observed during different stages of flower development; however, the precise role of this molecule and the significance of its level fluctuations during flowering remain unclear (Erland et al., 2015; Erland et al., 2018). Given that SER possesses antioxidant activity and tends to accumulate in the tissues of developing reproductive organs, which are characterized by intense metabolic activity, it has been hypothesized that, like MEL, SER could exert a protective role (Erland et al., 2015). The lack of clear and unequivocal experimental evidence regarding the role of SER in plant reproductive development makes it difficult to draw definitive conclusions about the observed phenotypes. The interplay between SER and MEL, the chemical-structural similarities between these two indolamines, and the incomplete and often contradictory information available in the literature further complicate the

attribution of specific functions to SER, which has been much less studied compared to MEL. To interpret the observed phenotypes in the *SlTDC1*-OE and *sltdc1* lines, further analyses will be necessary, particularly focusing on the levels of TAM, SER, and MEL in apical leaves and the shoot apex during the pre-flowering phase, as well as in floral buds, and flowers at anthesis.

*7.2.2 Phenotypic divergence in SlT5H-*OE *and slt5h lines: implications for stem growth and floral bud emergence*

Preliminary phenotypic analysis of the *SlT5H*-OE and *slt5h* lines revealed different outcomes compared to those obtained from the characterization of the *SlTDC1*-OE and *sltdc1* lines. Both the *SlT5H*-OE and *slt5h* lines exhibited shorter stems compared to the control. Similar to the *SlTDC1*-OE lines, the *SlT5H*-OE lines also showed a reduction in the number of true leaves, accompanied by the earlier emergence of floral buds. However, unlike the *SlTDC1*-OE lines, in the *SlT5H*-OE lines, the faster transition from the vegetative to the reproductive phase did not result in an earlier onset of anthesis. These results — early emergence of floral buds without an earlier onset of anthesis and without changes in metabolite levels — adds an additional layer of complexity to the interpretation of the observed phenotypes. In contrast to the *SlT5H*-OE lines, the shorter stem observed in the *slt5h* lines was associated solely with the reduction in overall plant size, without the decrease in the number of true leaves or the earlier emergence of floral buds. Therefore, the mechanisms underlying the phenotypes observed in the *SlT5H*-OE and *slt5h* lines appear to be different. This is consistent with the differing levels of TAM and SER observed in the knockout lines compared to those in the overexpressing lines. The *slt5h* lines exhibited, as expected, a significant accumulation of TAM in both the roots and leaves, along with a complete depletion of SER in the roots and an almost complete depletion of SER in the leaves. Several studies have highlighted the role of MEL in upregulating genes associated with biosynthesis of gibberellic acid (GA), a plant hormone that influences various morphological traits, including stem elongation (Arnao and Hernández-Ruiz, 2018). Thus, it can be hypothesized that the significant depletion

of SER observed in the *slt5h* lines leads to a reduction in endogenous MEL levels, which in turn inhibits GA synthesis and results in stem shortening. Furthermore, the observed changes in TAM and SER levels could also have disrupted auxin signaling, although this hypothesis seems less likely, as the plants, despite exhibiting reduced height, did not show altered apical dominance. In *Zea mays*, SER has been shown to promote phosphoinositide turnover and function as a primary messenger in the activation of far-red phytochrome (Pfr), which operates upstream of nitrate reductase—an enzyme essential for nitrogen metabolism and, consequently, for vegetative development. Therefore, it can be hypothesized that a reduction in SER may negatively impact vegetative development, potentially accounting for the reduced size of the *slt5h* lines (Mishra and Sarkar, 2023). It should be noted that the literature presents conflicting results regarding the role of SER in regulating vegetative development. For example, Byeon et al. (2016) observed that in *snat* rice mutants, characterized by an accumulation of SER and a depletion of MEL, the seedlings exhibited slower stem elongation (Byeon and Back, 2016). Conversely, Kang et al. (2007) reported no phenotypic effects in transgenic rice lines overexpressing the *TDC* gene and characterized by high levels of SER (Kang et al., 2007). MEL levels were not measured in this study, suggesting that the effects observed by Byeon et al. (2016) may be attributed to an imbalance in the MEL/SER ratio rather than to SER accumulation alone. In light of the data obtained from the characterization of the *SlT5H*-OE and *slt5h* lines, and considering the limited scientific literature on the subject, it remains challenging to attribute the observed phenotypes solely to TAM and SER levels. The overlap between SER and MEL in regulating these phenotypes is once again evident. On the other hand, it is important to note that it seems highly unlikely that the predominant role of SER (and also of TAM in fruits and seeds, where TAM accumulates at high levels) is limited to its function as MEL intermediate. This is especially true given that the levels of SER in all measured organs, as well as the levels of TAM in reproductive tissues, are far higher than those required for MEL biosynthesis. The massive accumulation of these metabolites suggests that they

act locally (SER everywhere, TAM in fruits and seeds) not only as precursors of MEL but also as final metabolic products. Similar to the findings from the *SlTDC1*-OE and *sltdc1* lines, further phenotypic and molecular analyses will be necessary to elucidate the mechanisms underlying the results obtained from the phenotyping of the *SlT5H*-OE and *slt5h* lines.

7.2.3 Seeds from sltdc1 lines are characterized by a reduced germinability and exhibit a dark pigmentation of the seed coat

The most evident phenotypes emerging from the characterization of the *SlTDC1*-OE and *sltdc1* lines were observed in the seeds, particularly those produced by the *sltdc1* lines. Seeds of both *SlTDC1*-OE and *sltdc1* lines exhibited reduced germinability. In the *sltdc1* lines, this reduction was especially pronounced, with values falling below 50% across all three *sltdc1* genotypes, ranging from 16% in the KO-3 line to 37% in the KO-2 line. Additionally, the *sltdc1* lines displayed an increase in the Mean Days to Germination (MDG), a parameter that reflects not only the average time required for germination but also provides insights into overall seed viability. The *SlTDC1*-OE and *sltdc1* lines were characterized by a drastic reduction in TAM content compared to the control. In terms of SER, the *SlTDC1*-OE lines exhibited a marked reduction relative to the control, whereas the *sltdc1* lines were completely depleted. As mentioned in the previews paragraph, since SER has often been found at high concentrations in the tissues of reproductive organs, several authors have hypothesized that it plays a protective role in these organs (Anon, 2017; Erland, Turi, and Saxena, 2016/2018). SER tends to accumulate in the embryos and endosperm of various plant species, including *Juglans regia*, *Vitis vinifera*, and *Solanum lycopersicum* (Commisso et al., 2022; Erland et al., 2015; Negri et al., 2021). However, the mechanisms by which SER acts remain unclear, with its effects largely attributed to its antioxidant properties. SER has also been positively associated with the germination process and the development and growth of seedlings in various plant species, including *Capsicum annuum* L., *Zea mays*, *Raphanus sativus L.*, *Hordeum vulgare*, and *Helianthus annuus*, both under normal conditions and abiotic stress (Anon, 2017; Araz,

Yildirim, and Ekinci, 2021; Mukherjee et al., 2014; Zhao et al., 2023). However, most of these studies have been conducted thorough the exogenous application of SER or have been limited to analyzing variations in SER content during germination and seedling development, without providing detailed insights into the mechanisms by which SER exerts its stimulatory or protective functions. In this context, the available literature often overlaps with studies on MEL. It is likely that the MEL/SER ratio, along with their cross-talk with other plant hormones, including auxins and cytokinins, also plays an important role in germination and seedling development. Regarding the dark pigmentation observed in the seeds of the *sltdc1* lines, it has recently been observed that MEL can influence the synthesis of anthocyanins and proanthocyanidins (PAs) in the seeds of *A. thaliana*. In the double mutants *sant1-1/comt1*, characterized by MEL depletion, the *KFB39* gene (*KIP-RELATED PROTEIN 39*), a transcription factor involved in the negative regulation of anthocyanin biosynthesis, was downregulated. Conversely, genes involved in flavonoid biosynthesis, including *4CL* (*4-Coumaroyl-CoA Ligase*), *CHI* (Chalcone Isomerase), and *KAN4* (a transcription factor involved in the positive regulation of flavonoid biosynthesis), were upregulated. In these mutants, an increased accumulation of anthocyanins and proanthocyanidins (PAs) was observed in the seed coat (Li et al., 2020). Conversely, the exogenous application of MEL resulted in a reduction in anthocyanin and PAs levels in mature seeds. In another study conducted on *A. thaliana*, the exogenous application of PAs reduced seed germinability. Following MEL treatment, the authors observed an increase in ABA levels, which inhibited endosperm weakening and radicle elongation, negatively affecting the germination process (Jia et al., 2012). Other studies conducted on *A. thaliana* and *V. vinifera* have shown that excessive accumulation of proanthocyanidins (PAs) in leaves can have deleterious effects, even leading to plant death (Bogs et al., 2007; Sharma and Dixon, 2005). Based on these findings, it can be hypothesized that the dark seed coat pigmentation and the reduced germinability observed in the seeds of the *sltdc1* lines may be attributed to the depletion of MEL and the consequent accumulation of PAs, rather than the

depletion of SER. This hypothesis seems to be supported by the observation that seeds produced by the *slt5h* lines, despite being characterized by SER depletion, did not exhibit the reduced germinability observed in the seeds of the *sltdc1* lines. The absence of dark seed coat pigmentation in the seeds of the *slt5h* lines may be explained by the fact that the excess TAM present in these seeds could be partly utilized for MEL production via an alternative SER-independent pathway. This pathway does not rely on SER and instead uses TAM, which is converted into N-acetylserotonin by the SNAT enzyme (Byeon et al., 2014). To confirm the hypotheses formulated in this paragraph, further analyses will be necessary, particularly the determination of MEL, PAs, and ABA levels in developing and mature seeds of the *sltdc1* and *slt5h* mutants.

7.3 Conclusion and future perspective

Although definitive conclusions cannot be drawn, this study has provided significant insights into the regulatory mechanisms governing the biosynthesis of TAM and SER in the analyzed organs of tomato plants, as well as their roles in regulating vegetative and reproductive development. Analysis of *SlTDC1* and *SlT5H* expression in *SlTDC1*-OE lines demonstrated that *SlT5H* activity is linked to *SlTDC1* activity and consequently, to endogenous TAM levels. Specifically, TAM levels influence both *SlT5H* activity and SER levels in roots and leaves. In fruits and seeds, TAM and SER levels appear to be regulated by a process that prevents excessive accumulation of these molecules, although the underlying mechanisms remain unclear. It is likely that in these organs, TAM exerts control over *SlTDC1* activity, either at the transcript or enzyme level, helping the plant maintain TAM and SER levels within a specific range. Analysis of indolamine levels in *sltdc1* and *slt5h* lines confirmed the fruit- and seed-specific activity of *SlTDC1* and the ubiquitous activity of *SlT5H*, as proposed in the model developed by Commisso et al. (2022). The most interesting results emerged from the phenotypic analysis of these lines, particularly in *SlTDC1*-OE lines, which exhibited faster vegetative-to-reproductive transition and reduced seed germinability, and in *sltdc1* lines, which showed a strong reduction in seed germinability and viability, along with dark pigmentation of the seed coat. In these lines, although not clearly, the observed phenotypes correlate with variations in TAM and SER levels. Similarly, in *slt5h* lines, characterized by reduced stem length, this phenotype may be associated with increased TAM and depleted SER levels in roots and leaves. In contrast, associating phenotypes with indolamine levels in *SlT5H*-OE lines is more challenging, as these lines showed no significant variation in TAM and SER levels in the analyzed organs, except for increased SER in ripe fruits. Interpretation of the results is complicated by the lack of literature on TAM's role in physiological processes, the frequent overlap in roles attributed to MEL and SER, and the proven interplay between SER and MEL, as well as between these molecules and various plant hormones. Additionally, the mechanisms of action for MEL and SER remain unclear. For

instance, regarding the evident phenotypes observed in *sltdc1* seeds (reduced germinability and dark phenotype), there is no clear information on SER's role in the germination process. However, literature suggests a negative correlation between MEL levels in seeds and the synthesis of polyamines (PAs), which could be responsible for the dark seed coat pigmentation and reduced germinability observed in the *sltdc1* lines. Future studies should integrate the quantification of MEL, key hormones (auxins, gibberellins, ABA), anthocyanins, and PAs in organs exhibiting observed phenotypes, such as stems, apical leaves, floral buds, flowers at anthesis, and seeds, to clarify the roles of TAM and SER in plant vegetative and reproductive development and the biochemical processes they regulate. Untargeted metabolomic analyses in these genotypes could identify unknown downstream molecules influenced by the modulation of *TDC1* and *T5H* activity. Additionally, analyzing the expression profiles of the genes located downstream of SER, would provide additional insights into how TAM and SER levels affect downstream metabolites, refining the proposed models for TAM and SER regulation in roots and leaves, and fruits and seeds. Optimizing protocols for TAM exogenous application, including the use of deuterium-labeled TAM, could help to clarify the hypothesized alternative biosynthetic pathways for SER in leaves and MEL in seeds of *slt5h* lines. Further insights into TAM and SER roles in development could also be gained by characterizing *SlTDC2*-KO and triple-*SlTDC1/SlTDC2/SlTDC3*-knockout lines. Finally, although TAM's deterrent effect on herbivorous insects is documented, research is limited, and the underlying mechanisms remain largely unexplored, especially in tomatoes. Investigating interactions between *slt5h* lines with elevated TAM levels and phytophagous insects could provide valuable insights into TAM's proposed role in enhancing plant defense against pests.

Bibliography

Akcay, Ufuk Celikkol, and Nilgun Okudan. 2023. “Exogenous Serotonin Improves Drought and Salt Tolerance in Tomato Seedlings.” *Plant Growth Regulation* 101(1):239–49. doi: 10.1007/s10725-023-01016-x.

Al-Soqeer, Abdulrahman A., Qasi D. Alsubaie, Mohamed I. Motawei, Hassan M. Mousa, and Ahmed M. Abdel-Salam. 2017. “Isolation and Identification of Allergens and Biogenic Amines of Prosopis Juliflora Genotypes.” *Electronic Journal of Biotechnology* 30:24–32. doi: 10.1016/j.ejbt.2017.08.005.

Araújo, Ana Margarida, Félix Carvalho, Maria de Lourdes Bastos, Paula Guedes de Pinho, and Márcia Carvalho. 2015. “The Hallucinogenic World of Tryptamines: An Updated Review.” *Archives of Toxicology* 89(8):1151–73. 10.1007/s00204-015-1513-x.

Arnao, Marino B., and J. Hernández-Ruiz. 2018. “Melatonin and Its Relationship to Plant Hormones.” *Annals of Botany* 121(2):195–207. doi: 10.1093/aob/mcx114.

Arnao, Marino B., and J. Hernández-Ruiz. 2020. “Melatonin in Flowering, Fruit Set and Fruit Ripening.” *Plant Reproduction* 33(2):77–87. doi: 10.1007/s00497-020-00388-8.

Arnao, Marino B. 2014. “Phytomelatonin: Discovery, Content, and Role in Plants.” *Advances in Botany* 2014:1–11. doi: 10.1155/2014/815769.

Arnao, Marino B., Antonio Cano, and Josefa Hernández-Ruiz. 2022. “Phytomelatonin: An Unexpected Molecule with Amazing Performances in Plants.” *Journal of Experimental Botany* 73(17):5779–5800. doi: doi.org/10.1093/jxb/erac009.

Back, Kyoungwhan. 2021. “Melatonin Metabolism, Signaling and Possible Roles in Plants.” *Plant Journal* 105(2):376–91. doi: 10.1111/tpj.14915.

Back, Kyoungwhan, Dun Xian Tan, and Russel J. Reiter. 2016a. “Melatonin Biosynthesis in Plants: Multiple Pathways Catalyze Tryptophan to Melatonin in the Cytoplasm or Chloroplasts.” *Journal of Pineal Research* 61(4):426–37. doi: 10.1111/jpi.12364.

Bajguz, Andrzej, and Alicja Piotrowska-Niczyporuk. 2023. “Biosynthetic Pathways of Hormones in Plants.” *Metabolites* 13(8). doi: 10.3390/metabo13080884.

Bhattarai, Yogesh, Brianna B. Williams, Eric J. Battaglioli, Weston R. Whitaker, Lisa Till, Madhusudan Grover, David R. Linden, Yasutada Akiba, Karunya K. Kandimalla, Nicholas C. Zachos, Jonathan D. Kaunitz, Justin L. Sonnenburg, Michael A. Fischbach, Gianrico Farrugia, and Purna C. Kashyap. 2018. “Gut Microbiota-Produced Tryptamine Activates an Epithelial G-Protein-Coupled Receptor to Increase Colonic Secretion.” *Cell Host and Microbe* 23(6):775-785.e5. doi: 10.1016/j.chom.2018.05.004.

Bradley, Samuel A., Beata J. Lehka, Frederik G. Hansson, Khem B. Adhikari, Daniela Rago, Paulina Rubaszka, Ahmad K. Haidar, Ling Chen, Lea G. Hansen, Olga Gudich, Konstantina Giannakou, Bettina Lengger, Ryan T. Gill, Yoko Nakamura, Thomas Dugé de Bernonville, Konstantinos Koudounas, David Romero-Suarez, Ling Ding, Yijun Qiao, Thomas M. Frimurer, Anja A. Petersen, Sébastien Besseau, Sandeep Kumar, Nicolas Gautron, Celine Melin, Jillian Marc, Remi Jeanneau, Sarah E. O'Connor, Vincent Courdavault, Jay D. Keasling, Jie Zhang, and Michael K. Jensen. 2023. "Biosynthesis of Natural and Halogenated Plant Monoterpene Indole Alkaloids in Yeast." *Nature Chemical Biology* 19(12):1551–60. doi: 10.1038/s41589-023-01430-2.

Byeon, Yeong, and Kyoungwhan Back. 2016. "Low Melatonin Production by Suppression of Either Serotonin N-Acetyltransferase or N-Acetylserotonin Methyltransferase in Rice Causes Seedling Growth Retardation with Yield Penalty, Abiotic Stress Susceptibility, and Enhanced Coleoptile Growth under Anoxic Conditions." *Journal of Pineal Research* 60(3):348–59. doi: 10.1111/jpi.12317.

Byeon, Yeong, Hyoung Yool Lee, Kyungjin Lee, and Kyoungwhan Back. 2014. "Caffeic Acid O-Methyltransferase Is Involved in the Synthesis of Melatonin by Methylating N-Acetylserotonin in Arabidopsis." *Journal of Pineal Research* 57(2):219–27. doi: 10.1111/jpi.12160.

Clay, Nicole K., Adewale M. Adio, Carine Denoux, Georg Jander, and Frederick M. Ausubel. 2009. "Glucosinolate Metabolites Required for an Arabidopsis Innate Immune Response". *Science*, *323*(5910), 95-101. doi: 10.1126/science.1164627.

Commisso, Mauro, Stefano Negri, Elisa Gecchele, Emanuela Fazion, Cecilia Pontoriero, Linda Avesani, and Flavia Guzzo. 2022. "Indolamine Accumulation and TDC/T5H Expression Profiles Reveal the Complex and Dynamic Regulation of Serotonin Biosynthesis in Tomato (Solanum lycopersicum L.)." *Frontiers in Plant Science* 13. doi: 10.3389/fpls.2022.975434.

Dangol, Anuma, Reut Shavit, Beery Yaakov, Susan R. Strickler, Georg Jander, and Vered Tzin. 2022. "Characterizing Serotonin Biosynthesis in Setaria Viridis Leaves and Its Effect on Aphids." *Plant Molecular Biology* 109(4–5):533–49. doi: 10.1007/s11103-021-01239-4.

Danilovich, M. E., M. R. Alberto, and M. S. Juárez Tomás. 2021. "Microbial Production of Beneficial Indoleamines (Serotonin and Melatonin) with Potential Application to Biotechnological Products for Human Health." *Journal of Applied Microbiology* 131(4):1668–82. doi: 10.1111/jam.15012.

Doench, John G., Nicolo Fusi, Meagan Sullender, Mudra Hegde, Emma W. Vaimberg, Katherine F. Donovan, Ian Smith, Zuzana Tothova, Craig Wilen, Robert Orchard, Herbert W. Virgin, Jennifer Listgarten, and David E. Root. 2016. "Optimized SgRNA Design to Maximize Activity and Minimize Off-Target Effects of CRISPR-Cas9." *Nature Biotechnology* 34(2):184–91. doi: 10.1038/nbt.3437.

Erb, Matthias, and Daniel J. Kliebenstein. 2020. “Plant Secondary Metabolites as Defenses, Regulators, and Primary Metabolites: The Blurred Functional Trichotomy1[OPEN].” *Plant Physiology* 184(1):39–52. doi: 10.1104/pp.20.00433.

Erland, Lauren A. E., Susan J. Murch, Russel J. Reiter, and Praveen K. Saxena. 2015. “A New Balancing Act: The Many Roles of Melatonin and Serotonin in Plant Growth and Development.” *Plant Signaling and Behavior* 10(11). doi: 10.1080/15592324.2015.1096469.

Erland, Lauren A. E., Christina E. Turi, and Praveen K. Saxena. 2016. “Serotonin: An Ancient Molecule and an Important Regulator of Plant Processes.” *Biotechnology Advances* 34(8):1347–61. doi: 10.1016/j.biotechadv.2016.10.002.

Erland, Lauren A. E., and Praveen K. Saxena. 2017. "Beyond a neurotransmitter: the role of serotonin in plants." *Neurotransmitter* 4.5 1-12. doi: 10.14800/nt.1538.

Erland, Lauren A. E., Christina E. Turi, and Praveen K. Saxena. 2018. “Serotonin in Plants.” Pp. 23–46 in *Serotonin: The Mediator that Spans Evolution*. Elsevier.

Facchini, Peter J., Kara L. Huber-Allanach, and Leslie W. Tari. 2000. Plant Aromatic L-Amino Acid Decarboxylases: Evolution, Biochemistry, Regulation, and Metabolic Engineering Applications. Phytochemistry, 54(2), 121-138. doi: 10.1016/S0031-9422(00)00050-9.

Fernie, Alisdair R., and Eran Pichersky. 2015. “Focus Issue on Metabolism: Metabolites, Metabolites Everywhere.” *Plant Physiology* 169(3):1421–23. doi: 10.1104/pp.15.01499.

Fujiwara, Tadashi, Sylvie Maisonneuve, Masayuki Isshiki, Masaharu Mizutani, Letian Chen, Hann Ling Wong, Tsutomu Kawasaki, and Ko Shimamoto. 2010. “Sekiguchi Lesion Gene Encodes a Cytochrome P450 Monooxygenase That Catalyzes Conversion of Tryptamine to Serotonin in Rice.” *Journal of Biological Chemistry* 285(15):11308–13. doi: 10.1074/jbc.M109.091371.

Gill, Rishi I. S., and Brian E. Ellis. 2006. “Over-Expression of Tryptophan Decarboxylase Gene in Poplar and Its Possible Role in Resistance against Malacosoma Disstria.” *New Forests* 31(2):195–209. doi: 10.1007/s11056-005-2719-1.

Gonçalves, Sara, Daniela Nunes-Costa, Sandra Morais Cardoso, Nuno Empadinhas, and John David Marugg. 2022a. “Enzyme Promiscuity in Serotonin Biosynthesis, From Bacteria to Plants and Humans.” *Frontiers in Microbiology* 13. doi: 10.3389/fmicb.2022.873555.

Gonçalves, Sara, Daniela Nunes-Costa, Sandra Morais Cardoso, Nuno Empadinhas, and John David Marugg. 2022b. “Enzyme Promiscuity in Serotonin Biosynthesis, From Bacteria to Plants and Humans.” *Frontiers in Microbiology* 13. doi: 10.3389/fmicb.2022.873555.

González-Aguilera, Karla L., Carolina F. Saad, Ricardo A. Chávez Montes, Marcio Alves-Ferreira, and Stefan de Folter. 2016. “Selection of Reference Genes for

Quantitative Real-Time RT-PCR Studies in Tomato Fruit of the Genotype MT-Rg1." *Frontiers in Plant Science* 7(September). doi: 10.3389/fpls.2016.01386.

Grobe, Wolfgang. "Function of serotonin in seeds of walnuts." Phytochemistry 21.4 (1982): 819-822. doi: 10.1016/0031-9422(82)80071-X.

Grosse, W., M. Karisch, and P. Schröder. 1983. "Serotonin Biosynthesis and Its Regulation in Seeds of Juglans Regia L." *Zeitschrift Für Pflanzenphysiologie* 110(3):221–29. doi: 10.1016/s0044-328x(83)80104-4.

Gupta, Poulami, and Bratati De. 2017. "Metabolomics Analysis of Rice Responses to Salinity Stress Revealed Elevation of Serotonin, and Gentisic Acid Levels in Leaves of Tolerant Varieties." *Plant Signaling and Behavior* 12(7). doi: 10.1080/15592324.2017.1335845.

Hayashi, Keiko, Yoshikatsu Fujita, Taketo Ashizawa, Fumihiko Suzuki, Yoshiaki Nagamura, and Yuriko Hayano-Saito. 2016. "Serotonin Attenuates Biotic Stress and Leads to Lesion Browning Caused by a Hypersensitive Response to Magnaporthe Oryzae Penetration in Rice." *Plant Journal* 85(1):46–56. doi: 10.1111/tpj.13083.

Ishihara, Atsushi, Yumi Hashimoto, Chihiro Tanaka, Joseph G. Dubouzet, Takahito Nakao, Fumio Matsuda, Takaaki Nishioka, Hisashi Miyagawa, and Kyo Wakasa. 2008. "The Tryptophan Pathway Is Involved in the Defense Responses of Rice against Pathogenic Infection via Serotonin Production." *Plant Journal* 54(3):481–95. doi: 10.1111/j.1365-313X.2008.03441.x.

Kang, Sei, Kiyoon Kang, Kyungjin Lee, and Kyoungwhan Back. 2007a. "Characterization of Rice Tryptophan Decarboxylases and Their Direct Involvement in Serotonin Biosynthesis in Transgenic Rice." *Planta* 227(1):263–72. doi: 10.1007/s00425-007-0614-z.

Kerwin, Rachel E., Jose M. Jimenez-Gomez, Daniel Fulop, Stacey L. Harmer, Julin N. Maloof, and Daniel J. Kliebensteina. 2011. "Network Quantitative Trait Loci Mapping of Circadian Clock Outputs Identifies Metabolic Pathway-to-Clock Linkages in Arabidopsis." *Plant Cell* 23(2):471–85. doi: 10.1105/tpc.110.082065.

khan, Muhammad zahid, and Waqas nawaz. 2016. "The Emerging Roles of Human Trace Amines and Human Trace Amine-Associated Receptors (HTAARs) in Central Nervous System." *Biomedicine and Pharmacotherapy* 83:439–49. doi: 10.1016/j.biopha.2016.07.002.

Khokon, Md Atiqur Rahman, Md Sarwar Jahan, Taniya Rahman, Mohammad Anowar Hossain, Daichi Muroyama, Ikuko Minami, Shintaro Munemasa, Izumi C. Mori, Yoshimasa Nakamura, and Yoshiyuki Murata. 2011. "Allyl Isothiocyanate (AITC) Induces Stomatal Closure in Arabidopsis." *Plant, Cell and Environment* 34(11):1900–1906. doi: 10.1111/j.1365-3040.2011.02385.x.

Kliebenstein, Daniel J., Virginia M. Lambrix, Michael Reichelt, Jonathan Gershenzon, and Thomas Mitchell-Olds. 2001. "Gene Duplication in the Diversification of Secondary Metabolism: Tandem 2-Oxoglutarate-Dependent Dioxygenases Control

Glucosinolate Biosynthesis in Arabidopsis". *The Plant Cell* 13(3), 681-693. doi: 10.1105/tpc.13.3.681.

Knecht, Leslie D., Gregory O'Connor, Rahul Mittal, Xue Z. Liu, Pirouz Daftarian, Sapna K. Deo, and Sylvia Daunert. 2016. "Serotonin Activates Bacterial Quorum Sensing and Enhances the Virulence of Pseudomonas Aeruginosa in the Host." *EBioMedicine* 9:161–69. doi: 10.1016/j.ebiom.2016.05.037.

Köllner, Tobias G., Christiane Schnee, Jonathan Gershenzon, and Jörg Degenhardt. 2004. "The Variability of Sesquiterpenes Emitted from Two Zea Mays Cultivars Is Controlled by Allelic Variation of Two Terpene Synthase Genes Encoding Stereoselective Multiple Product Enzymes." *Plant Cell* 16(5):1115–31. doi: 10.1105/tpc.019877.

Kumar, Gyanendra, Kirti R. Saad, Monisha Arya, Bijesh Puthusseri, Paramesha Mahadevappa, Nandini P. Shetty, and Parvatam Giridhar. 2021. "The Synergistic Role of Serotonin and Melatonin during Temperature Stress in Promoting Cell Division, Ethylene and Isoflavones Biosynthesis in Glycine Max." *Current Plant Biology* 26:100206. doi: 10.1016/j.cpb.2021.100206.

Lass-Flörl, Cornelia, Dietmar Fuchs, Maximilian Ledochowski, Cornelia Speth, Manfred P. Dierich, and Reinhard Würzner. 2003. "Antifungal Properties of 5-Hydroxytryptamine (Serotonin) against Candida Species in Vitro." *Journal of Medical Microbiology* 52(2):169–71. doi: 10.1099/jmm.0.04987-0.

Lee, Hyoung Yool, Kyungjin Lee, and Kyoungwhan Back. 2019. "Knockout of Arabidopsis Serotonin N-Acetyltransferase-2 Reduces Melatonin Levels and Delays Flowering." *Biomolecules* 9(11). doi: 10.3390/biom9110712.

Lembeck, Fred, and Gerhard Skofitsch. 1984. "Distribution of Serotonin in Juglans Regia Seeds During Ontogenetic Development and Germination." *Zeitschrift Für Pflanzenphysiologie* 114(4):349–53. doi: 10.1016/s0044-328x(84)80090-2.

Li, Lin, Minghui Zheng, Hai Long, Guangbing Deng, Atsushi Ishihara, Feng Liu, Junjun Liang, Zhifen Pan, and Maoqun Yu. 2016a. "Molecular Cloning and Characterization of Two Genes Encoding Tryptophan Decarboxylase from Aegilops Variabilis with Resistance to the Cereal Cyst Nematode (Heterodera Avenae) and Root-Knot Nematode (Meloidogyne Naasi)." *Plant Molecular Biology Reporter* 34(1):273–82. doi: 10.1007/s11105-015-0909-3.

Li, Lin, Minghui Zheng, Hai Long, Guangbing Deng, Atsushi Ishihara, Feng Liu, Junjun Liang, Zhifen Pan, and Maoqun Yu. 2016b. "Molecular Cloning and Characterization of Two Genes Encoding Tryptophan Decarboxylase from Aegilops Variabilis with Resistance to the Cereal Cyst Nematode (Heterodera Avenae) and Root-Knot Nematode (Meloidogyne Naasi)." *Plant Molecular Biology Reporter* 34(1):273–82. doi: 10.1007/s11105-015-0909-3.

De Luca, Vincenzo, Jesus Alvarez Fernandez2, Douglas Campbell3, and Wolfgang G. W. Kurz. 1988. "Developmental Regulation of Enzymes of Indole Alkaloid Biosynthesis

in Catharanthus Roseus". Plant physiology, 86(2), 447-450. doi: 10.1104/pp.86.2.447.

Luetje, Charles W., and Sisi Chen. 2014. "Trace Amines Inhibit Insect Odorant Receptor Function through Antagonism of the Co-Receptor Subunit." *F1000Research* 3. doi: 10.12688/f1000research.3825.1.

Manchester, Lucien C., Ana Coto-Montes, Jose Antonio Boga, Lars Peter H. Andersen, Zhou Zhou, Annia Galano, Jerry Vriend, Dun Xian Tan, and Russel J. Reiter. 2015. "Melatonin: An Ancient Molecule That Makes Oxygen Metabolically Tolerable." *Journal of Pineal Research* 59(4):403–19. doi: doi.org/10.1111/jpi.12267.

Mannino, Giuseppe, Carlo Pernici, Graziella Serio, Carla Gentile, and Cinzia M. Bertea. 2021a. "Melatonin and Phytomelatonin: Chemistry, Biosynthesis, Metabolism, Distribution and Bioactivity in Plants and Animals—an Overview." *International Journal of Molecular Sciences* 22(18). doi: doi.org/10.3390/ijms22189996.

Mishra, Vishnu, and Ananda K. Sarkar. 2023b. "Serotonin: A Frontline Player in Plant Growth and Stress Responses." *Physiologia Plantarum* 175(4). doi: doi.org/10.1111/ppl.13968.

Mohammad-Zadeh, L. F., L. Moses, and S. M. Gwaltney-Brant. 2008. "Serotonin: A Review." *Journal of Veterinary Pharmacology and Therapeutics* 31(3):187–99. doi: 10.1111/j.1365-2885.2008.00944.x.

Moore, Ben D., Rose L. Andrew, Carsten Külheim, and William J. Foley. 2014. "Explaining Intraspecific Diversity in Plant Secondary Metabolites in an Ecological Context." *New Phytologist* 201(3):733–50. doi: 10.1111/nph.12526.

Mukherjee, Soumya, Anisha David, Sunita Yadav, František Baluška, and Satish Chander Bhatla. 2014. "Salt Stress-Induced Seedling Growth Inhibition Coincides with Differential Distribution of Serotonin and Melatonin in Sunflower Seedling Roots and Cotyledons." *Physiologia Plantarum* 152(4):714–28. doi: 10.1111/ppl.12218.

Murch, Susan J., Skye S. B. Campbell, and Praveen K. Saxena. 2001. "The role of serotonin and melatonin in plant morphogenesis: regulation of auxin-induced root organogenesis in in vitro-cultured explants of St. John's wort (Hypericum perforatum l.)." In Vitro Cellular & Developmental Biology-Plant, 37, 786-793. doi: 10.1007/s11627-001-0130-y.

Muszyńska, Bozena, Katarzyna Sułkowska-Ziaja, and Halina Ekiert. 2011. "Indole Compounds in Fruiting Bodies of Some Edible Basidiomycota Species." *Food Chemistry* 125(4):1306–8. doi: 10.1016/j.foodchem.2010.10.056.

Negre, Florence, Christine M. Kish, Jennifer Boatright, Beverly Underwood, Kenichi Shibuya, Conrad Wagner, David G. Clark, and Natalia Dudareva. 2003. "Regulation of Methylbenzoate Emission after Pollination in Snapdragon and Petunia Flowers." *Plant Cell* 15(12):2992–3006. doi: 10.1105/tpc.016766.

Negri, Stefano, Mauro Commisso, Linda Avesani, and Flavia Guzzo. 2021. "The Case of Tryptamine and Serotonin in Plants: A Mysterious Precursor for an Illustrious

Metabolite." *Journal of Experimental Botany* 72(15):5336–55. doi: Negri, Stefano, Mauro Commisso, Linda Avesani, and Flavia Guzzo. 2021. "The Case of Tryptamine and Serotonin in Plants: A Mysterious Precursor for an Illustrious Metabolite." Journal of Experimental Botany 72(15):5336–55.

Oliver, Stephen G., Michael K. Winson, Douglas B. Kell, and Frank Baganz. 1998. "Systematic Functional Analysis of the Yeast Genome." *Trends in Biotechnology* 16(9):373–78. doi: https://doi.org/10.1016/S0167-7799(98)01214-1.

Pang, Zhiqiang, Jia Chen, Tuhong Wang, Chunsheng Gao, Zhimin Li, Litao Guo, Jianping Xu, and Yi Cheng. 2021. "Linking Plant Secondary Metabolites and Plant Microbiomes: A Review." *Frontiers in Plant Science* 12, 621276. doi: 10.3389/fpls.2021.621276.

Park, Sangkyu, Kyungjin Lee, Young Soon Kim, and Kyoungwhan Back. 2012. "Tryptamine 5-Hydroxylase-Deficient Sekiguchi Rice Induces Synthesis of 5-Hydroxytryptophan and N-Acetyltryptamine but Decreases Melatonin Biosynthesis during Senescence Process of Detached Leaves." *Journal of Pineal Research* 52(2):211–16. doi: 10.1111/j.1600-079X.2011.00930.x.

Pelagio-Flores, Ramón, Randy Ortíz-Castro, Alfonso Méndez-Bravo, Lourdes Macías-Rodríguez, and Jose López-Bucio. 2011. "Serotonin, a Tryptophan-Derived Signal Conserved in Plants and Animals, Regulates Root System Architecture Probably Acting as a Natural Auxin Inhibitor in Arabidopsis Thaliana." *Plant and Cell Physiology* 52(3):490–508. doi: 10.1093/pcp/pcr006.

Perkhofer, Susanne, Harald Niederegger, Gerhard Blum, Wolfgang Burgstaller, Maximilian Ledochowski, Manfred P. Dierich, and Cornelia Lass-Flörl. 2007. "Interaction of 5-Hydroxytryptamine (Serotonin) against *Aspergillus* Spp. in Vitro." *International Journal of Antimicrobial Agents* 29(4):424–29. doi: 10.1016/j.ijantimicag.2006.12.003.

Pichersky, Eran, Joseph P. Noel, and Natalia Dudareva. 2006. "Biosynthesis of Plant Volatiles: Nature's Diversity and Ingenuity". *Science,* 311(5762), 808-811. doi: 10.1126/science.1118510.

Runguphan, Weerawat, Justin J. Maresh, and Sarah E. O'connor. 2009. "Silencing of Tryptamine Biosynthesis for Production of Nonnatural Alkaloids in Plant Culture". *Proceedings of the National Academy of Sciences*, *106*(33), 13673-13678. 10.1073/pnas.090339310.

S Gill, Rishi I., Brian E. Ellis, and Murray B. Isman. 2003. "Tryptamine-induced resistance in tryptophan decarboxylase transgenic poplar and tobacco plants against their specific herbivores". *Journal of chemical ecology*, 29, 779-793. doi: 10.1023/A:1022983529555.

Salehin, Mohammad, Baohua Li, Michelle Tang, Ella Katz, Liang Song, Joseph R. Ecker, Daniel J. Kliebenstein, and Mark Estelle. 2019. "Auxin-Sensitive Aux/IAA Proteins Mediate Drought Tolerance in Arabidopsis by Regulating Glucosinolate Levels." *Nature Communications* 10(1). doi: 10.1038/s41467-019-12002-1.

Schwab, Wilfried. 2003. “Metabolome Diversity: Too Few Genes, Too Many Metabolites?” *Phytochemistry* 62(6):837–49. doi: 10.1016/S0031-9422(02)00723-9.

Shan, Qiaobo, Weicheng Liu, Xiaoxiao Ni, Min Li, Yifan Sun, Lixian Liao, and Chunfang Zheng. 2025. “Serotonin Mitigates ColdStress-Induced Damage in *Kandelia Obovata* Through Modulating the Endogenous Melatonin- and Abscisic Acid Biosynthesis.” *International Journal of Molecular Sciences* 26(4):1635. doi: 10.3390/ijms26041635.

Songstad, David D., Vincenzo De Luca, Normand Brisson, Wolfgang G. W. Kurz, and Craig L. Nessler5. 1990. “High Levels of Tryptamine Accumulation in Transgenic Tobacco Expressing Tryptophan Decarboxylase”. *Plant physiology*, 94(3), 1410-1413. doi: 10.1104/pp.94.3.1410.

Sravanthi, T. V., and S. L. Manju. 2016. “Indoles - A Promising Scaffold for Drug Development.” *European Journal of Pharmaceutical Sciences* 91, 1–10. DOI: 10.1016/j.ejps.2016.05.025.

Sun, Chengliang, Lijuan Liu, Luxuan Wang, Baohai Li, Chongwei Jin, and Xianyong Lin. 2021. “Melatonin: A Master Regulator of Plant Development and Stress Responses.” *Journal of Integrative Plant Biology* 63(1):126–45. DOI: 10.1111/jipb.12993.

Tholl, Dorothea, Feng Chen, Jana Petri, Jonathan Gershenzon, and Eran Pichersky. 2005. “Two Sesquiterpene Synthases Are Responsible for the Complex Mixture of Sesquiterpenes Emitted from Arabidopsis Flowers.” *Plant Journal* 42(5):757–71. doi: 10.1111/j.1365-313X.2005.02417.x.

Thomas, John C., Edward F. Saleh, Nouha Alammar, and Andann M. Akroush. 1998. “The Indole Alkaloid Tryptamine Impairs Reproduction in Drosophila Melanogaster”. *Journal of economic entomology*, 91(4), 841-846. doi: 10.1093/jee/91.4.841.

Tong, Xiwen, Yundan Wang, Pengcheng Yang, Chengshu Wang, and Le Kang. 2020. “Tryptamine Accumulation Caused by Deletion of MrMao-1 in Metarhizium Genome Significantly Enhances Insecticidal Virulence.” *PLoS Genetics* 16(4). doi: 10.1371/journal.pgen.1008675.

Tsunoda, Yui, Shohei Hano, Nozomi Imoto, Tomoki Shibuya, Hiroki Ikeda, Kayoko Amagaya, Kazuhisa Kato, Hitoshi Shirakawa, Hisashi Aso, and Yoshinori Kanayama. 2021. “Physiological Roles of Tryptophan Decarboxylase Revealed by Overexpression of SlTDC1 in Tomato.” *Scientia Horticulturae* 275. doi: 10.1016/j.scienta.2020.109672.

Turlejski, Krzysztof. 1996. “Evolutionary Ancient Roles of Serotonin: Long-Lasting Regulation of Activity and Development”. *Acta neurobiologiae experimentalis*, 56(2), 619-636.

Ueno, Makoto, Hitoshi Shibata, Junichi Kihara, Yuichi Honda, and Sakae Arase. 2003. “Increased Tryptophan Decarboxylase and Monoamine Oxidase Activities Induce

Sekiguchi Lesion Formation in Rice Infected with Magnaporthe Grisea." *Plant Journal* 36(2):215–28. doi: 10.1046/j.1365-313X.2003.01875.x.

Veenstra-Vanderweele, Jeremy, George M. Anderson, and Edwin H. Cook. 2000. "Pharmacogenetics and the Serotonin System: Initial Studies and Future Directions". *European journal of pharmacology*, 410(2-3), 165-181. doi: 10.1016/S0014-2999(00)00814-1.

Wan, Jinpeng, Ping Zhang, Ruling Wang, Liangliang Sun, Qiong Ju, and Jin Xu. 2018. "Comparative Physiological Responses and Transcriptome Analysis Reveal the Roles of Melatonin and Serotonin in Regulating Growth and Metabolism in Arabidopsis." *BMC Plant Biology* 18(1). doi: 10.1186/s12870-018-1548-2.

Wang, Gangzheng, Xianglian Chen, Chenghua Zhang, Min Li, Chengyuan Sun, Ning Zhan, Xueshuang Huang, Taihui Li, and Wangqiu Deng. 2021. "Biosynthetic Pathway and the Potential Role of Melatonin at Different Abiotic Stressors and Developmental Stages in Tolypocladium Guangdongense." *Frontiers in Microbiology* 12. doi: 10.3389/fmicb.2021.746141.

Wegner, Andre, Johannes Meiser, Daniel Weindl, and Karsten Hiller. 2015. "How Metabolites Modulate Metabolic Flux." *Current Opinion in Biotechnology* 34:16–22. doi: 10.1016/j.copbio.2014.11.008.

Williams, Brianna B., Andrew H. Van Benschoten, Peter Cimermancic, Mohamed S. Donia, Michael Zimmermann, Mao Taketani, Atsushi Ishihara, Purna C. Kashyap, James S. Fraser, and Michael A. Fischbach. 2014. "Discovery and Characterization of Gut Microbiota Decarboxylases That Can Produce the Neurotransmitter Tryptamine." *Cell Host and Microbe* 16(4):495–503. doi: 10.1016/j.chom.2014.09.001.

Wink, Michael. 2010. "Introduction: Biochemistry, Physiology and Ecological Functions of Secondary Metabolites." *Biochemistry of Plant Secondary Metabolism: Second Edition* 40:1–19. doi: 10.1002/9781444320503.ch1.

Wishart, David S., Dan Tzur, Craig Knox, Roman Eisner, An Chi Guo, Nelson Young, Dean Cheng, Kevin Jewell, David Arndt, Summit Sawhney, Chris Fung, Lisa Nikolai, Mike Lewis, Marie Aude Coutouly, Ian Forsythe, Peter Tang, Savita Shrivastava, Kevin Jeroncic, Paul Stothard, Godwin Amegbey, David Block, David D. Hau, James Wagner, Jessica Miniaci, Melisa Clements, Mulu Gebremedhin, Natalie Guo, Ying Zhang, Gavin E. Duggan, Glen D. MacInnis, Alim M. Weljie, Reza Dowlatabadi, Fiona Bamforth, Derrick Clive, Russ Greiner, Liang Li, Tom Marrie, Brian D. Sykes, Hans J. Vogel, and Lori Querengesser. 2007. "HMDB: The Human Metabolome Database." *Nucleic Acids Research* 35(SUPPL. 1). doi: 10.1093/nar/gkl923.

Wu, Jianqiang, and Ian T. Baldwin. 2010. "New Insights into Plant Responses to the Attack from Insect Herbivores." *Annual Review of Genetics* 44:1–24. doi: 10.1146/annurev-genet-102209-163500.

Xie, Xiaotong, Dongqin Ding, Danyang Bai, Yaru Zhu, Wei Sun, Yumei Sun, and Dawei Zhang. 2022. "Melatonin Biosynthesis Pathways in Nature and Its Production in

Engineered Microorganisms." *Synthetic and Systems Biotechnology* 7(1):544–53. doi: 10.1016/j.synbio.2021.12.011.

Xu, Peipei, Shan Fang, Haiying Chen, and Weiming Cai. 2020. "The Brassinosteroid-Responsive Xyloglucan Endotransglucosylase/Hydrolase 19 (XTH19) and XTH23 Genes Are Involved in Lateral Root Development under Salt Stress in Arabidopsis." *Plant Journal* 104(1):59–75. doi: 10.1111/tpj.14905.

Ye, Tiantian, Xiaoming Yin, Lei Yu, Shu Jian Zheng, Wen Jing Cai, Yan Wu, and Yu Qi Feng. 2019. "Metabolic Analysis of the Melatonin Biosynthesis Pathway Using Chemical Labeling Coupled with Liquid Chromatography-Mass Spectrometry." *Journal of Pineal Research* 66(1). doi: 10.1111/jpi.12531.

Yonekura-Sakakibara, Keiko, and Kazuki Saito. 2009. "Functional Genomics for Plant Natural Product Biosynthesis." *Nat. Prod. Rep.* 26(11):1466–87. doi: 10.1039/B817077K.

Zhang, Jianzhi. 2003. "Evolution by Gene Duplication: An Update." *Trends in Ecology and Evolution* 18(6):292–98. doi: 10.1016/S0169-5347(03)00033-8.

Zhang, Yanxia, Yiyun Li, Thijs de Zeeuw, Kilian Duijts, Dorota Kawa, Jasper Lamers, Kristina S. Munzert, Hongfei Li, Yutao Zou, A. Jessica Meyer, Jinxuan Yan, Francel Verstappen, Yixuan Wang, Tom Gijsberts, Jielin Wang, Nora Gigli-Bisceglia, Timo Engelsdorf, Aalt D. J. van Dijk, and Christa Testerink. 2023. "Root Branching in Salt Requires Auxin-Independent Modulation of LBD16 Function". *bioRxiv*, 2023, 2023.04. 25.538210. doi: 10.1101/2023.04.25.538210.

Zhao, Dake, Yang Yu, Yong Shen, Qin Liu, Zhiwei Zhao, Ramaswamy Sharma, and Russel J. Reiter. 2019. "Melatonin Synthesis and Function: Evolutionary History in Animals and Plants." *Frontiers in Endocrinology* 10, 441357. doi: doi.org/10.3389/fendo.2019.00249.

Zhao, Daqiu, Xiayan Zhang, Rong Wang, Ding Liu, Jing Sun, and Jun Tao. 2019. "Herbaceous Peony Tryptophan Decarboxylase Confers Drought and Salt Stresses Tolerance." *Environmental and Experimental Botany* 162:345–56. doi: 10.1016/j.envexpbot.2019.03.013.

Zhou, Yuanze, Lijing Liao, Xikai Liu, Biao Liu, Xinxin Chen, Yan Guo, Chuanlong Huang, Yucheng Zhao, and Zhixiong Zeng. 2020. "Crystal Structure of Oryza Sativa TDC Reveals the Substrate Specificity for TDC-Mediated Melatonin Biosynthesis." *Journal of Advanced Research* 24:501–11. doi: 10.1016/j.jare.2020.06.004.

Web References

https://gbcloning.upv.es/

https://gbcloning.upv.es/tools/crisprs/

http://crispor.gi.ucsc.edu/